

**Okinawa Institute of Science and Technology  
Graduate University**

**Thesis submitted for the degree  
Doctor of Philosophy**

---

**SynGAP Condensates Recruit PSD95, and Selectively Retain  
Multivalent Receptors, Functioning as the Basic Platform  
for Generating Neuronal Excitatory Synapses**

---

by

**Saahil Acharya**

**Supervisor: Prof. Akihiro Kusumi**

September 2022




## Declaration of Original and Sole Authorship

I, Saahil Acharya, declare that this thesis entitled “**SynGAP condensates recruit PSD95, and selectively retain multivalent receptors, functioning as the basic platform for generating neuronal excitatory synapses**” and the data presented in it are original and my own work.

I confirm that:

- No part of this work has previously been submitted for a degree at this or any other university.
- References to the work of others have been clearly acknowledged. Quotations from the work of others have been clearly indicated, and attributed to them.
- In cases where others have contributed to part of this work, such contribution has been clearly acknowledged and distinguished from my own work.
- None of this work has been previously published elsewhere.

Signature: 

Date: 2022/09/21

## **Abstract**

The post-synaptic structure consists of nano-scale domains that need to be precisely apposed to pre-synaptic neurotransmitter release sites. This exquisite assembly of post-synaptic receptors and scaffold proteins is essential for proper synaptic function. However, the biophysical mechanisms that retain receptors and scaffold proteins at the post-synapse are not well understood. Specifically, a mechanism that can induce clusters of PSD95, a key scaffold protein, at low concentrations, such as those expected before the formation of functional post-synapses, and which can induce long-term retention of post-synaptic receptors, remains to be postulated. In this thesis, I show that SynGAP forms phase-separated condensates through homophilic interactions mediated by its C-terminal coiled-coil domain as well as its intrinsically disordered region. SynGAP recruits PSD95 into these condensates, and this allows recruitment and immobilization of receptors such as Neuroligin and AMPA receptors (via TARPs), which have PDZ binding sites. I also found that oligomerization of Neuroligin and AMPA receptors anchors these receptors in SynGAP condensates. Functional oligomeric Neuroligin and AMPA receptors (GluA1 subunits linked to TARP  $\gamma 2$ ) are immobilized for longer durations as they diffuse through phase-separated condensates containing PSD95, compared to monomeric Neuroligin and TARP  $\gamma 2$ . Together, these discoveries reveal how liquid-like assemblies of SynGAP can recruit PSD95 molecules, and retain trans-membrane receptors like Neuroligin and AMPA receptors depending on their oligomerization state.

## Acknowledgement

The work presented in this thesis would not have been possible without the steadfast support, encouragement, scientific and intellectual discussions, and mentorship of Prof. Akihiro Kusumi, in whose lab I spent the years from 2016 onwards at OIST. I would also like to thank all members of the Membrane Cooperativity unit (past and present) for their help, encouragement, cooperation, and collaboration. These members include but are not limited to Dr. Taka A. Tsunoyama, Dr. Amine Aladag, Dr. HooiCheng Lim, Dr. Peng Zhou, Dr. Irina Meshcheryakova, Ms. Aya Nakamura, Ms. Hiroko Hijikata, Dr. Yuri L. Nemoto, and Dr. An-An Liu. Special thanks to Prof. Takahiro K. Fujiwara of Kyoto University for the development of scientific and analysis software tools, as well as his mentorship and collaboration, that were essential for the completion of this project, and to Prof. Ikuko Koyama-Honda, for teaching me the methods related to viral vector production and viral transduction. Many thanks also to the members of my thesis committee, Prof. Bernd Kuhn and Prof. Yoko Yazaki-Sugiyama, who also played important roles in mentoring me.

I also thank Prof. Rinshi Kasai for his kind gift of L cells, Dr. Yuri L. Nemoto for her kind gift of PSD95 cDNA, and Prof. Michiyuki Matsuda for his gift of pCMV-mPbase plasmid.

The examiners of my thesis, Prof. Frederick Meunier and Prof. Thomas Blanpied, provided excellent feedback on my written thesis and presentation, and suggested very useful changes in the thesis, and provided advice on scientific writing and presentation. These have been invaluable in making this thesis better, and I would like to thank them for their generosity.

I would like to express my gratitude for the support of the Graduate School of OIST, and in particular the long serving members of the Graduate School, who have always helped students and served in their best interests.

The members of the OIST community, and particularly the friends I made during my years as a PhD student at OIST, played an important role in my life, and I will forever cherish our memories and friendship, built in and around OIST. Special thanks to my friend and partner Larisa Sheloukhova for her encouragement and support through the difficult times as well as the good ones.

Lastly, I must express my gratitude for the people of Japan, and particularly the people of Okinawa, who taught me that a society can exist where people are friendlier, more helpful, and more cooperative than I ever imagined was possible.

## List of abbreviations

AMPA –  $\alpha$ -amino-3-hydroxy-5-methyl-4-isoxazolepropionic acid receptor  
AZ – active zone (presynaptic)  
CaMKII –  $\text{Ca}^{2+}$ /calmodulin dependent protein kinase II  
DM – (Neuroigin) dimerization-null mutant construct  
GluA1/GluA2/GluA3/GluA4 – AMPA receptor subunits  
IDR – intrinsically disordered region (of a protein)  
LLPS – liquid-liquid phase separation (also used as liquid-liquid phase separated condensates)  
LRRTM2 – Leucine-rich repeat trans-membrane neuronal protein 2  
LTP – long term potentiation  
Nlg – Neuroigin  
NMDAR – N-methyl-D-aspartate receptor  
Nxn – Neurexin  
PDZ – protein domain, named after PSD95, Dlg, and ZO-1 proteins  
PKA – protein kinase A  
PKC – protein kinase C  
PSD – post-synaptic density  
PSD95 – post-synaptic density protein 95  
SynGAP – synaptic Ras GTPase activating protein  
TARP2 – trans-membrane AMPA receptor regulatory protein  $\gamma$  2  
WT – (Neuroigin) wild-type or fully functional construct

## Table of Contents

### Declaration of Original and Sole Authorship

### Abstract

### Acknowledgement

### List of abbreviations

### Table of Contents

### List of figures

<b>Chapter 1. Introduction</b>	<b>1</b>
1.1 Structure and function of the synapse	1
1.2 Dynamics and regulation of the post-synapse	7
1.3 Problem statement	14
<b>Chapter 2. Liquid-liquid phase separation of SynGAP and assembly of PSD95 molecules as clients in SynGAP condensates</b>	<b>17</b>
2.1 Results	17
2.1.1 SynGAP forms LLPS condensates by itself, and recruits PSD95 as a client	17
2.1.2 Revealing the protein domains responsible for LLPS of SynGAP	19
2.1.3 SynGAP LLPS condensates are recruited to the plasma membrane	22
2.1.4 SynGAP LLPS condensates are dissolved by CaMKII	23
2.2 Summary and discussion	24
<b>Chapter 3. Retention of receptors at SynGAP LLPS condensates</b>	<b>27</b>
3.1 Introduction	27
3.2 Results	27
3.2.1 Creating a functional tagged version of Neuroligin	27
3.2.2 Role of Neuroligin dimerization in its retention at the synapse	32
3.2.3 Valency dependent retention of receptors at the synapse: comparing tetrameric GluA1 to dimeric and monomeric versions	39
3.3. Summary and discussion	47
<b>Chapter 4. General discussion and future directions</b>	<b>49</b>
4.1 SynGAP's role at the post-synapse: reconciling my results with other studies	49
4.2 Future experiments	50
4.3 Final Summary	51
<b>Chapter 5. Materials and methods</b>	<b>52</b>
<b>Bibliography</b>	<b>57</b>



## List of figures

Fig 1	Electron micrograph of a mammalian glutamatergic synapse.....	2
Fig 2	Electron micrograph 3D reconstruction of a mammalian glutamatergic synapse.....	2
Fig 3	Schematic of major proteins present at a typical glutamatergic synapse.....	4
Fig 4	Schematic of the concept of synaptic “nano-columns” .....	6
Fig 5	Schematic of the concept of liquid-liquid phase separation at the post-synapse.....	11
Fig 6	FRAP assay of LLPS condensates comprising of post-synaptic proteins.....	11
Fig 7	Schematic of the protein domains of PSD95.....	12
Fig 8	Schematic of the protein domains of SynGAP.....	12
Fig 9	Schematic showing the N and C-terminal post-transcriptional modification of SynGAP.....	13
Fig 10	Structure of the SynGAP parallel coiled-coil trimer, and the interaction of SynGAP PBM with PSD95.....	13
Fig 11	Schematic highlighting the key outstanding questions about the assembly and regulation of the post-synapse.....	15
Fig 12	LLPS of SynGAP in L cells, and the recruitment of PSD95 to SynGAP ‘QTRV’ isoform clusters.....	17
Fig 13	Fluorescence recovery after photobleaching of SynGAP LLPS condensates.....	18-19
Fig 14	Concentration dependent LLPS of SynGAP, and the domains of SynGAP responsible for LLPS.....	20-21
Fig 15	Calibration of intensity of mEGFP-SynGAP constructs to that of titrated amounts of purified EGFP in solution.....	22
Fig 16	SynGAP LLPS condensates can be brought to the plasma membrane by Nlg1.....	23
Fig 17	CaMKII dissolves SynGAP LLPS condensates.....	24
Fig 18	Intrinsic disorder prediction for the amino-acid sequence of SynGAP.....	25
Fig 19	Schematic showing role of SynGAP in nucleating the formation of the post-synapse....	26
Fig 20	Schematic showing how Nlg1 forms homodimers via cis-interactions as well as binds to Neurexin via trans-synaptic interactions.....	28
Fig 21	Schematic showing various Nlg1 constructs used in this study with the sites of tag insertion.....	29
Fig 22	Cell aggregation experiments to test the function of different Nlg1 constructs.....	30
Fig 23	Estimation of plasma membrane expression of Nlg1 constructs used in the cell-cell aggregation experiments.....	31
Fig 24	Synaptic localization of Nlg-Halo-687 construct.....	31
Fig 25	Schematic of fully functional Nlg construct (Nlg-Halo-687 WT) and its dimerization-null mutant (Nlg-Halo-687 DM) .....	32



Fig 26 Nlg-Halo DM molecules show impaired localization to neuronal spines compared to Nlg-Halo WT molecules.....	32
Fig 27 Schematic illustrating the oligomerization state of Nlg-Halo WT, Nlg-Halo DM, and Nlg-Halo DM clustered with antibodies.....	34
Fig 28 Estimation of the fractions of monomers, dimers, trimers, and tetramers, and the mean cluster size of Nlg-Halo WT, Nlg-Halo DM, and Nlg-Halo DM clustered with antibodies.....	34-35
Fig 29 Immobilization of Nlg-Halo WT, Nlg-Halo DM, and Nlg-Halo DM clustered with antibodies in SynGAP LLPS condensates via PSD95.....	37-39
Fig 30 Schematic of Halo tagged TARP2, GluA1-TARP2, and GluA1- $\Delta$ NTD-TARP2 constructs.....	42
Fig 31 Estimation of the fractions of monomers, dimers, trimers, and tetramers, and the mean cluster size of Halo-TARP2, Halo-GluA1-TARP2, and Halo-GluA1- $\Delta$ NTD-TARP2.....	41-42
Fig 32 Immobilization of Halo-TARP2, Halo-GluA1-TARP2, and Halo-GluA1- $\Delta$ NTD-TARP2 in SynGAP LLPS condensates via PSD95.....	43-45
Fig 33 Illustration of the concept of LLPS condensates of SynGAP, with PSD95 as a client, selectively recruiting and immobilizing receptors based on their oligomerization state..	48

## Chapter 1. Introduction

The human nervous system, comprising of billions of neurons in the brain, spinal cord, and throughout the body, is perhaps the most important system from a biomedical perspective. Disorders affecting all human experience are connected to the nervous system, and therefore it is of utmost importance that we thoroughly understand its structure and function. Despite this, the nervous system is arguably the least understood system of the human body. This is because at every level of organization, the nervous system is exquisitely complex. The information processing part of the nervous system comprises of billions of cells called neurons that connect to each other. The connection between two neurons is called the synapse, and this is where information is conveyed from a pre-synaptic neuron across a cleft to the post-synaptic neuron. The synapse is the fundamental structural and functional unit of the nervous system.

The study of the structure, formation, and function of synapses is of great biomedical importance. Synaptic dysfunction is implicated in a variety of diseases and disorders. Moreover, the changes that occur at the synapse in response to signals, underlie fundamental brain functions like learning and memory. Specifically, what enables synaptic transmission is the machinery of proteins present at the pre and post-synapse. And when a synapse changes, it is the arrangement, number, and turnover of pre and post-synaptic proteins that results in the change in function of the synapse. Therefore, understanding the mechanisms behind the assembly and regulation of these pre and post-synaptic proteins is essential to understand brain function and dysfunction. This is also why the complex machinery of proteins both at the pre-synaptic side and the post-synaptic side have also been extensively examined over the last several decades. In this introduction, I will provide a brief explanation of the structure of the synapse, the pre and post-synaptic machinery of proteins, their function in relaying signals or “action potentials” and undergoing long-term changes, and the nanoscale organization of the pre and post-synaptic proteins, and their dynamics. Finally, I will discuss the focus of this thesis, which is the role of phase separation in clustering a key post-synaptic scaffold protein and in retaining post-synaptic receptors.

Since the model system I am studying is the typical excitatory synapse, where glutamate is the neurotransmitter released, in the following parts, I simply use the word "synapse" to indicate glutamatergic excitatory synapse.

### 1.1 Structure and function of the synapse

As shown in Fig 1 and Fig 2, the synapse is the region where a pre-synaptic neuron communicates with the post-synaptic neuron. In mammalian neurons, the presynaptic side of the synapse consists of a protrusion from a neuron’s axon, called a pre-synaptic bouton. This contains active zones, where synaptic vesicles, which carry neurotransmitters, fuse with the plasma membrane and release neurotransmitters into the synaptic cleft. A network of scaffolding proteins organizes the vesicles and other proteins in and near the active zone. The neurotransmitters released from a pre-synaptic neuron are molecules that diffuse across the synaptic cleft, and can activate receptors on the post-synaptic neuron. At the post-synaptic side, there are several types of receptors that can bind to neurotransmitters, and these trigger electric or chemical signals in the post-synaptic neuron. A scaffolding protein network also exists in the post-synaptic zone, which holds the post-synaptic zone together, and organizes receptors so that they are closely opposed to pre-synaptic release sites.

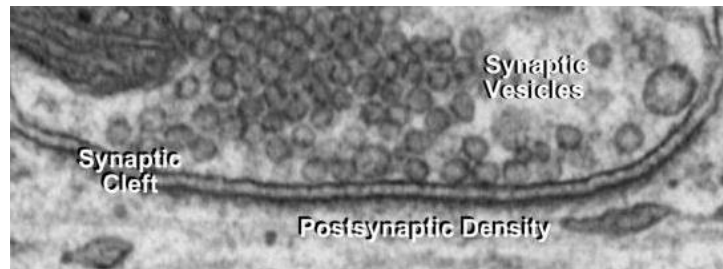


**Fig 1. Electron micrograph showing a typical mammalian excitatory synapse**

The pre-synaptic terminal containing synaptic vesicles, the synaptic cleft, and the post-synaptic density are labelled (image courtesy of Dr. X. Liu, UT Southwestern)

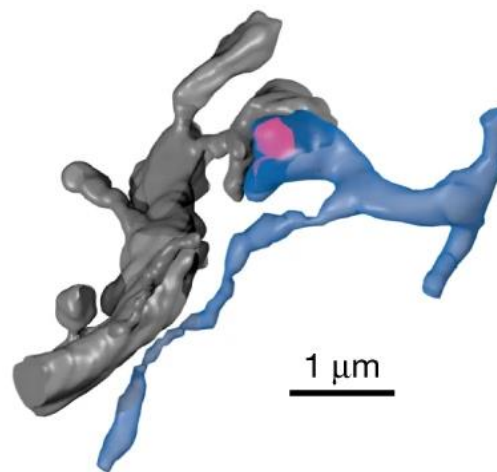


**Fig 2. High-resolution 3D reconstruction of a synapse**

Electron microscopy reconstruction of a synapse (magenta) formed between the pre-synaptic (blue) neuron and the post-synaptic (grey) neuron (Adapted from Holler et al., 2021)

### *Pre-synapse*

The site of pre-synaptic activity is often referred to as the active zone (sometimes abbreviated to AZ). The essential role of the AZ is the release of neurotransmitters when an electrical signal arrives. This function comprises a variety of different processes, such as calcium channels that respond to incoming signals by allowing the entry of calcium ions into the pre-synapse, fusion of synaptic vesicles, which contain molecules of neurotransmitters, in response to calcium influx, recycling of synaptic vesicles by endocytosis, adhesion across the synapse by homophilic and heterophilic adhesion molecules, and adaptor proteins (also called scaffold proteins) that allow all the functional proteins to be held in place, and eventually linked to structural proteins like actin. See Fig 3 for a schematic of the various proteins involved in the processes just described.

### *Post-synapse*

On the post-synaptic side is an equally complex machinery of proteins that enable efficient detection of neurotransmitter release from the pre-synapse. These comprise of glutamate-sensitive ion channels such as  $\alpha$ -amino-3-hydroxy-5-methyl-4-isoxazolepropionic acid receptor (abbreviated as AMPAR) and N-methyl-D-aspartate receptor (abbreviated as NMDAR), among others, which are ion channels that open in response to glutamate.

In the cytoplasmic region close to the post-synaptic membrane is a dense area of numerous scaffold proteins such as PSD95 (named after the **p**ost-**s**ynaptic **d**ensity, which is described later), GKAP (guanylate kinase-associated protein), Homer, and Shank (among others). This region, because of its obvious density in electron micrographs, is called the post-synaptic density (abbreviated as PSD). Individual PSDs range from about 200 to 800 nm wide, and 30 to 50 nm thick (Carlin et al., 1980), and contain an extremely high density of proteins, equivalent to about 10,000 copies of proteins with an average size of 100 kDa (Sheng et al., 2007). The most well-studied protein in the PSD, PSD95, is also one of the most abundant, existing at about 300 copies at a typical PSD (Sugiyama et al., 2005). PSD95 is widely considered the key protein responsible for the dense assembly of scaffold and receptors at the PSD (Chen et al., 2011). Synaptic Ras GTPase activating protein (abbreviated as SynGAP), a modulator of small GTPases, is also present in similar numbers as PSD95, and is therefore one of the most abundant PSD proteins (Sheng et al., 2007). SynGAP plays an important structural role as well, and binds with PSD95 (Zeng et al., 2016). The only protein reported to be present in greater numbers is  $\text{Ca}^{2+}$ /calmodulin dependent protein kinase II (abbreviated as CaMKII), a kinase that phosphorylates a large number of synaptic proteins, and is involved in LTP. About 3000 copies of CaMKII are reported to exist at a typical PSD, roughly ten times the number of PSD95 molecules (Lowenthal et al., 2015). One of the key outstanding questions is how the extremely high density of scaffold proteins and enzymes which comprise the PSD is maintained, and how the numbers of these proteins are regulated in response to synaptic activation.

The post-synaptic plasma membrane also consists of adhesion proteins such as N-cadherin and Neuroligin (abbreviated as Nlg), which bind with their pre-synaptic partners (either the same or different proteins). N-cadherins are capable of homophilic interactions, while Nlgs bind with Neurexins (abbreviated as Nxn) on the presynaptic side. Adhesion proteins like N-cadherin physically link the pre and post-synaptic sides (Uchida et al., 1996), while the heterophilic pair Nxn (pre-synaptic) and Nlg (post-synaptic) also play an important role in proper synaptic transmission (Chanda et al., 2017) and LTP (Shipman et al., 2012), by aligning the pre-synaptic neurotransmitter machinery with the post-synaptic receptors to enable efficient detection of neurotransmitters (Haas et al., 2018).

Fig 3. gives an illustration of the main proteins on the pre and post-synaptic side of a typical glutamatergic excitatory synapse.

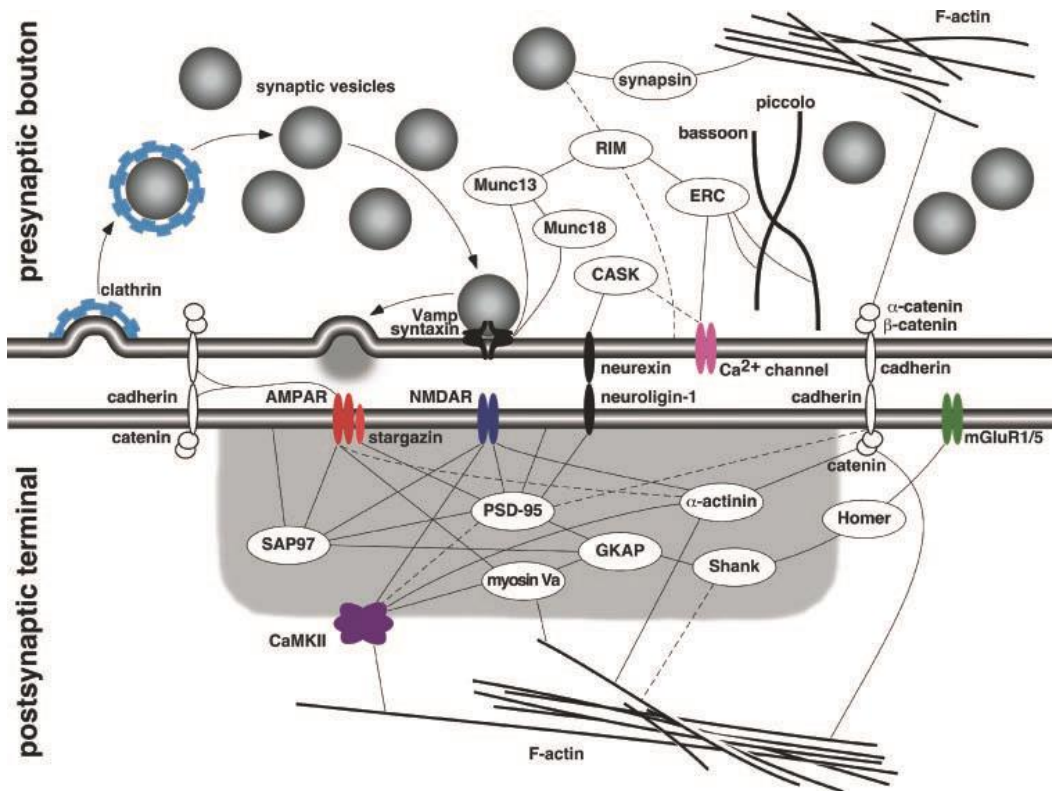


**Fig 3. The major proteins present at the pre-synaptic active zone and post-synaptic PSD (adapted from Specht et al., 2008)**

### *Action potential*

Synapses communicate with each other through a very fast process called the action potential. The action potential starts when an incoming “depolarization” (explained later) activates voltage gated calcium channels in the pre-synaptic membrane. The entry of calcium ions into the presynaptic membrane triggers the fusion of neurotransmitter laden vesicles, called synaptic vesicles, to the pre-synaptic plasma membrane, releasing neurotransmitters (in the case of our typical excitatory synapses, this neurotransmitter is glutamate) into the synaptic cleft. A complex machinery of proteins (see Fig 3) enables the almost instantaneous fusion of synaptic vesicles to the pre-synaptic plasma membrane, and more vesicles are held in reserve a short distance from the pre-synaptic plasma membrane.

The neuronal plasma membrane is maintained at an electro-chemical gradient, with more sodium ions outside the cell and more potassium ions inside (a chemical potential), and an uneven distribution of net charge (an electrical potential). When glutamate-sensitive ion channels such as AMPAR bind with glutamate, they open, and allow the entry of sodium ions into the cell and potassium ions out of the cell, due to the difference in their resting concentrations inside and outside the cell. This initial entry of positive sodium ions induces a change in the plasma membrane potential, and triggers the opening of voltage-sensitive ion channels. Glutamate sensitive ion channels like AMPAR shut off quickly, while voltage-sensitive ion channels continue the process of letting in sodium ions into the cell, further “depolarizing” adjacent membrane areas. As the plasma membrane becomes “depolarized”, voltage-gated sodium channels become inactivated,

stopping the flow of sodium ions into the cells, but voltage-gated potassium channels then open and potassium ions continue to exit, and bring the potential of the local membrane back towards its resting state. The original concentrations of sodium and potassium ions across the neuronal plasma membrane are maintained by a separate group of proteins called sodium-potassium pumps. The transient depolarization of the neuronal plasma membrane, which can get transmitted along the neuronal plasma membrane from the site of initial depolarization, is called an action potential. Action potentials represent the unit of signal transduction of a neuron, since they can propagate across the neuron and pass information to connecting neurons. Action potentials enable the quick transfer, processing, and output of information in the central nervous system, and the machinery of pre and post-synaptic proteins are finely tuned to allow action potentials to occur. The study of the mechanisms that regulate pre and post-synaptic proteins that allow action potentials to occur is therefore very important.

### *LTP*

While the entry and exit of sodium and potassium ions respectively are the biophysical basis for the action potential and therefore neuronal signaling, the entry of calcium ions is important in the induction of long-term changes to the characteristics of the synapse. When the initial pre-synaptic release of glutamate reaches AMPAR and NMDAR, they can only conduct sodium and potassium ions. NMDAR are capable of conducting calcium ions, but they are initially blocked by magnesium ions. When a high-frequency stimulation of the presynaptic neuron occurs, glutamate is released in bursts, and results in repeated entry of sodium ions into the postsynaptic neuron, and repeated depolarizations of the post-synaptic plasma membrane. This can relieve the magnesium ion “block” on NMDAR, and allow them to conduct calcium ions into the cell. The entry of calcium into the post-synapse causes a wide range of effects, and is the basis for long lasting changes in the numbers of receptors and scaffold proteins, as well the size and volume of spines. This “response” on the post-synaptic side is called long-term potentiation (abbreviated as LTP). While LTP as a phenomenon was discovered and is studied at the level of cells and molecules, it is likely that LTP plays an important role in higher order functions like learning and memory. Impairing various pathways in the expression of LTP at the post-synapse has been shown to block learning and memory in mice (Giese et al., 1998, Moser et al., 1998).

LTP is expressed as an increase in the numbers of AMPAR on the post-synapse, making the post-synapse more sensitive to glutamate release. One interesting sub-case of LTP expression is the conversion of so-called “silent synapses”, which only contain NMDA receptors but no AMPAR, to functional synapses by the addition of AMPAR (Isaac et al., 1995), although LTP can also potentiate synapses that already contain AMPAR. LTP also results in a general enlargement of the spine (Matsuzaki et al., 2004), and involves changes in various structural components including the actin cytoskeleton (Bosch et al., 2014), an increase in AMPAR due to an increase in exocytosis of AMPAR (Jurado et al., 2013) and capture of freely diffusing AMPAR at the post-synapse (Choquet et al., 2003).

Thus, the increase in the AMPA receptor numbers at the post-synapse is an important aspect of LTP. The relative roles of exocytosis and receptor diffusion in the increase of AMPA receptor numbers are still unclear, although both processes could be involved. Recent research suggests AMPA receptor diffusion may even have a role to play in the pathophysiology of diseases like Huntington’s (Zhang et al., 2018), and in fear-conditioning in rodents (Penn et al., 2017). Therefore, studying the mechanisms that modulate anchoring of AMPAR at the post-synapse is of

great importance, and could reveal specific targets to address diseases and disorders caused by AMPA receptor dysfunction.

### *Nano-scale organization of the pre and post-synapse*

Recent studies, using super-resolution imaging, have revealed that important proteins at both the pre-synaptic side and the post-synaptic side are organized into nano-scale domains, or “nano-domains”. At the pre-synapse, neurotransmitter vesicle release sites, proteins involved in vesicle priming and docking, as well as adhesion proteins and calcium channels, are all reported to exist in clusters rather than diffusely across the AZ (Tang et al., 2016; Eggermann et al., 2012; Bademosi et al., 2016; Trotter et al., 2019). Most pre-synaptic proteins reported to exist in nano-domains have not been shown to exist in the same nano-domains, and many other essential pre-synaptic proteins appear to localize in a more diffuse manner across the pre-synapse. In spite of this, the nano-scale organization of many of these essential pre-synaptic proteins points to the possibility that an intricate machinery exists that targets fusion of synaptic vesicles to specific sites at the pre-synapse.

Meanwhile, at the post-synapse, PSD95, a key scaffold protein of the post-synapse, and AMPAR, the major receptors involved in fast synaptic transmission, are reported to cluster in nano-domains of the diameter of 70 nm. Moreover, nano-domains of AMPAR and PSD95 are often colocalized, indicating that AMPAR are likely clustered by the nano-domains of PSD95 (Nair et al., 2013; MacGillavry et al., 2013). NMDAR are also reported to be clustered in nano-domains (Kellermayer et al., 2018), although it is unclear if AMPAR and NMDAR nano-domains overlap. This nano-scale organization of post-synaptic receptors and scaffold proteins strikingly mirrors the organization of pre-synaptic proteins, and suggests that nano-scale domains may serve a physiological function.

Indeed, pre and post-synaptic nano-scale organization is not merely coincidental, and it has been shown that nano-scale organization is maintained across the synapse, with key adhesion proteins like Neurexin on the pre-synaptic side, and Neuroligin and Leucine-rich repeat transmembrane neuronal protein (LRRTM) on the post-synaptic side, serving to align the pre-synaptic vesicle priming and release machinery and post-synaptic receptors (Tang et al., 2016; Haas et al., 2018). Interestingly, these studies also suggested that lateral misalignment of pre and post-synaptic nano-domain sites by several nanometers could affect the strength of synaptic transmission. The nano-scale organization and alignment of pre and post-synaptic nano-domains (termed “nanocolumns”) could therefore be an essential feature of synapse function.

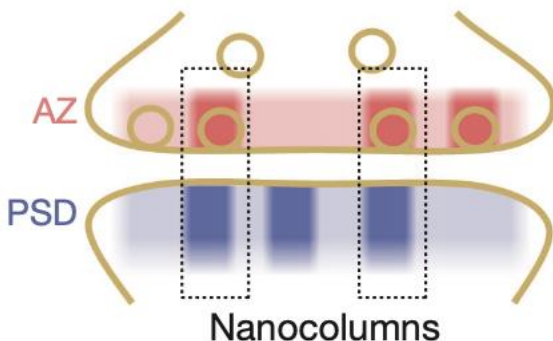


**Fig 4. Pre and post alignment across the synapse plays a role in synaptic transmission**

Pre-synaptic nano-domains at the active zone (AZ) and post-synaptic nano-domains at the post-synaptic density (PSD) align across the synapse to form “nanocolumns” (adapted from Tang et al., 2016).



## 1.2 Dynamics and regulation of the post-synapse

The synapse is a very dynamic structure. The earliest evidence of the ability of synapses to change in response to stimulation came from electrophysiology studies, in which a brief high-frequency electrical stimulation (called a tetanus) of excitatory synapses of hippocampal slices induced a long-lasting increase in synaptic strength (Lomo, 1966). The changes seen at these synapses were rapid (within minutes) and long lasting (for up to days) in response to a stimulus lasting only a second. Obviously, such precise and rapid change brought about by a brief stimulus meant that a sophisticated cellular machinery existed that could accommodate and maintain such changes in synaptic transmission. Subsequent studies revealed the role of ion channels such as AMPA and NMDA channels in synaptic transmission and potentiation respectively, and how the entry of calcium ions into the post-synapse leads to signals that can induce lasting change at the post-synapse, leading to LTP. Pre-synaptic changes were also found in response to LTP induction, although most of our molecular understanding of LTP favors post-synaptic changes (Bliss et al., 2013).

### *Dynamics of post-synaptic receptors*

It required advances in electron microscopy, light microscopy (including fluorescence imaging), and most recently, super-resolution imaging methods to establish which molecular constituents of the post-synapse changed in response to synaptic transmission, and how. The most well studied post-synaptic indicator of LTP is the number and dynamics of AMPAR. Functional AMPAR consist of four subunits, which can comprise of GluA1, GluA2, GluA3, or GluA4 subunits. It was reported that greater than 80% of AMPAR comprise of GluA1 and GluA2 hetero-tetramers (Sheng et al., 2007), but a more recent study indicates that GluA3 and GluA4 may comprise a much higher fraction of hetero-tetramers (Zhao et al., 2019). GluA1 and GluA2 can form homo-tetramers as well (Morise et al., 2019). The number of AMPAR at a synapse vary, with silent synapses having zero AMPAR (Kerchner et al., 2008), but the average synapse has about 60 AMPAR subunits (Cheng et al., 2006). AMPAR are now considered the main variable in the modulation of synaptic plasticity. AMPAR exchange between the synapse and extra-synaptic areas by diffusion as well as endocytosis and exocytosis. Endocytosis of AMPAR was thought to occur at sites located about 100-500 nm away from the PSD (Racz et al., 2004), but a very recent study using super-resolution imaging has revealed that proteins required for endocytosis are located as near as 10 nm from the PSD edge (Catsburg et al., 2022). Single-molecule studies of AMPAR showed that AMPAR exchange between the synapse and adjacent extrasynaptic membrane region rapidly by diffusion, and are transiently immobilized in a few nano-scale regions, called “nano-domains” of ~70 nm in diameter in the synapse (Nair et al., 2013; MacGillavry et al., 2013). Single molecule studies of GluA1 and GluA2 subunits report that these subunits join to form tetrameric receptors, and fall apart into trimers, dimers, and monomers, at time scales of 100-200 ms, and that most of the turnover of AMPAR between the synapse and the dendritic shaft happens by monomers diffusing in and out of synapses, while tetramers are less mobile (Morise et al., 2019). AMPAR are thus highly dynamic, and constantly exchange between synaptic and extra-synaptic regions as well as between the synaptic and the dendritic-shaft membranes. Other receptors such as NMDAR (Groc et al., 2006), Glycine receptors (Dahan et al., 2003), Gamma-amino butyric acid receptors (GABAR) (Jacob et al., 2005) have also been found to be cycling between freely diffusing and confined phases outside and inside the synapse, respectively, albeit with varying



retention durations at the post-synapse, likely due to their varying affinities for binding sites on scaffold proteins.

Synaptic adhesion proteins such as Neuroligin1 (abbreviated as Nlg1) and LRRTM2 have also been studied using super-resolution imaging techniques, showing that both Nlg1 and LRRTM2 molecules exhibit slower diffusion at synaptic sites compared to molecules in dendritic regions, and they assemble into nano-domains of the size of 80-100 nm (Chamma et al., 2016). While the dynamics of adhesion proteins and ion channels differ quantitatively, it is clear that these trans-membrane post-synaptic receptors are dynamic and diffuse in and out of the synapse, where they are retained by interactions with scaffold proteins.

### *Retention of receptors at the post-synapse*

Most of the receptors in the post-synapse bind to one particular domain that has been found to be present in the most abundant scaffold proteins- the PDZ domain (named after the proteins PSD95, Dlg1 and ZO-1). The prevailing hypothesis for the retention of receptors such as AMPAR at the synaptic plasma membrane is that “slots” made of PDZ domain binding sites can be occupied by diffusing receptors. PDZ domains exist on a number of synaptic proteins, such as PSD95, but also related proteins like PSD93, GRIP1, PICK1, etc. (Kim et al., 2004). These PDZ domains can be occupied by diffusing receptors, whose affinity for these PDZ domain “slots” can be tuned by various modifications (such as phosphorylation) induced by synaptic activity (Opazo et al., 2012).

The binding affinities of receptors like Nlg and NMDAR for their binding sites on PDZ domains are of the order of  $10^{-7}$  M as measured by in-vitro experiments using the cytoplasmic domains of these proteins (Irie et al., 1997), resulting in the presence of unbound molecules in the postsynaptic membrane that will diffuse away from the post-synapse. For longer term immobilization of synaptic receptors such as Nlg and AMPAR, a very high density of binding sites must be available to them within the area of their confinement, such that detachment of these receptors would be followed by instantaneous rebinding with an adjacent binding site. Another way that receptors may be immobilized is by multivalent binding, such that receptors contain multiple binding sites for various synaptic proteins. Indeed, NMDAR is reported to bind with Nlg1 via extracellular domain interactions, in addition to binding with PSD95 (Budreck et al., 2013). Nlg1 itself binds to Neurexin trans-synaptically with an affinity of the order of  $10^{-9}$  M (Tsetsenis et al., 2014), while also binding with PSD95, albeit at a much lower affinity (Irie et al., 1997). Retention of post-synaptic receptors might therefore be accomplished by a combination of multiple binding sites (either due to binding with multiple different protein partners, or via multiple binding domains for the same protein partner), as well as a high density of binding sites available at the post-synapse. However, this picture is that of an already assembled mature post-synapse. The initial retention of receptors at nascent post-synaptic sites may be difficult to achieve with low affinity interactions of receptors and scaffold proteins (of the order  $10^{-7}$  M). This presents a major question about how synapses are initially assembled.

The binding affinities of post-synaptic receptors (such as Nlg and AMPAR) for scaffold proteins can be modulated through phosphorylation. Phosphorylation of Nlg1 at Y782 has been shown to prevent its binding to gephyrin (an inhibitory synapse scaffold protein) (Giannone et al., 2013), and phosphorylation of Nlg1 at S839 blocks its binding with PSD95 (Jeong et al., 2019). It is likely that a dynamic equilibrium is maintained such that a majority of Nlg1 binds with PSD95 and therefore localizes to post-synapses. NMDAR are phosphorylated at multiple sites by kinases such as protein kinase A (PKA) and protein kinase C (PKC), which can modulate its channel properties, gating, as well as its interaction with PSD95 (Chen et al., 2007). The phosphorylation

of trans-membrane AMPA receptor regulatory protein  $\gamma 2$  (TARP  $\gamma 2$ , also called Stargazin), an auxiliary trans-membrane protein that links AMPAR to PSD95, at its PDZ binding domain disrupts its binding to PSD95 (Chetkovich et al., 2002). Therefore, the affinities of receptors for PDZ domains can also be dynamically tuned by modifications like phosphorylation, often in response to synaptic activity.

More recently, the discovery of liquid-liquid phase separation (LLPS) of some post-synaptic proteins, such as SynGAP, PSD95 (Zeng et al., 2016) and CaMKII (Hosokawa et al., 2021) has introduced a new concept that may help explain the assembly of scaffolding proteins as well as receptors such as ion channels and adhesion proteins in nano-scale domains at the post-synapse (LLPS will be discussed in detail in the latter part of this chapter). Even the receptors with low binding affinities with scaffolding proteins could be assembled in the post-synapse due to the very high local density of binding sites in LLPS condensates. In addition, after the binding of receptors with the scaffolding proteins, although the receptors might dissociate quickly due to low affinity, they would soon encounter another binding site, ensuring the subsequent binding to a new site before they escape the region of the LLPS condensate by lateral diffusion. Trans-membrane receptors, such as Stargazin (TARP  $\gamma 2$ , henceforth called TARP2), which help anchor AMPAR to PSD95 slots, and NMDAR, could bind with PDZ domains of PSD95 highly concentrated in the LLPS condensates (Zeng et al., 2019; Zeng et al 2018).

LLPS condensates could be also assembled or dispersed by synaptic activity induced protein modifications, allowing for dynamic modulation of receptor binding sites, and thereby receptor density/numbers at the post-synapse. Thus, it is an attractive concept to explain the assembly and regulation of post-synaptic receptors.

#### *Retention of cytoplasmic PSD proteins at the post-synapse*

Similar to receptors, post-synaptic scaffold proteins are also dynamically exchanged between the synapse and extra-synaptic pools. The most abundant and well-studied post-synaptic scaffold protein is PSD95. On average, a synapse contains about 300 PSD95 molecules (Chen et al., 2005; Sugiyama et al., 2005). This typical PDZ domain containing protein has three PDZ domains, and is known to be recruited to the post-synaptic density region by N-terminal palmitoylation (Craven et al., 1999). PSD95 is from a family of proteins called membrane-associated guanylate kinases (MAGUKs), which have homologous PDZ domains, allowing them to recruit a variety of proteins that can interact with the PDZ domains, like Nlg1, TARPs, NMDAR, etc. as well as providing redundancy. The dynamics of PSD95 molecules within single synapses in-vivo were studied by Gray et al. (Gray et al., 2006), who found that photoactivated PSD95 turned over in time scales of 30-100 min, depending on the age of the animal and size of the PSD, whereas a control molecule, photoactivated GFP, turned over 4,000-10,000 times faster, in 0.47 s. PSD95 is therefore largely retained at the synapse by interactions with PSD proteins instead of spine geometry. A different study using mVenus-tagged PSD95 knock-in mice found a much slower turnover of PSD95, with only about 20% PSD95 turnover in 60 min. Other scaffold proteins have been studied with similar experiments, albeit mostly in primary hippocampal neurons. These studies provide a range of retention times, but almost all scaffold proteins studied have a large fraction of molecules that are bound to the synapse, and retention times of 10-100 min (Specht et al., 2008). While PSDs themselves are structurally intact for days (Okabe et al., 1999), the scaffold proteins that make up the majority of the molar mass of PSDs turn over at much faster time scales.

### *PSD95 clustering at the post-synapse*

How are scaffold proteins themselves retained at the synapse? While there is a lot of evidence for the direct binding of PSD95 to cytoplasmic tails of various trans-membrane receptors, and while such interactions could be an important mechanism for PSD95 retention into the dense PSD, direct evidence of PSD95 forming clusters by itself is scarce. It was shown that the N-terminal homophilic interactions of PSD95 can induce dimerization and clustering (Hsueh et al., 1999; Xu et al., 2008). Xu et al. showed that the N-terminal 32 amino acids of PSD95 can coimmunoprecipitate full-length PSD95 in HEK293 cells. It is therefore assumed that N-terminal interactions somehow induce dimerization, and perhaps even oligomerization of PSD95. There is however the possibility that even if N-terminal homophilic interactions of PSD95 exist, they may be too weak to induce clustering at relatively low concentrations. If PSD95 homophilic interactions are indeed weak, it would then require a different mechanism for the initial recruitment and clustering of PSD95 to occur in the early phases of synapse formation, when scaffold components are diffusely present in the dendrite and no spines have formed.

### *Liquid-liquid phase separation as a biophysical mechanism of protein clustering*

However, a promising theory that could be the mechanism for the formation of synaptic scaffold protein clusters has been proposed. PSD95 was shown to recruit SynGAP and other post-synaptic proteins to form dense condensates due to liquid-liquid phase-separation (LLPS) (Zeng et al., 2016; Zeng et al., 2018). In this phenomenon, molecules of proteins or nucleic acids in solution separate into a dense phase, different from their soluble phase, much like the separation of oil droplets in water, under favorable environmental conditions. Molecules in the dense phase constantly exchange with molecules in the soluble phase. Importantly, LLPS can be tuned or regulated by environmental conditions such as pH, or even by modifications that change the structure of the protein, such as phosphorylation.

In subsequent studies, multi-valent interactions of a mixture of synaptic proteins like PSD95, GKAP, Shank3, and SynGAP and the C-terminal tails of receptors like NMDAR subunits were shown to lead to PSD-like dense assemblies via liquid-liquid phase separation, or LLPS (Zeng et al., 2018), as shown in Fig 5. It is an appealing idea that provides a biophysical explanation for the dense clustering of synaptic scaffolds at the post synapse. Fluorescence recovery after photobleaching (FRAP) experiments of these condensates in-vitro, shown in Fig 6, reveal that up to 50% of PSD95 in condensates exchanges with the bulk molecules after 4 min (Zeng et al., 2018), suggesting that these condensates have a “hydrogel” characteristic. These data do not match the data observed from in-vivo FRAP experiments of PSD95 previously discussed, likely due to the widely different experimental platform of in-vitro experiments and in-vivo conditions- FRAP of a portion of a protein condensate in-vitro would show faster recovery due to proteins being unconfined and having an almost unlimited availability in solution. Moreover, the study of Zeng et al., used fragments of various post-synaptic proteins at relatively high concentrations of up to 20  $\mu$ M each. Nevertheless, the recruitment of PSD95 and other scaffolds into “hydrogel” like LLPS condensates could be one explanation for the relatively slow exchange rate of PSD95 in neuronal spines.

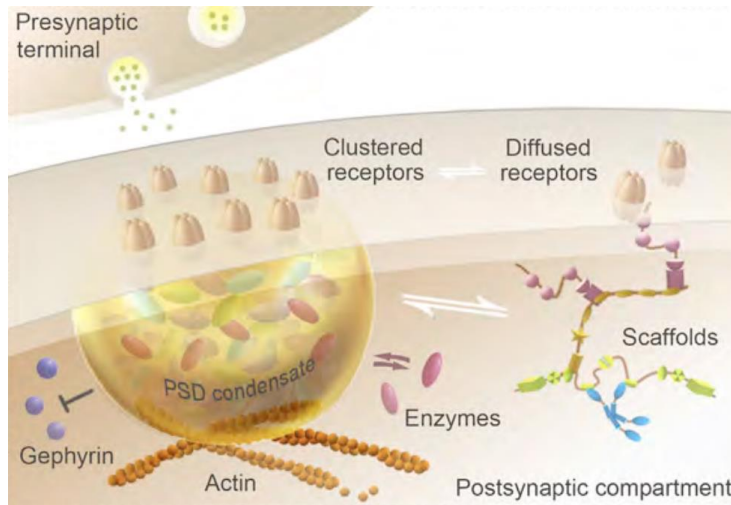


**Fig 5. Liquid-liquid phase separation may be a mechanism for protein clustering at the post-synapse**

Liquid-liquid phase separation of key post-synaptic proteins to form condensates could help recruit trans-membrane receptors as well as cytoskeletal proteins like actin, to the post-synapse, as proposed by Zeng et al. (adapted from Zeng et al., 2018).

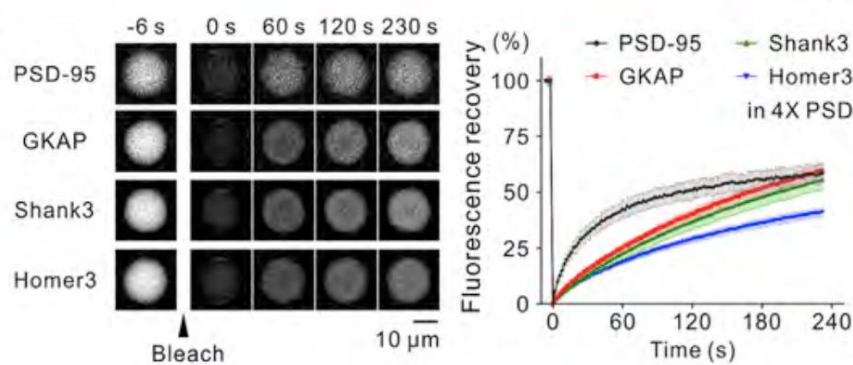


**Fig 6. LLPS condensates of post-synaptic proteins behave as a “hydrogel”**

FRAP assay of LLPS condensates containing key post-synaptic scaffold proteins like PSD95, GKAP, etc. show limited recovery, suggesting a “hydrogel” nature of these condensates.

### *PSD95 and SynGAP*

PSD95 has three PDZ domains that can bind with various receptors, such as Neuroligins, AMPAR, NMDAR, etc. At the N-terminus, PSD95 has two cysteine residues that can be palmitoylated. The bound palmitoyl chains help bring PSD95 to the PSD by their affinity to the plasma membrane (Sturgill et al., 2009). PSD95 interacts with other abundant post-synaptic cytoplasmic proteins, such as GKAP (Kim et al., 1997) and SynGAP (Kim et al., 1998), with its C-terminal Src-homology-3 (SH3) domain and guanylate kinase (GK) domains. It was proposed that PSD95 molecules can form dimers or oligomers due to N-terminal interactions (Xu et al., 2008). Therefore, PSD95 was generally considered to form clusters at the post-synaptic plasma membrane through multivalent interactions with trans-membrane receptors, other scaffold proteins, as well as homo-dimerization/oligomerization. With the report that PSD95 and SynGAP could

form LLPS condensates in vitro (Zeng et al., 2016), a new mechanism, i.e., multivalent interactions leading to LLPS, is being postulated as the biophysical mechanism of PSD95 clustering at the post-synapse.



**Fig 7. Tertiary protein structure of PSD95**

PSD95 has three PDZ (named after **P**SD95, **D**lg, and **Z**o-1 protein) domains, an SH3 (Src-homology-3) domain and a GK (guanylate kinase) domain.

SynGAP is an abundant synaptic protein that was discovered in 1998 as a GTPase activating protein (GAP) in the neuronal synapse (Chen et al., 1998; Kim et al., 1998). Since SynGAP is present at similar copy numbers at the PSD as PSD95, it was suspected that SynGAP may also play a structural role at the post-synapse. The study by Zeng et al. (2016) hinted at the role of SynGAP as a structural component of the post-synaptic density, when they showed that PSD95 and SynGAP can form LLPS condensates in-vitro.

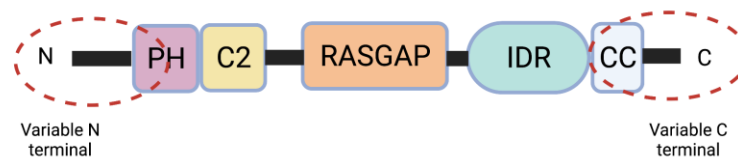


**Fig 8. Tertiary protein structure of SynGAP**

The N-terminal region, before the pleckstrin homology (PH) domain and the C-terminal region after the coiled-coil (CC) domain are often variable in different isoforms. The C2 domain, the RasGAP domain, and the IDR (intrinsically disordered region) are unchanged between isoforms.

SynGAP has various isoforms, which result from different transcription start sites and alternative splicing at the N and C terminal ends of SynGAP, as shown in Fig 9. The canonical isoform, which contains a PDZ Binding Motif (referred to as PBM) that enables it to interact with PSD95, is called the  $\alpha 1$  isoform. Since the study of Zeng et al. showed that PSD95 binding is essential to induce LLPS condensates with SynGAP, it is also assumed that only the  $\alpha 1$  isoform of SynGAP containing the PBM can form phase separated condensates. Indeed, a subsequent study looking at the role of different isoforms of SynGAP in synaptic plasticity and dendrite development (Araki et al., 2020) implied the same, using biochemical and live cell experiments of SynGAP isoforms with full length PSD95.

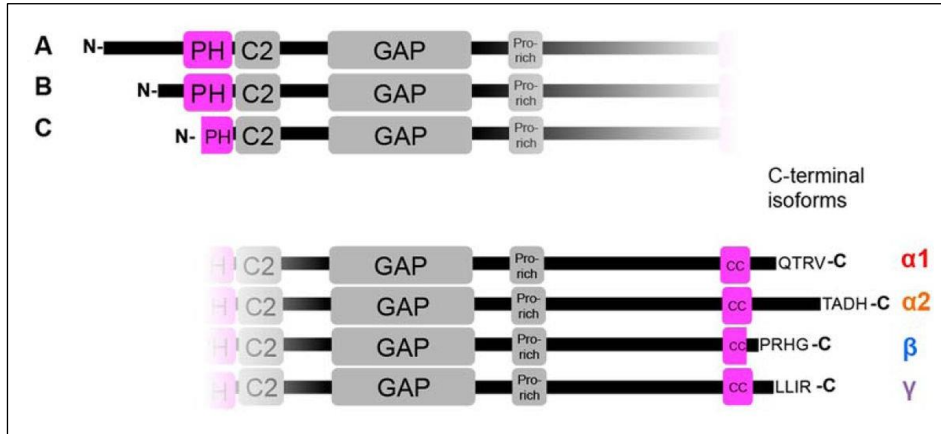


**Fig 9. SynGAP has various isoforms**

N and C terminal modifications of SynGAP result in different isoforms (from Gamache et al., 2020). Note the C terminal isoform α1 is the only one with the ‘QTRV’ PDZ binding motif (PBM).

The study of Zeng et al. (2016), using fragments of PSD95 and SynGAP in-vitro, reports that PSD95 and SynGAP form condensates by LLPS. The study provides crystallographic evidence as well as the data using isothermal calorimetry to show that SynGAP forms trimers by interactions in the C-terminal CC domain, and that SynGAP’s CC domain and C-terminal PDZ binding motif (PBM) interact with PSD95’s PDZ3-SH3-GK (PSG) domains to form LLPS condensates.

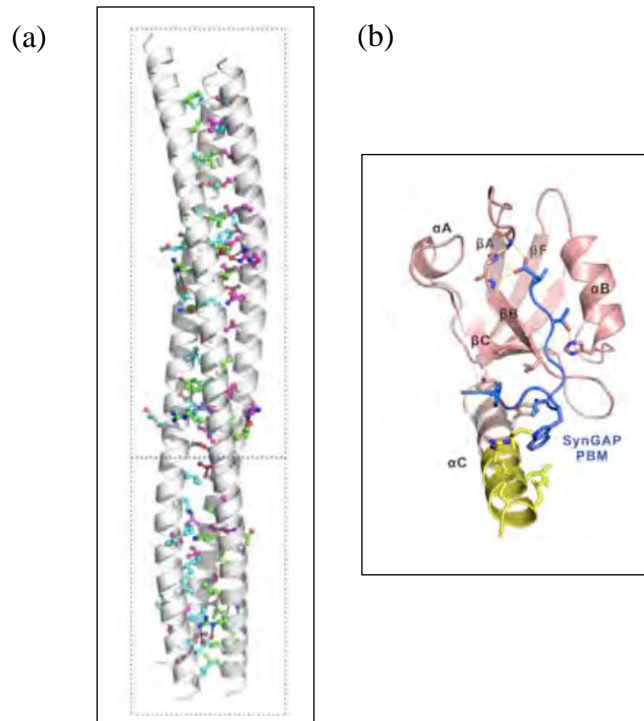


**Fig 10. SynGAP forms trimers and binds with PSD95 via the PBM at its C-terminus**

(a) The crystal structure showing the CC parallel trimer of SynGAP, showing the CC regions of each molecule in the trimer and the amino acid residues responsible for charge interactions (from Zeng et al., 2016).

(b) The crystal structure showing the interactions between SynGAP PBM and PSD95 PDZ3-C region (from Zeng et al., 2016).

1.3 Problem statement

The reports showing LLPS of post-synaptic proteins such as PSD95 used relatively high concentrations of proteins in-vitro (20-50  $\mu\text{M}$ ; Zeng et al., 2018). The concentrations of the most abundant cytoplasmic PSD proteins, such as PSD95 and SynGAP, are on the order of 1 to 10  $\mu\text{M}$  in the neuronal spine (assuming spine volumes between 0.1 - 0.01  $\mu\text{m}^3$ , and the number of molecules of PSD95, SynGAP and other abundant PSD proteins between 60 and 600 per spine, as estimated by Sugiyama et al., 2005). Local concentrations at the PSD, in the volume adjacent to the synaptic plasma membrane, are likely to be much higher, and thus LLPS condensates could exist at concentrations of  $>10 \mu\text{M}$  at the PSD. However, in the initial period of synapse formation, before the existence of a spine, the local concentration of scaffold proteins at the dendritic areas might be much lower. Therefore, several outstanding questions remain regarding the initial recruitment and assembly of PSD95 at the post-synapse. These can be summarized as:

- Does PSD95 cluster at relatively lower concentrations ( $<1 \mu\text{M}$ ) in a live cell system?
- If PSD95 does not cluster by itself, how can it be recruited into clusters at lower concentrations?
- Could the PSD95 and SynGAP LLPS (previously reported using small fragments of each protein) be replicated in live cells, and could LLPS be the way that PSD95 gets assembled at the post-synapse?
- If so, what are the key determinants of LLPS mediated assembly of PSD95?

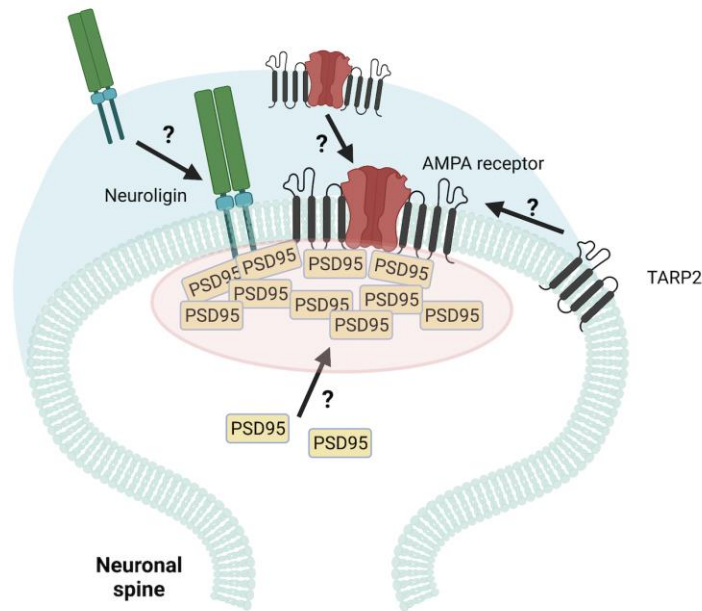


**Fig 11. Outstanding questions about the assembly of the post-synapse:**

How are PSD95 molecules assembled at the post-synapse? Is PSD95 able to cluster by itself at relatively low number densities? How do receptors such as Nlg and AMPAR get recruited and retained at the synapse, when they have relatively low binding affinities for PDZ domains?

Another important outstanding question is how receptors such as Nlg1 and AMPAR are assembled at the post-synapse for long periods, even though they have relatively low binding affinities for PDZ domains on PSD95 (of the order of  $10^{-7}$  M). A hint was provided by a study that found that dimerization of Nlg1 is essential for proper synaptic transmission (Shipman et al., 2012). Over-expression of dimerization-null Nlg1 and Nlg3 had a remarkably lowered ability to potentiate post-synaptic currents compared to wild-type Nlg1 or Nlg3. This suggests that the dimerized state of Nlg plays an important role in its function. Taking this concept further, oligomerization dependent capture of receptors at the post-synapse may be a universal mechanism affecting various oligomerized receptors.

- Could it be that dimers of Nlg, by virtue of having two binding sites for PDZ domains instead of one, are retained much longer at the post-synapse? If this hypothesis was true, could the clustering of Nlg by antibodies, mimicking the effect of clustering induced by binding of pre-synaptic Neurexin, further increase its retention at the post-synapse?
- Further, is the selective retention of receptors based on their oligomerized state a universal concept? How does the retention of oligomerized receptors, such as the tetrameric AMPAR, compare to that of a monomer or a dimer version?

To address these questions, I set out to replicate the post-synapse assembly in non-neuronal cells, and endeavored to produce a minimal PSD, such that the assembly of PSD95 into PSD-like clusters, as well as the retention of post-synaptic receptors such as Nlg and AMPAR could be



studied. The results of my experiments are detailed in the following two chapters, and summarized in the discussion chapter.

## Chapter 2. Liquid-liquid phase separation of SynGAP and assembly of PSD95 as clients in SynGAP condensates

### 2.1 Results

#### 2.1.1 SynGAP forms LLPS condensates by itself, and recruits PSD95 as a client

To reveal how PSD95 can be assembled and recruited to the post-synapse, I decided to replicate the results of Zeng et al. (2016), which showed that when the fragments of PSD95 and SynGAP are mixed, they can form LLPS condensates, in live cells. As the first test, I expressed the canonical full length SynGAP (referred to as SynGAP 'QTRV') and its full length  $\alpha 2$  isoform which lacks the PBM (referred to as SynGAP 'TADH') with the mEGFP tag at their N-termini, in L cells, which express neither SynGAP nor PSD95. Unexpectedly from the results of Zeng et al. (2016), this initial experiment showed the formation of clear condensates of both SynGAP proteins at expression levels as low as 0.5  $\mu\text{M}$ , in the absence of PSD95. It is important to note that the 'TADH' isoform of SynGAP, which does not bind to PSD95, forms LLPS condensates just as effectively as the canonical 'QTRV' isoform. PSD95 when expressed by itself does not form condensates. These results are contrary to the previous conclusions, obtained by using the protein fragments, that SynGAP requires the PBM and its binding to PSD95 to form LLPS condensates.

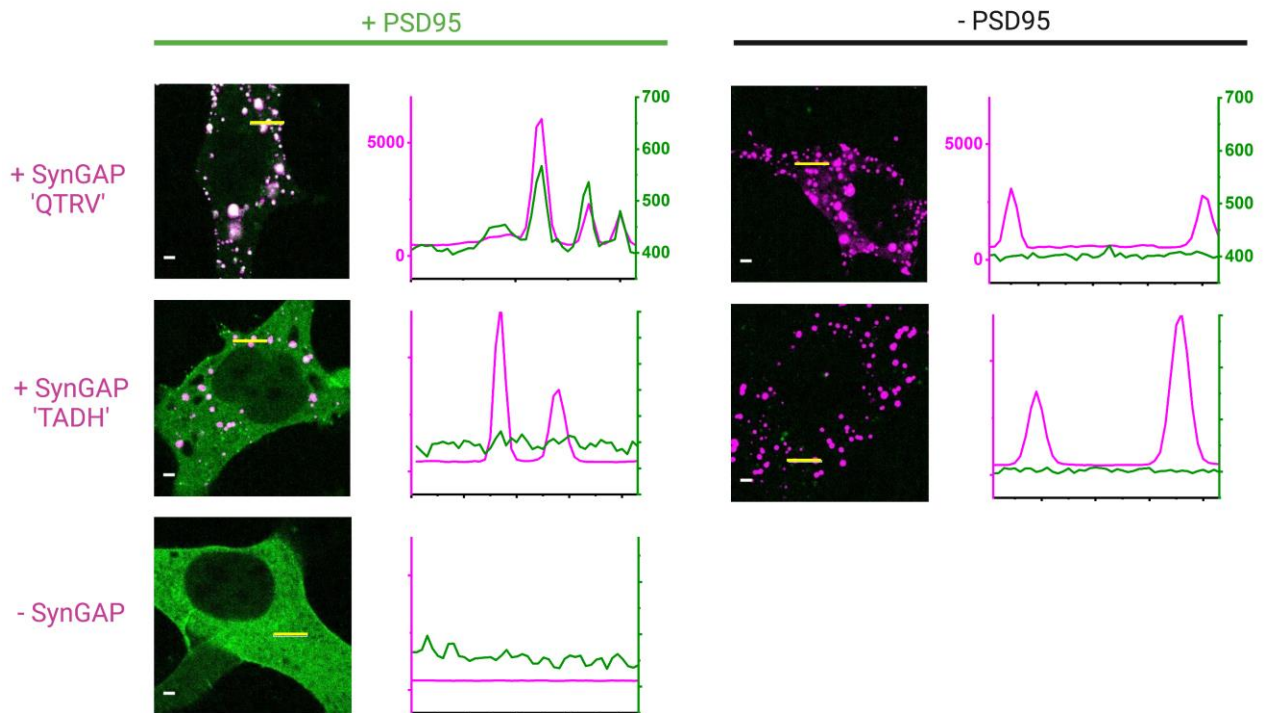


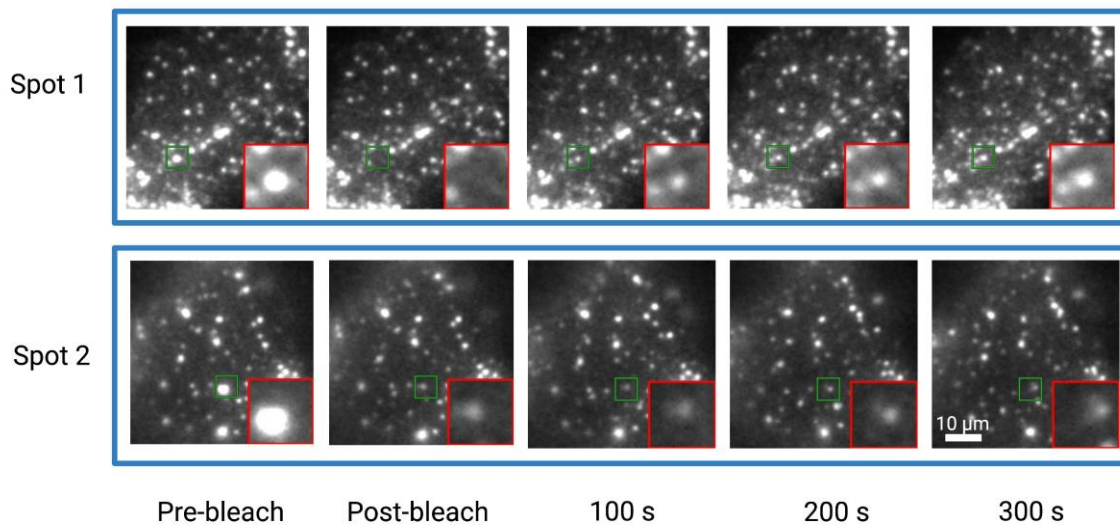
**Fig 12. SynGAP can form LLPS condensates by itself in live cells, and recruits PSD95**  
L cells were transfected with 1  $\mu\text{g}$  cDNA encoding either of the SynGAP isoforms and/or 1  $\mu\text{g}$  cDNA encoding PSD95 (using Effectene reagent), and imaged with confocal microscopy two days after transfection.

Right panels show isoforms mEGFP-SynGAP ‘QTRV’ and mEGFP-SynGAP ‘TADH’ can both form LLPS condensates, even in the absence of PSD95, when expressed in L cells. Left panels show that mEGFP-SynGAP ‘QTRV’ can recruit PSD95-Halo (labelled by incubating with 20 nM TMR-Halo ligand for 30 min) into LLPS condensates (top left), but mEGFP-SynGAP ‘TADH’, lacking the PDZ binding motif, cannot. PSD95-Halo by itself does not form LLPS condensates (bottom left) (Scale bar = 1  $\mu$ m).

When PSD95 (at the C-terminus tagged with the Halo-tag protein) is co-expressed with SynGAP, the ‘QTRV’ isoform of SynGAP recruits PSD95 into the condensates. However, this does not happen with the ‘TADH’ isoform of SynGAP. This shows that while PSD95 is not required for SynGAP LLPS condensate formation, only the ‘QTRV’ isoform, which contains the PBM, can recruit PSD95 into the condensates.

Fluorescence recovery after photobleaching (FRAP) experiments on SynGAP condensates show that SynGAP molecules in the condensates can exchange with those in the cytoplasm, but only partially, up to 25% in 300 s, as shown in Fig 13. Meanwhile, Zeng et al. (2016) employed the CC domain fragment containing the PDZ binding motif (CC-PBM), and PSD95 fragment consisting of the PDZ3-SH3-GK domains, to form condensates *in vitro*, which exhibited the FRAP recovery up to 50% in 120 s. Therefore, these results suggest that the condensates made of the full-length version of SynGAP without PSD95 in live cells behave substantially differently from the condensates made of the CC domain fragments and PSD95 fragments *in vitro*. This hints at a “hydrogel” nature of SynGAP condensates, which has been observed particularly for proteins containing long intrinsically disordered regions (IDRs), such as Nsp1 FG repeat domains, which also show a FRAP recovery of ~10-20% after 3 min (Frey et al., 2006).

(a)



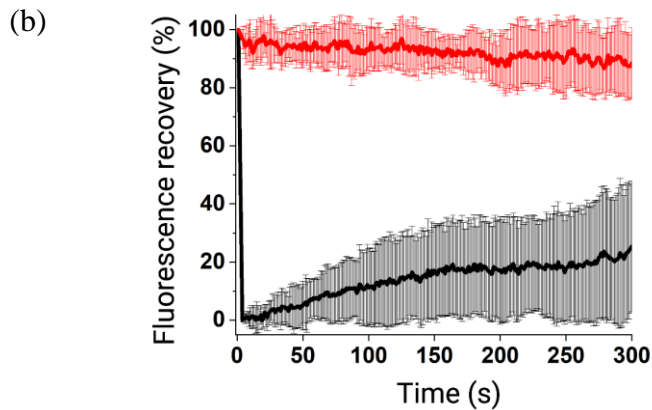


### Fig 13. Fluorescence recovery after photobleaching (FRAP) of SynGAP condensates

L cells were transfected with 1 $\mu$ g cDNA encoding mEGFP-SynGAP ‘QTRV’ (using Effectene reagent), and imaged with TIRF microscopy two days after transfection. Photobleaching was carried out with a focused 488-nm laser beam.

(a) Fluorescence recovery after photobleaching of two spots in mEGFP-SynGAP ‘QTRV’ expressing L cells (insets show zoomed-in view of the image shown by green squares), showing relatively slow recovery (top panels), and relatively quick recovery (bottom panels). (Scale bar = 5  $\mu$ m)

(b) Fluorescence recovery after photobleaching of SynGAP LLPS condensates in L cells (6 spots, from 6 cells; black curve), showing that on average SynGAP LLPS condensates exchange  $\approx$ 25% of their molecules after 300 s. Red curve shows the average photobleaching rate of unbleached spots (11 spots, 6 cells).

#### 2.1.2 Revealing the protein domains responsible for LLPS of SynGAP

To quantify SynGAP condensate formation and make it comparable between isoforms and mutants, I used confocal microscopy to image 2- $\mu$ m thick slices of the cytoplasmic area about 5  $\mu$ m inside the cell (from the basal plasma membrane), of L cells expressing mEGFP-SynGAP. I then used *ilastik*, a machine-learning image processing tool (Berg et al., 2019), to quantify the total cluster intensity within the 2- $\mu$ m deep image of the cell and normalized this with the total area of the cell being imaged. I call this metric the “clustering coefficient”. The clustering coefficient of SynGAP (in each cell) is plotted against the concentration of SynGAP (in each cell), as shown in Fig 14. The average concentration of SynGAP in each cell was measured as the average cytoplasmic pixel intensity and calibrated to the average pixel intensity of titrated amounts of EGFP in solution (Fig 15).

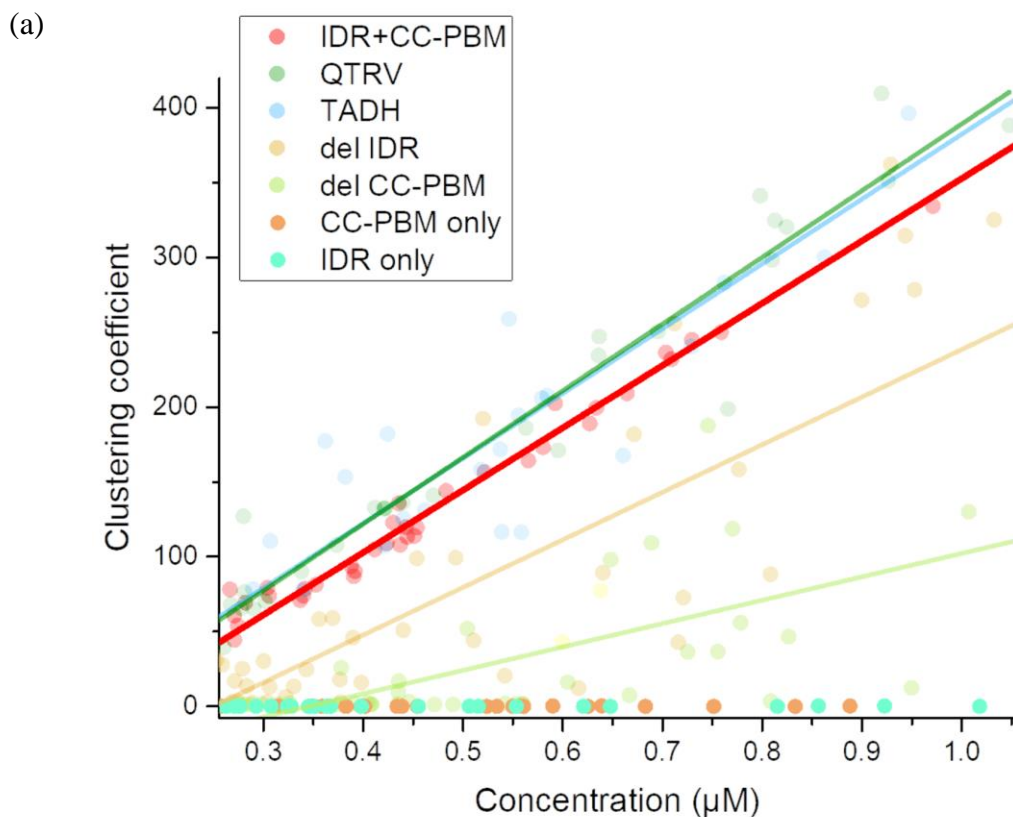
Both isoforms of SynGAP, SynGAP-QTRV containing the PBM and SynGAP-TADH lacking the PBM, form condensates. Their concentration dependences of clustering coefficients are virtually the same, further supporting that PSD95 is not required for the LLPS of either isoform of SynGAP.

Next, I examined the concentration dependence of clustering coefficients for deletion mutants of SynGAP-QTRV: those lacking the IDR or the CC + PBM domain, which are likely to be responsible for the formation of large condensates. The IDR is the 409 amino-acid-long region,

which could mediate multivalent interactions between SynGAP molecules. The CC domain induces SynGAP trimers, which might be essential for the formation of LLPS condensates by enhancing the weak multivalent interactions mediated by the IDR. Both mutants exhibited a distinct impairment in condensate formation, as shown in Fig 14. The threshold concentrations for the condensate formation was increased to 0.24 and 0.33  $\mu\text{M}$  for the mutant missing the IDR (referred to as mEGFP-SynGAP del IDR) and that missing the CC-PBM domain (referred to as mEGFP-SynGAP del CC-PBM) from  $<0.05 \mu\text{M}$  for the full-length SynGAPs. The slopes were decreased to 69% and 34% of that of the full length SynGAP for the del IDR and del CC-PBM mutants, respectively.

As the next step, I investigated whether the IDR and CC domains by themselves could form condensates (referred to as mEGFP-SynGAP-IDR only and mEGFP-SynGAP CC-PBM only, respectively). Both failed to form LLPS condensates at concentrations up to 1  $\mu\text{M}$ . Taken together, these results suggest that both the CC domain and IDR are required for SynGAP to form proper LLPS condensates.

To unequivocally examine this possibility, I expressed a SynGAP mutant containing only the IDR and CC+PBM domain, without its N-terminal PH, C2, and RasGAP domains (called mEGFP-SynGAP IDR+CC-PBM). This mutant exhibited the clustering coefficient-concentration plots only slightly lower than the full length SynGAP (Fig 14), showing that these two domains are basically responsible for the concentration dependent LLPS condensate formation property of SynGAP. Meanwhile, the slight reduction suggests that the N-terminal region of SynGAP, containing the PH, C2, and GAP domains, could also play a small role in SynGAP LLPS.



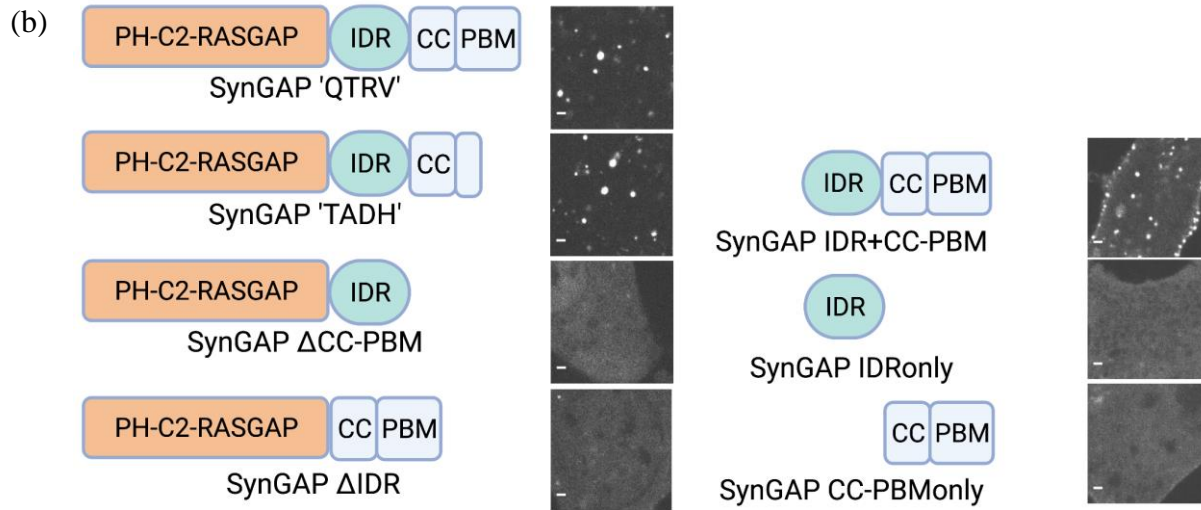


**Fig 14. SynGAP undergoes concentration dependent LLPS in live cells, mediated by its IDR and coiled-coil (CC+ PBM) domain**

L cells were transfected with  $1\mu\text{g}$  cDNA encoding each respective mEGFP-SynGAP construct (using Effectene reagent), and imaged with confocal microscopy two days after transfection.

(a) Concentration dependent LLPS of all SynGAP constructs, in L cells. The clustering coefficient is plotted as a function of the overall SynGAP concentration in the cytoplasm, with each dot representing a cell analyzed. mEGFP-SynGAP IDR only and mEGFP-SynGAP CC-PBM only could not form LLPS condensates at all in the concentration range employed here, as shown by the CC-PBM only dots (dark orange) and IDR only dots (cyan) at the bottom of the graph.

(b) Schematic of all SynGAP constructs used in the experiment, with the images of the typical cells expressing the respective SynGAP construct at approximately  $0.3\mu\text{M}$  (Scale bar =  $1\mu\text{m}$ ).



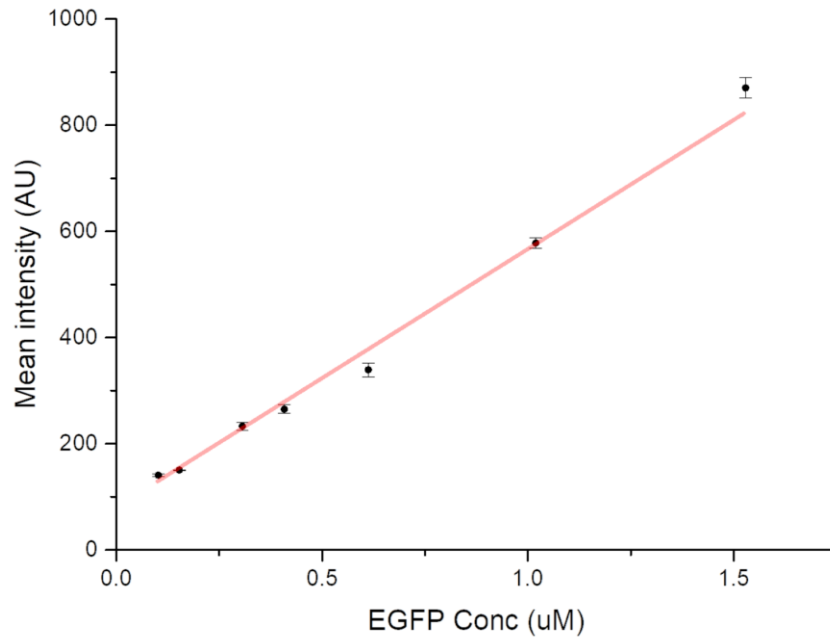


**Fig 15. Calibration of the intensity of mEGFP-SynGAP constructs to that of known concentrations of EGFP.**

Purified EGFP in solutions in the glass-bottom cell culture dishes were imaged using confocal microscopy operated under the same conditions employed for observing mEGFP tagged SynGAP expressed in L cells. The mean ( $\pm$  SEM) pixel intensities were plotted as a function of the EGFP concentration, and fitted with a linear function. Each dot represents the mean of at least three independent titrations of the EGFP solution and intensity measurements. The best-fit linear function was used to evaluate the mEGFP-SynGAP concentrations in the cytoplasm of live L cells.

### 2.1.3 SynGAP LLPS condensates are recruited to the plasma membrane

In neurons, the SynGAP condensates would be recruited to the PM via PSD95, whereas PSD95 association with the plasma membrane in the post-synaptic domain would be enhanced by the interaction with the transmembrane proteins in the synapse. As one of the key proteins involved in synapse formation with a capability of binding to PSD95, we considered the transmembrane adhesion protein Neuroligin (Nlg). Thus, I tested the hypothesis that Nlg1 can bring SynGAP condensates to the plasma membrane. I co-expressed PSD95 and SynGAP in L cells, with or without Nlg1 expression. To switch on the expression of SynGAP, I expressed it in a vector designed to have inducible expression with the addition of doxycycline (Shibata et al., 2012). SynGAP condensates were imaged at the basal PM as well as at 2  $\mu$ m above the PM in the cytoplasm, 3 h after doxycycline addition to induce SynGAP expression. SynGAP condensates were imaged with confocal microscopy. Clusters of SynGAP at the basal PM as well as in the cytoplasm were counted, and the fraction of clusters at the basal PM was estimated, as shown in Fig. 16.

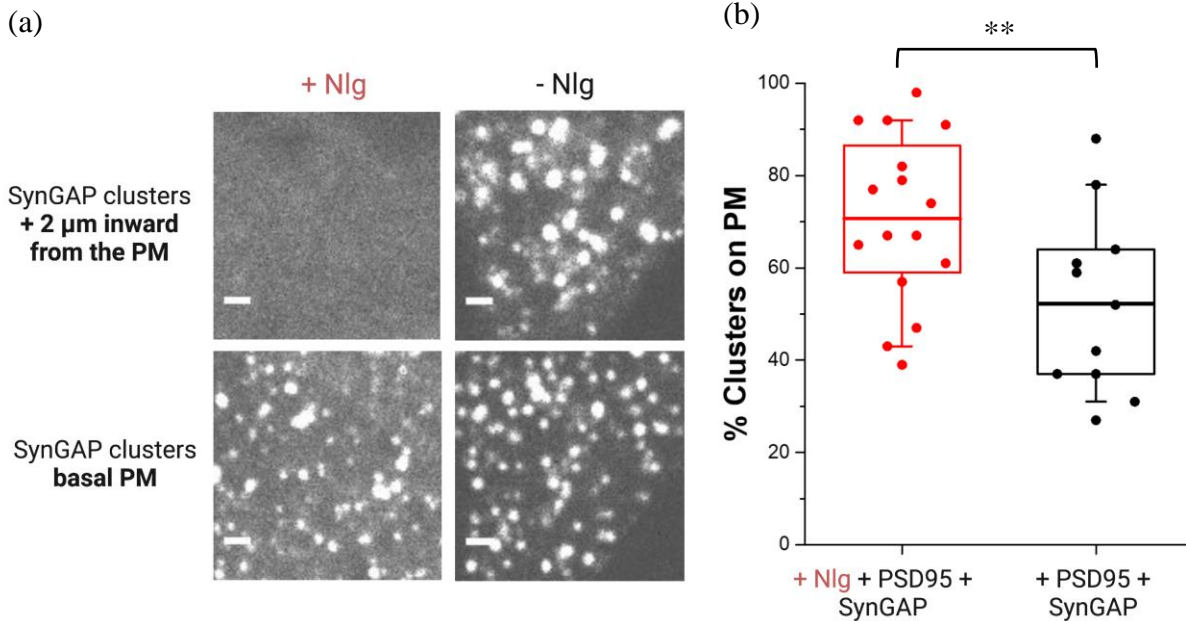


### Fig 16. Nlg1 recruits SynGAP condensates to the plasma membrane via PSD95

L cells stably expressing Nlg1 were transfected with 1 $\mu$ g cDNA encoding mEGFP-SynGAP ‘QTRV’ and PSD95-Halo each (using Effectene reagent), and imaged with confocal microscopy two days after transfection.

(a) Left panels show SynGAP clusters 2  $\mu$ m inside the cell from the basal plasma membrane versus those at the basal plasma membrane, in the presence of Nlg1 and PSD95. Right panels show SynGAP clusters 2  $\mu$ m inside the cell versus at the basal plasma membrane, with only PSD95 and without the presence of Nlg1. (Scale bar = 1  $\mu$ m)

(b) Percentage of SynGAP clusters at the basal plasma membrane (estimated as: clusters on PM/total clusters within 2  $\mu$ m slices), in the presence of Nlg1 expression (n = 16 cells; red) and in the absence of Nlg1 expression (n = 11 cells; black). Bars, boxes, and whiskers indicate mean values, inter-quartile range (25% - 75%), and 10% - 90% range, respectively. Statistical P-values: \*p<0.05, \*\*p<0.01, \*\*\*p<0.001.

Nlg1 greatly enhances the recruitment of SynGAP condensates to the plasma membrane. By doing so, Nlg1 could have an important function in the formation of the post-synapse. The above result is the first mechanistic evidence of the so called “synapse organizer” role of Nlg1, which was observed when pre-synaptic Neurexin multimers could induce the assembly of post-synapse like structures via Nlg1 (Mondin et al., 2011), and has since been observed in various other proteins such as SynCAM and LRRTM (Ribic et al., 2019).

#### 2.1.4 SynGAP LLPS condensates are dissolved by CaMKII

CaMKII is known to phosphorylate several residues in the IDR of SynGAP (Dosemeci et al., 2010; Araki et al., 2015), some of which are reported to cause SynGAP to be dispersed from the spine (Araki et al., 2015). These results lead me to hypothesize that synaptic activity induced CaMKII activation controls the dissolution and reformation of SynGAP condensates, allowing the receptors immobilized within SynGAP LLPS condensates, such as Nlg1 and AMPAR, to be



released. The dissolution of SynGAP condensates would also reduce SynGAP's ability to recruit PSD95, since PSD95 participates in SynGAP LLPS condensates as a "client". To test this hypothesis, I expressed full length Halo-SynGAP with mEGFP-CaMKII in L cells. Co-expression with CaMKII clearly dissolved SynGAP LLPS condensates, at the same expression levels, as shown in Fig 17.

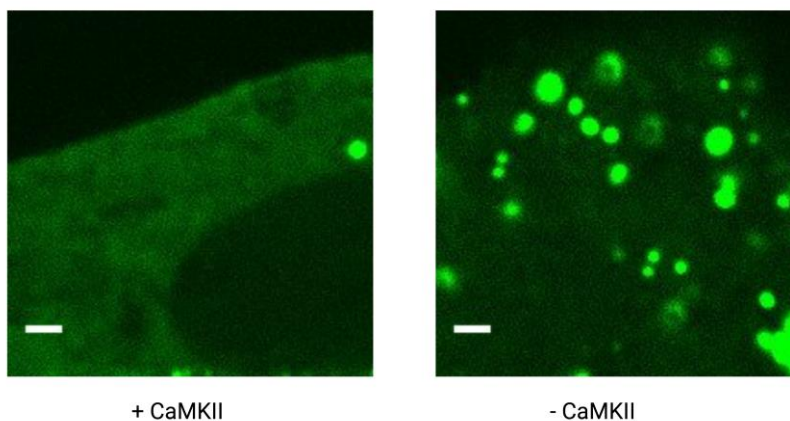


**Fig 17. CaMKII dissolves SynGAP condensates in live cells**

L cells were transfected with 1  $\mu$ g cDNA encoding Halo-SynGAP 'QTRV' (and mEGFP-CaMKII each) (using Effectene reagent), and imaged with confocal microscopy two days after transfection. CaMKII co-expressed in L cells with SynGAP (left) results in dissolution of SynGAP LLPS condensates, while SynGAP expressed without CaMKII (right) readily forms LLPS condensates, at similar expression levels of SynGAP. Scale bar = 1  $\mu$ m.

## 2.2 Summary and discussion

The results described in this chapter show that full-length SynGAP forms LLPS condensates on its own. Moreover, the LLPS of SynGAP requires both the C-terminal CC domain and the IDR, but not the PSD95 binding site. These results do not match the previous conclusions obtained by using protein fragments in vitro, which suggested that only SynGAP 'QTRV' isoform can form LLPS condensates, and it can only do so by binding with PSD95 (Zeng et al., 2016; Araki et al., 2020). The study of Zeng et al. (2016) used partial sequences of SynGAP (157 out of 1,308 amino acids) and PSD95 (416 out of 724 amino acids) in vitro, at an extremely high concentration of 100  $\mu$ M each, to observe LLPS. This made the applicability of the conclusions to live neurons doubtful.

Another important finding from my experiments is the role of SynGAP's large intrinsically disordered region (IDR) in its LLPS. IDRs are domains of a protein that although functional, do not fold into ordered and stable three-dimensional structures. IDRs instead are "dynamically disordered", meaning that they rapidly fluctuate in structure all the time. IDRs within proteins, and even proteins that are fully disordered (called intrinsically disordered proteins, or IDPs), are found among eukaryotic proteins and especially involved in cell signaling and regulation functions (Wright et al., 2014). IDRs can mediate multi-domain interactions between proteins, and within the structure of a protein, often due to low affinity polar, electrostatic, or hydrophobic interactions.

These can be tuned dynamically by post-translational modifications like phosphorylation (Brangwynne et al., 2015). Specifically in the context of synaptic function, IDRs have been shown to be involved in LLPS of Synapsin at the pre-synapse, and phosphorylation of the IDR of Synapsin by CaMKII can disperse these LLPS condensates (Milovanovic et al., 2018). My results show that SynGAP's IDR is required for proper LLPS and clustering, and that the CC domain itself is not sufficient. This again contradicts the results of Zeng et al. (2016).

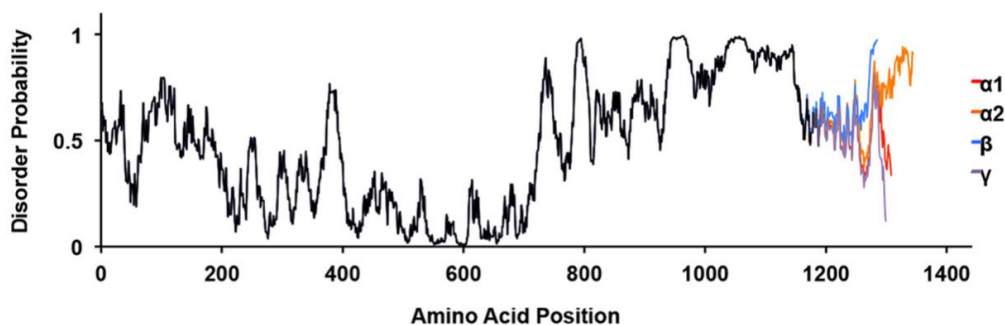


**Fig 18. Roughly 30% of SynGAP's amino acid sequence consists of an intrinsically disordered region (IDR)**

Intrinsic disorder probability at various parts of the amino-acid sequence of SynGAP, calculated using IUPred2A. A large IDR exists at amino acids ~800 to ~1150. The C-terminal end shows the disorder probabilities for various isoforms of SynGAP, with  $\alpha 1$  being the canonical isoform containing the PDZ binding motif (adapted from Gamache et al., 2020).

I also show that, remarkably, SynGAP can form LLPS condensates at concentrations of less than 1  $\mu\text{M}$  in live cells. Most studies showing LLPS of synaptic proteins have used concentrations of proteins higher by at least a factor of 10, and in the case of the study of Zeng et al. (2016), by a factor of 100. With its ability to form LLPS condensates at such low concentrations in live cells, SynGAP could be a good candidate for the initial recruitment of essential post-synapse proteins such as PSD95 during synapse formation. By recruiting multivalent proteins such as PSD95 into LLPS condensates, SynGAP could dramatically increase the local density of binding sites available for receptors, and be the nucleating factor for the formation of the mature post-synapse. Such condensates could offer a very high local density of binding sites for immobilizing post-synaptic receptors, including Nlg1 and AMPARs. Moreover, LLPS condensates could be dynamically regulated to induce retention or dispersion of receptors and signaling molecules as needed. I show that CaMKII expression dissolves SynGAP LLPS condensates. It is likely that a dynamic equilibrium exists at the synapse, such that SynGAP condensates are regulated in size and “liquidity” by phosphorylation by CaMKII. Synaptic activity induced activation of CaMKII could thus be a major regulatory mechanism of SynGAP at the post-synapse.

LLPS condensates of SynGAP can be effectively recruited to the plasma membrane by Nlg1, which can bind to PSD95 molecules present in SynGAP condensates. This result suggests the mechanism by which Nlg1 could work as a “synaptic organizer”- Nlg1 could induce a positive feedback loop by recruiting SynGAP condensates to the plasma membrane, which in turn can recruit more SynGAP and PSD95 molecules, which in turn can assemble even more Nlg1 and other synaptic receptors. This hypothesis is the basis for the next chapter, which discusses the

ability of SynGAP LLPS condensates to recruit receptors such as Nlg1 and AMPAR (linked to TARP2).

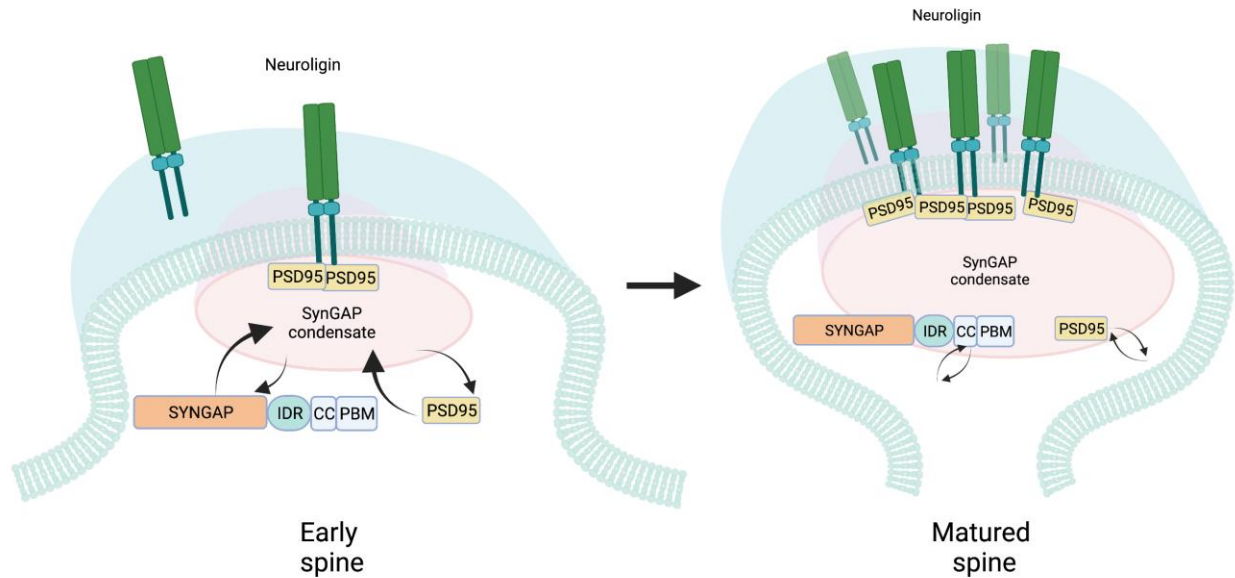


**Fig 19. Proposed model for the role of SynGAP and Nlg1 in the formation of the post-synapse** Nlg1 recruits SynGAP condensates via PSD95 to the plasma membrane during synapse formation, and SynGAP further recruits PSD95 into LLPS condensates, leading to the formation of the mature synapse. Therefore, we propose that SynGAP is the nucleating factor for the post-synapse formation.

## Chapter 3. Retention of receptors at SynGAP LLPS condensates

### 3.1 Introduction

The results of the previous chapter, showing that SynGAP forms LLPS condensates by itself, and recruits PSD95 into these condensates, allowing these condensates to then be recruited to the plasma membrane by a trans-membrane receptor such as Nlg1, are the first step in demonstrating the function of LLPS condensates in live cells. This chapter focuses on further demonstrating the function of post-synaptic LLPS condensates to recruit post-synaptic trans-membrane receptors in live cells.

Receptor dimerization and tetramerization, which is known to occur in many types of post-synaptic receptors such as adhesion molecules (Neuroligins) and ion channels (AMPA and NMDAR), could prolong the immobilizations of receptors in LLPS condensates by increasing the probability of receptor binding to PDZ domain binding sites. Nlg1 is known to exist as a constitutive dimer (Arac et al., 2007; Pouloupoulos et al., 2012). The importance of Nlg1's dimerization was discussed in a 2003 study that created dimerization-null mutants of Nlg1, where it was found that dimerization-null mutations dramatically reduced the Neurexin binding ability of Nlg1, as estimated by cell aggregation experiments (Dean et al., 2003). Evidence for the importance of dimerization for Nlg1's function was also shown in a study using electrophysiology, where dimerization-null mutants of Nlg1 could not show enhancements of excitatory post-synaptic currents (EPSCs) in hippocampal slice cultures, compared to wild-type Nlg1. This was further reinforced by the study's use of a chemical dimerizer to force dimerization of monomeric Nlg1, which rescued the wild-type Nlg1's phenotype (Shipman et al., 2012). While these studies suggest a role for dimeric Nlg1 in the recruitment of trans-synaptic Neurexin, neither of them considered if the dimerization-null mutant could have decreased retention in the synapse due to fewer binding sites for PDZ domain binding. Indeed, the study by Shipman et al. found that dimerization-null mutants of Nlg1 could not enhance post-synaptic PSD95 recruitment to the same level as dimeric Nlg1. Therefore, the question of whether multiple binding sites of receptors such as Nlg1 are important in enhancing their binding to PDZ domains at the post-synapse, remains unanswered.

### 3.2 Results

#### 3.2.1 Creating a functional tagged version of Nlg1

To create a fully functional version of Nlg1 tagged with Halo tag, I first looked for studies that have found suitable tag insertion sites for Nlg1. Although various studies have used both N-terminal (Feinberg et al., 2008) and C-terminal (Banovic et al., 2010) tags on Nlg1, it was unclear if these strategies produced fully functional Nlg1. Nlg1 binds with its trans-synaptic partner Neurexin via its extracellular domain, and dimerizes with the help of residues in its extracellular domain. In addition, Nlg1 interacts with PDZ domains of PSD95 with its C-terminal PDZ binding site. This is illustrated in Fig 20. Therefore, finding a place for a tag such as Halo tag with a size of 33kDa (about half the size of Nlg1's extracellular domain), without disrupting any of the functions of Nlg1, was a challenge.

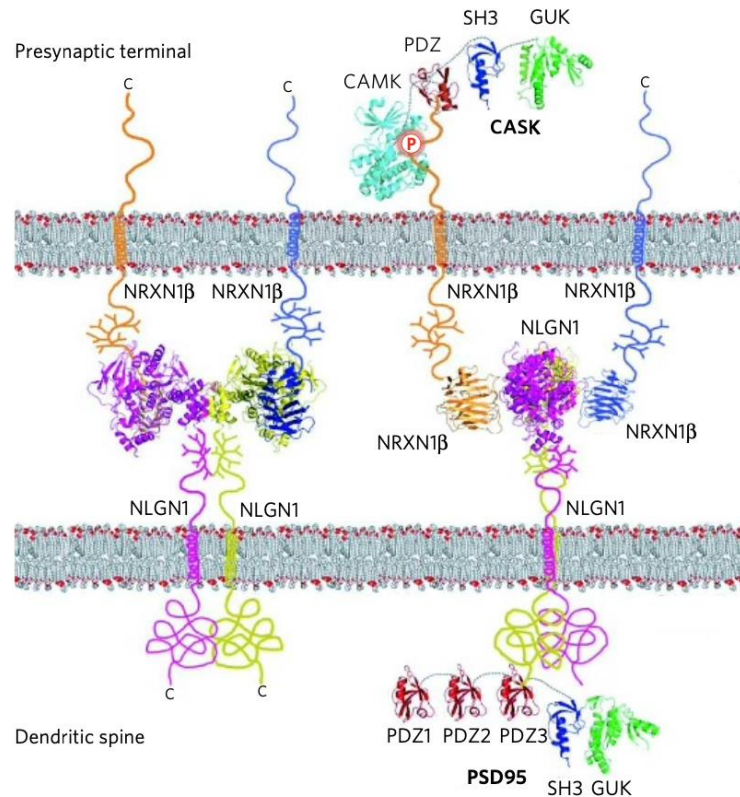


**Fig 20. Schematic showing functional Nlg1 takes part in at least 3 different interactions, via both its extra-cellular and intra-cellular domains**

Nlg1 forms dimers via interactions of the extra-cellular domain (left); Nlg1 also interacts with Neurexin1B via the extra-cellular domain and with PSD95 via its C-terminal PDZ binding domain (right), (adapted from Sudhof et al., 2008).

Tsetsenis et al. endeavored to introduce a “split GFP” tag into Nlg1, while preserving its function (Tsetsenis et al., 2014). This study produced a synaptic tagging system using Nlg1 and Neurexin1β (Nxn1β), whereby the reconstitution of split GFP occurs across the synapse when Nlg1 binds to Nxn1β. Using a wide range of experiments, including biochemical binding affinity measurements, synapse formation experiments with co-culture of neurons and non-neuronal cells, and confocal imaging to assess localization of Nlg1 in neurons, the study convincingly showed that adding a GFP-derived peptide of 1.78 kD (GFP11) between amino acids 641 and 642 of rat Nlg1 fully preserved the function of Nlg1 (see Fig 21a). This study was the basis for my early endeavors to produce a fully functional Halo-tagged Nlg1. However, the main concern with using the same insertion site for the Halo tag was that Halo tag (33kDa) is a much bigger tag than the GFP 11 peptide. The larger Halo tag could interfere with the extracellular domain functions, i.e. the Nlg1 dimerization interactions and the Nxn1-Nlg1 adhesion interactions. So a thorough test to check extracellular domain function was required. To assess the Nxn1β binding function of Halo-tagged Nlg1, I used an assay developed in an early paper showing the adhesion properties of E-cadherin (Nose et al., 1988). The assay involved dispersing L cells expressing E-cadherin with trypsin-EDTA, and then allowing them to aggregate over time in the medium containing  $Ca^{2+}$ . A

similar assay was used in a subsequent study showing the adhesion properties of Nlg1 (Dean et al., 2003) using PC12 cells.

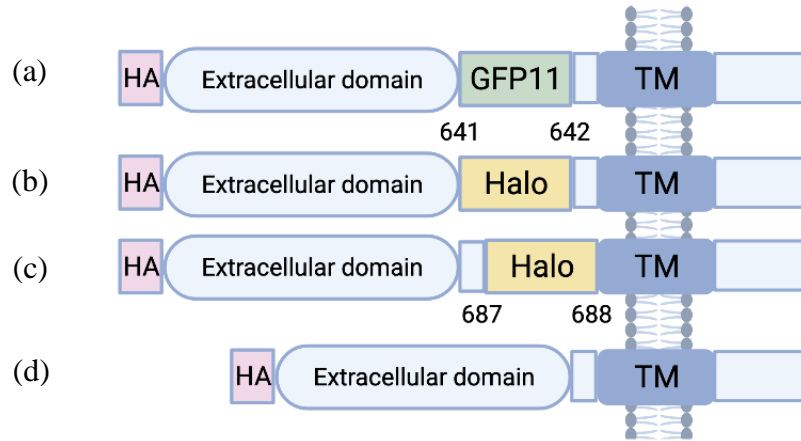


**Fig 21. Schematic of various Nlg1 constructs used in this study, showing the sites of tag insertion**

(a) Nlg1 with GFP11 tag insertion between amino acids 641 and 642, as used by Tsetsenis et al. (2014)

(b) Nlg1 with Halo tag insertion between amino acids 641 and 642, called Nlg-Halo-641

(c) Nlg1 with Halo tag insertion between amino acids 687 and 688 (tried for the first time in this study), called Nlg-Halo-687

(abbreviations: HA, HA tag; TM, Transmembrane region)

(d) Control Nlg1 construct, without Halo tag, called HA-Nlg

I created an L cell clone stably expressing E-cadherin, which served as adhesion positive control (Fig. 22). I also created clones of L cells stably expressing N-terminal HA-tagged Nlg1 and those stably expressing N-terminal HA-tagged Nrx1 $\beta$ . The HA-tag was useful to examine the expression levels of these molecules and its effects on the functions of these proteins were considered limited. As shown in Fig. 22, these cells exhibited cell aggregation. The aggregation level was lower than that of the L cells expressing E-cadherin, but this might be due to lower affinities of the HA-tagged Nlg1 and Nrx1 $\beta$  compared with the homophilic binding of E-cadherin and/or the lower expression levels of HA-tagged Nlg1 and Nrx1. All of the Nlg1 constructs used in this work contained the HA-tag at the Nlg1's N-terminus, and thus the cell aggregation assay results using the HA-tagged Nlg1 and Nrx1 served as the control for the same assays using L cells expressing various Nlg1 constructs. These L cells expressed similar levels of tagged Nlg1, as estimated by immunolabelling with anti-HA antibodies conjugated to Alexa Fluor<sup>®</sup> 555, followed by the imaging using total internal reflection fluorescence (TIRF) microscopy (Fig 23).

The L cells expressing Nlg1-Halo-641 construct (Fig. 21b) did not exhibit cell aggregation to the same extent as the HA-Nlg1 control cells (Fig 22), suggesting that the larger Halo tag placed between amino acids 641 and 642 interfered with Nlg1's interactions with Nrx1 $\beta$ . I then created a new Nlg1 construct, with a Halo tag attached between amino acids 687 and 688 (called Nlg-



Halo-687; Fig. 21c). This construct provided an extra length of 46 amino acids of the Nlg1 stalk region between the Halo tag and Nlg1's extracellular domain, likely decreasing the probability that the Halo tag might interfere with Nxn1 $\beta$  binding. This construct performed just as well as the control construct HA-Nlg1 in cell aggregation experiments. For all further experiments, this construct was used, and is referred to as Nlg1 WT when used with other mutants.

When Nlg-Halo-687 was over-expressed in dissociated hippocampal cultured neurons along with a spine marker, Homer1b-EGFP, and labeled with the TMR-Halo-ligand, Nlg-Halo-687 exhibited very good synaptic localization, as shown in Fig 24.

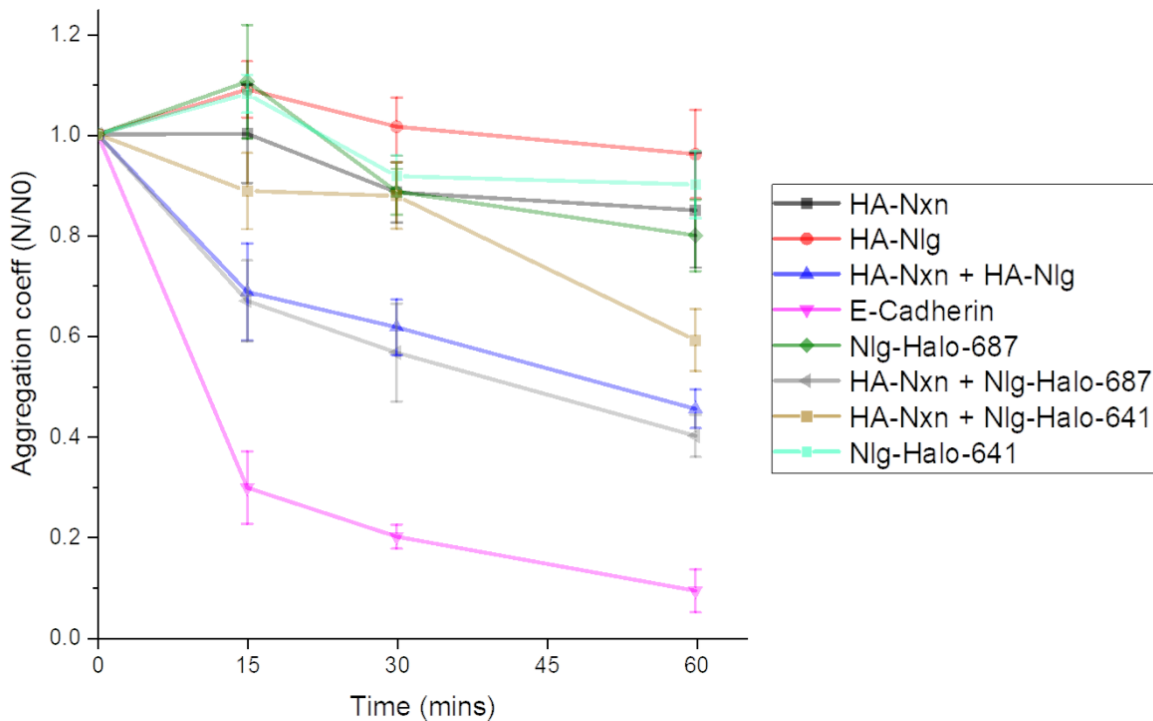


**Fig 22. Nlg1 with Halo tag at amino acid position 687 can form functional trans adhesions with Nxn, assessed via cell aggregation experiments.**

L cells stably expressing each construct, were incubated at 37°C in 1.5 mL tubes for the indicated durations with shaking, and aliquots at each time point taken and imaged with a phase-contrast microscope.

The aggregation coefficient is estimated as the number of cells or cell clusters at each time point (T) divided by the number of cells or cell clusters at time 0 (n = at least 3 separate experiments for each construct). Error bars indicate standard error of mean.

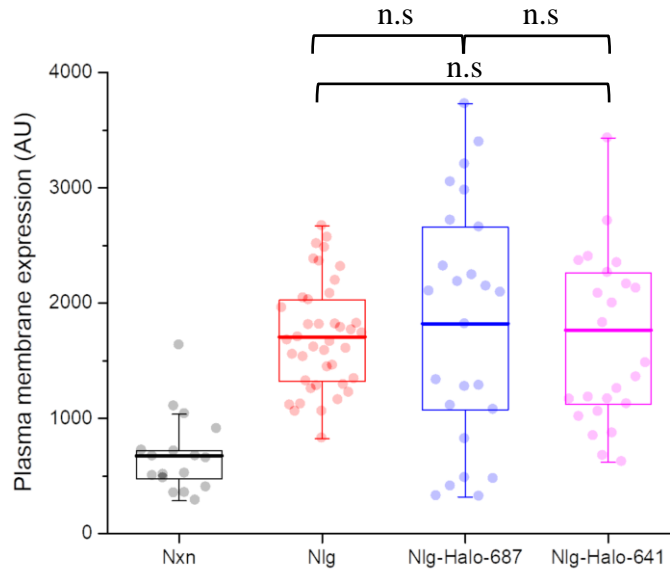
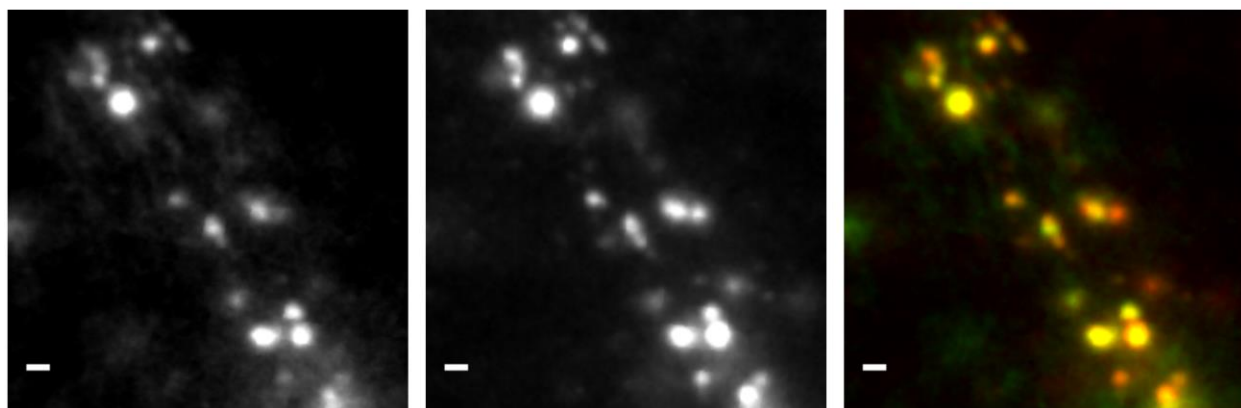


**Fig 23. All L cells stably expressing Nlg1 constructs (used for cell aggregation experiments) had similar plasma membrane expression**

L cells stably expressing each construct were immuno-labelled for HA tag and imaged with TIRF microscopy.

Mean plasma membrane (PM) expression of each construct used was estimated as the mean fluorescence intensity of an area of  $42.25 \mu\text{m}^2$  ( $6.5 \times 6.5 \mu\text{m}$ ) of the PM, under TIRF microscopy. HA-Nxn1 $\beta$  construct (left most) was used with all Nlg1 constructs for cell aggregation experiments. Bars, boxes, and whiskers indicate mean values, inter-quartile range (25% - 75%), and 10% - 90% range, respectively. Statistical P-values: \* $p < 0.05$ , \*\* $p < 0.01$ , \*\*\* $p < 0.001$ .



Homer1b-EGFP

Nlg-Halo-687

Nlg-Halo-687 + Homer1b-EGFP

**Fig 24. Nlg-Halo-687 construct localizes to the post-synapse**

Nlg-Halo-687 (labelled by incubating with 20 nM TMR-Halo ligand for 30 min) co-expressed with Homer1b-EGFP in DIV 18 hippocampal neurons, imaged with widefield fluorescent microscopy. Scale bar =  $1 \mu\text{m}$ .



### 3.2.2 Role of Neuroligin dimerization in its retention at the synapse

To understand the role of dimerization in the retention of Nlg1 at the synapse, I created two variants of Nlg1, a fully-functional Halo tagged variant, Nlg-Halo-687, as described in the previous section, and a dimerization-null mutant of the same, based on the dimerization sites suggested by the crystal structure of Nlg1 (Arac et al., 2007), and also used in the study of Shipman et al. for electrophysiology experiments (Shipman et al., 2012). See Fig 25 for a schematic of these constructs. These are henceforth called Nlg-Halo WT (wild type) and Nlg-Halo DM (dimerization-null mutant) respectively.

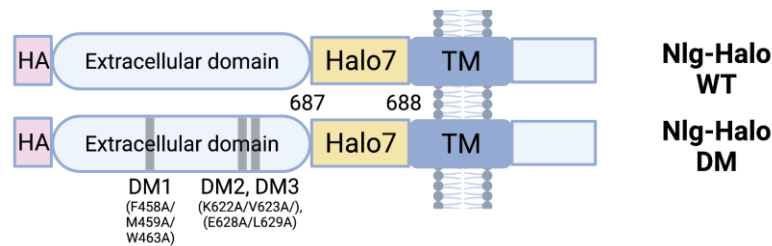


**Fig 25. Schematic of Nlg1 WT and Nlg1 dimer mutant constructs used for experiments**

Top schematic shows Nlg-Halo-687, used henceforth as Nlg-Halo WT and bottom schematic shows Nlg-Halo-687 dimerization-null mutant, used henceforth as Nlg-Halo DM.

To test the hypothesis that dimeric Nlg1 can be better retained at the post-synapse, I over-expressed Nlg-Halo WT and Nlg-Halo-DM in primary rat hippocampal neurons, labeled with TMR, and imaged the labeled molecules at the level of single Nlg1 molecules in neurons using the co-expressed Homer1b-EGFP as a spine marker. Nlg-Halo WT molecules localized to neuronal spines twice as well as Nlg-Halo DM molecules, as shown in Fig 26.

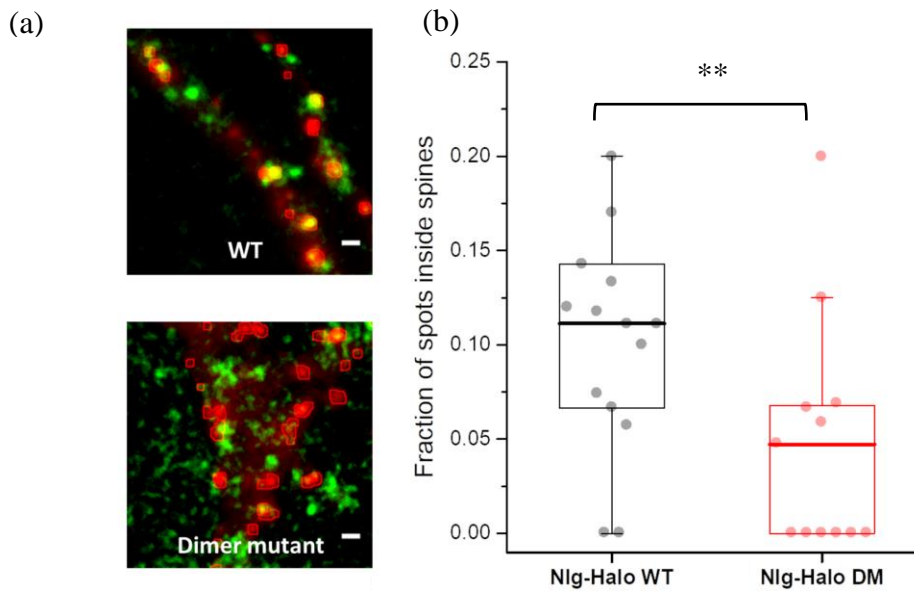


## Fig 26. Dimerization plays an important role in the proper localization of Nlg1 at the post-synapse

Nlg-Halo WT and Nlg-Halo DM (labelled by incubating with 20 nM TMR-Halo ligand for 30 min) were respectively co-expressed with Homer1b-EGFP by lentiviral transfection in DIV 18-22 rat primary hippocampal neurons, and imaged with TIRF microscopy.

(a) Single Nlg-Halo WT (top right) and Nlg-Halo DM (bottom right) molecules in green, with spine regions marked by Homer1b in red. Red lines indicate binarized spine areas. Scale bar = 1 $\mu$ m.

(b) Nlg-Halo WT molecules (n = 15 neurons) localize to neuronal spines of DIV 18-21 rat primary hippocampal neurons twice as well as Nlg-Halo DM molecules (n = 12 neurons). Bars, boxes, and whiskers indicate mean values, inter-quartile range (25% - 75%), and 10% - 90% range, respectively. Statistical P-values: \*p<0.05, \*\*p<0.01, \*\*\*p<0.001.

The results from experiments in neurons show that Nlg1 may indeed rely on its dimerization state to be retained at neuronal spines. In order to understand better how Nlg1 molecules could be retained at neuronal spines, and to quantitatively assess the difference between Nlg-Halo WT and Nlg-Halo DM in their interactions with post-synaptic assemblies, I decided to image Nlg1 molecules at the level of single molecules in the presence of SynGAP LLPS condensates containing PSD95, in non-neuronal cells. Using non-neuronal L cells, the interactions of Nlg1 with SynGAP condensates containing PSD95 can be specifically investigated. An additional advantage is that L cells offer large basal plasma membrane area, making it easier to image single molecules. L cells, a type of fibroblasts that are deficient in adhesion molecules such as E-cadherin, were the system of choice for non-neuronal experiments in this research. Before I could begin experiments to observe Nlg1 molecules in the presence of LLPS condensates of SynGAP and PSD95, I needed to estimate the fraction of molecules that existed as dimers and monomers at Nlg1 number densities similar to those used in all future experiments.

Nlg-Halo WT, Nlg-Halo DM, and a monomeric control, consisting of the transmembrane region of the LDL receptor linked to the Halo tag (Halo-TM), were labelled with the TMR-Halo ligand dye, to achieve labelling efficiency of greater than 90% (Appendix 1). In addition, a mixture of antibodies against HA tag and Halo tag were used to induce dimers and greater oligomers of Nlg-Halo DM (called Nlg-Halo DM+Ab), as controls for stable dimers and oligomers (Fig 27). The L cells expressing these molecules before and after the Ab treatment were imaged at the level of single molecules by TIRF microscopy. The average number densities of fluorescent spots were approximately 0.6 spots/ $\mu$ m<sup>2</sup>. To quantify the fractions of monomers, dimers, and greater oligomers, the signal intensities of all the individual fluorescent spots detected in the initial twenty frames in the single fluorescent-molecule imaging movies were determined. The signal intensity distributions for monomers were obtained by imaging Halo-TM, and all the signal intensities of individual fluorescent spots of each Nlg1 construct were normalized by using the mean signal intensity of Halo-TM.

The distributions of the normalized signal intensities of individual spots distributions are plotted in Fig 28a. These distributions were fitted by the sum of multiple lognormal functions, such that each of the constituent lognormal functions represents the signal intensity distributions of monomers, dimers, trimers, and tetramers etc. (Mehta et al., 2006; Mutch et al., 2007). This method of estimating the relative stoichiometries has been previously used by our group for similar analyses (Morise et al., 2019). This analysis yields an estimate of spot fractions, which is the

fraction of observed fluorescent spots that are monomers, dimers, trimers, or tetramers. While the larger oligomers in my experiments make up a small fraction of spots, the number of molecules within a single oligomeric spot are proportionally greater. Therefore, it is also useful to think of the fractions of molecules that represent the observed fluorescent spots of monomers, dimers, trimers, and tetramers. This can be estimated from the spot fractions by multiplying each spot fraction with the  $n^{\text{th}}$  mer, and dividing by the total number of molecules.

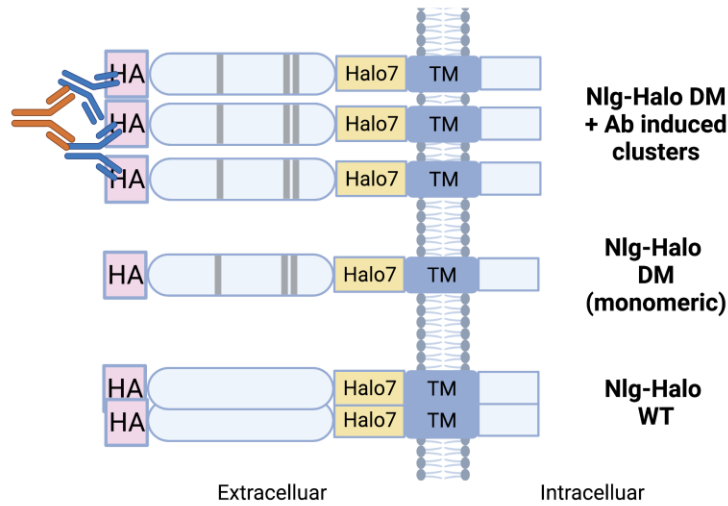
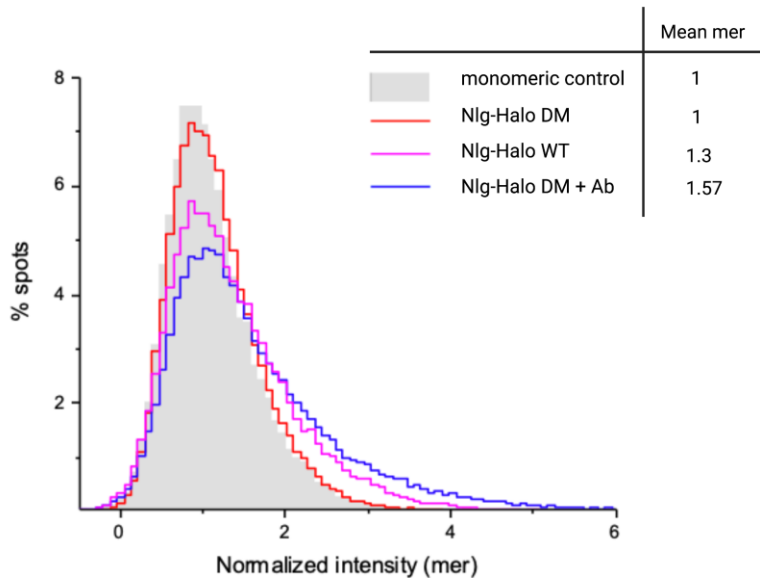


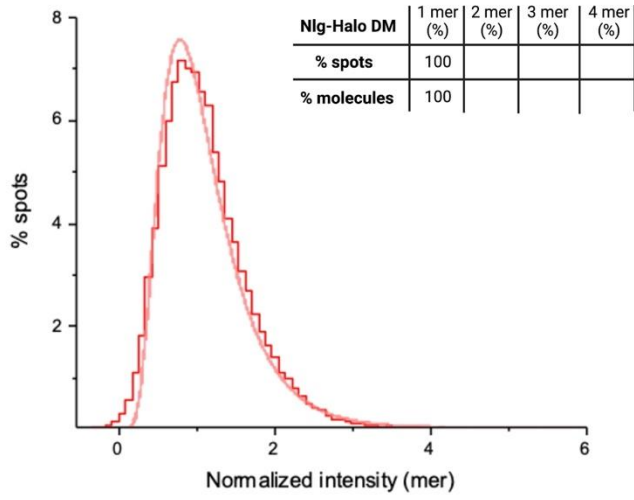
**Fig 27. Schematic of Nlg1 WT, Nlg1 dimer mutant, and Nlg1 dimer mutant clustered with antibodies, used for experiments**

Nlg-Halo WT (bottom), Nlg-Halo DM (middle), and Nlg-Halo DM+Ab (top; Nlg-Halo DM treated with a mixture of anti-HA and anti-Halo primary antibodies, and secondary antibodies)

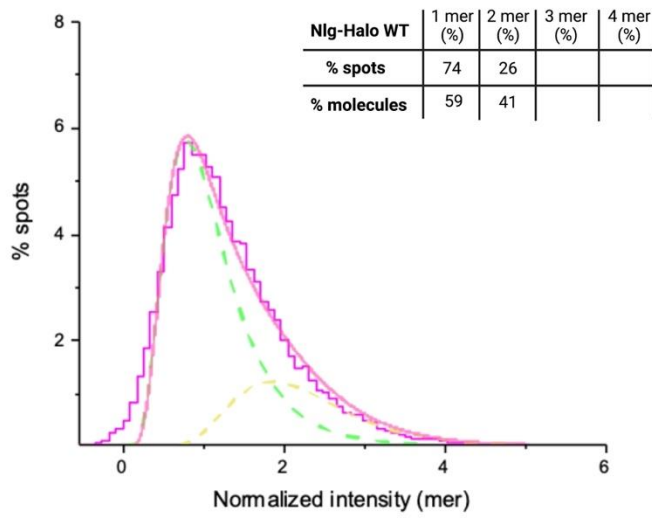
(a)



(b)



(c)



(d)

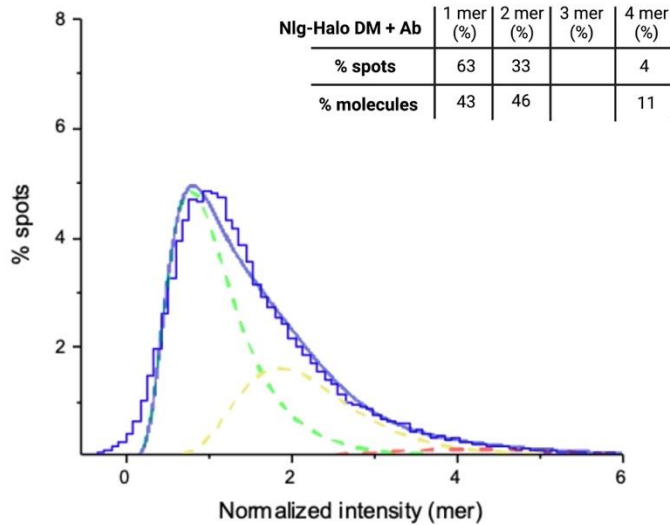


**Fig 28. Assessment of relative stoichiometry of monomers, dimers, and greater oligomers, and the average stoichiometry for each Nlg1 construct used for experiments**

L cells stably expressing each Nlg-Halo construct (or the monomeric control construct) were labelled by incubating with 20 nM TMR-Halo ligand for 30 min, and single fluorescent-molecule imaging was performed using TIRF microscopy.

(a) Superimposed histograms of the normalized signal intensities of Halo-TM (monomeric control, grey solid) Nlg-Halo DM (orange lines), Nlg-Halo WT (magenta lines), and Nlg-Halo DM+Ab (blue lines).

(b) The distribution for Nlg-Halo DM (histogram, step lines) could be fitted best by a single lognormal function (solid smooth curve), indicating that Nlg-Halo DM is monomeric.

(c) The distribution for Nlg-Halo WT (histogram, step lines) could be fitted best by the sum of two lognormal functions for monomers and dimers (green and yellow dashed smooth curves indicate individual lognormal distribution functions of monomers and dimers respectively; solid smooth curve indicates the sum), indicating that Nlg-Halo WT spots consist of 74% monomers, and 26% dimers, while 59% of the molecules are monomers and 41% dimers.

(d) The distribution for Nlg-Halo DM+Ab (histogram, step lines) could be fitted best by the sum of three lognormal functions for monomers, dimers, and tetramers (green, yellow, and red dashed smooth curves indicate lognormal distribution functions for monomers, dimers, and tetramers respectively; solid smooth curve indicates the sum), indicating that Nlg-Halo DM+Ab spots consist of 63% monomers, 33% dimers, and 4% tetramers, while 43% of the molecules are monomers, 46% dimers, and 11% tetramers.

Nlg-Halo DM is indeed monomeric, with the intensity of spots identical to the monomeric control (Fig 28b). 74% and 26% of Nlg-Halo WT spots exist as monomers and dimers respectively, at similar number densities (Fig 28c), suggesting that Nlg1 may form metastable dimers, that fall apart and rejoin continuously at the plasma membrane. Single spots of Nlg-Halo DM treated with the antibody mixture (Nlg-Halo DM+Ab), are represented by 33% dimers and 4% tetramers in addition to 63% monomers (Fig 28d), showing that monomeric Nlg-Halo DM can indeed be clustered to form dimers and tetramers with the help of antibodies. This serves as a positive control experiment, to observe the effect of inducing oligomerization of monomeric Nlg1. See Fig. 27 for a schematic of the Nlg1 constructs used in this set of experiments.

Next, Nlg-Halo WT, Nlg-Halo DM, and Nlg-Halo DM+Ab labelled with the Setau647-Halo ligand were imaged in L cells, where mCherry-SynGAP and PSD95-EGFP were co-expressed, using simultaneous triple-color single-molecule imaging. The time-lapse imaging using a frame integration time of 33 ms at 10 Hz was performed for 120 s. The time-lapse recording was necessary to track immobilized molecules beyond the observation periods permitted by imaging at typical video rate of 33 Hz due to photobleaching. Since SynGAP and PSD95 condensates did not move appreciably during several seconds to  $\approx 100$ -s scales, a time-lapse recording at 1 Hz was used to observe SynGAP and PSD95.

Since PSD95 was found condensed in all SynGAP LLPS condensates and behave exactly like SynGAP condensates, in the later experiments, only mCherry-SynGAP was observed. To establish the areas of SynGAP condensates, mCherry-SynGAP condensates were thresholded based on relative intensity, to create a binary mask.

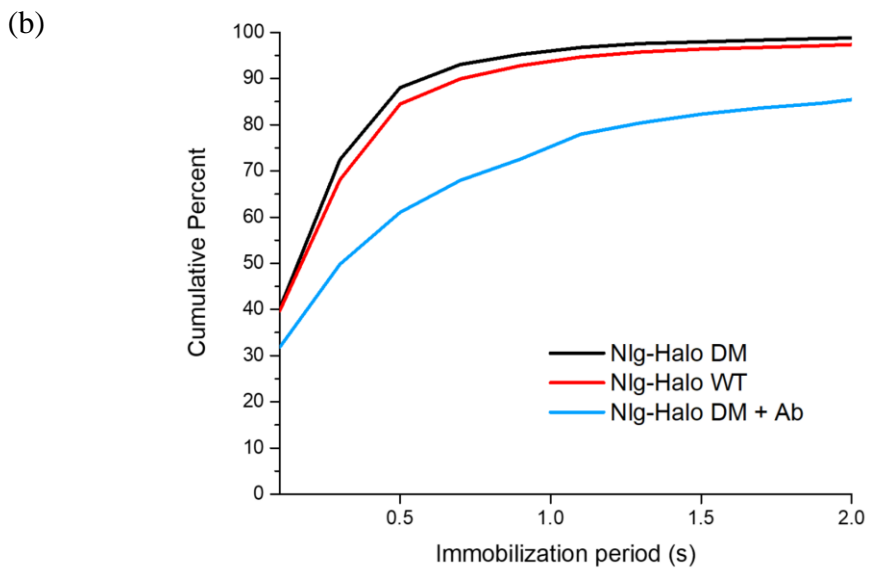
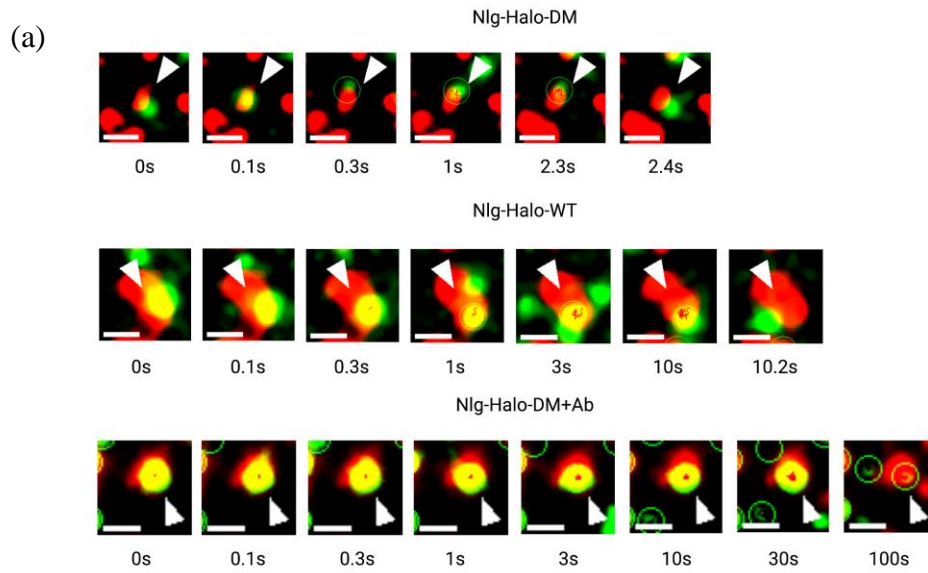
Single Nlg1 trajectories that exhibited immobilizations, defined as spots having an instantaneous diffusion coefficient of less than  $0.0083 \mu\text{m}^2/\text{s}$  for at least 500 ms, were analyzed to see if they resided within SynGAP condensates (Fig. 29a). Each immobilization period within the SynGAP condensates was measured and their cumulative distributions are shown in Fig 29b.

The mean immobilization durations for Nlg-Halo WT and Nlg-Halo DM indicate that the immobilization duration of Nlg-Halo WT is significantly longer than that of Nlg-Halo DM ( $p < 0.001$ ; Fig. 29c). This is consistent with the cumulative histograms, indicating that Nlg-Halo DM exhibited consistently shorter immobilizations within SynGAP condensates, compared to Nlg-Halo WT (Fig. 29b).

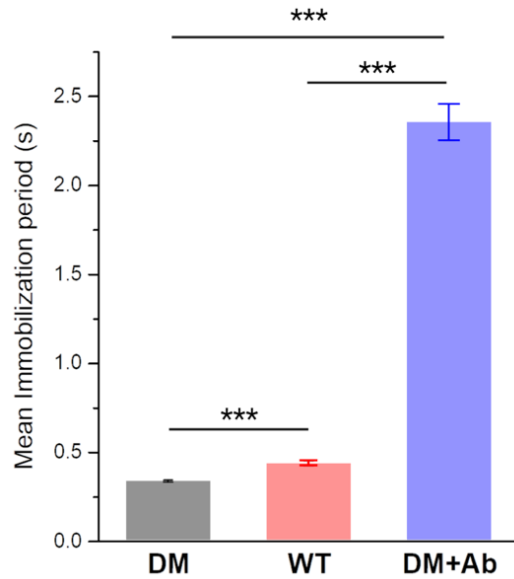
Since 74% of single-molecule spots of Nlg-Halo WT represent monomers (Fig 28c), it is likely that most immobilizations of Nlg-Halo WT observed were in fact monomers. To clarify the real difference between dimeric and monomeric Nlg1, it is necessary to observe only dimeric Nlg1 molecules. To do this, in the near future, I intend to use the split GFP system (Cabantous et al., 2005), to create two Nlg1 constructs labelled with GFP1-10 and GFP11 respectively, and observe the GFP fluorescence signal, which would occur only when real dimers are formed, and GFP1-10 and GFP11 are close enough to reconstitute the fluorescent GFP protein.

When Nlg-Halo DM was bound by the anti-Halo and anti-HA antibodies to induce dimers and tetramers (Fig. 28d), the Nlg-Halo DM+Ab exhibited remarkably longer immobilizations in SynGAP condensates (Fig 29b, 29c), indicating that oligomerization of Nlg1, such as that induced by its interactions with Nxn, could dramatically increase its immobilization in SynGAP condensates, and likely at the post-synapse. These results indicate that Nlg1 exhibits valency dependent immobilization in SynGAP condensates.

To assess if Nlg-Halo WT and Nlg-Halo DM+Ab molecules were indeed getting immobilized within SynGAP LLPS condensates, and not just immobilized uniformly due to clustering, the ratio of spots inside SynGAP LLPS condensates to the total number of spots detected, at time zero (the moment when single molecule imaging was started), was estimated, as shown in Fig 29d. Nlg-Halo DM + Ab spots were detected significantly more inside SynGAP LLPS condensates areas.



(c)



(d)

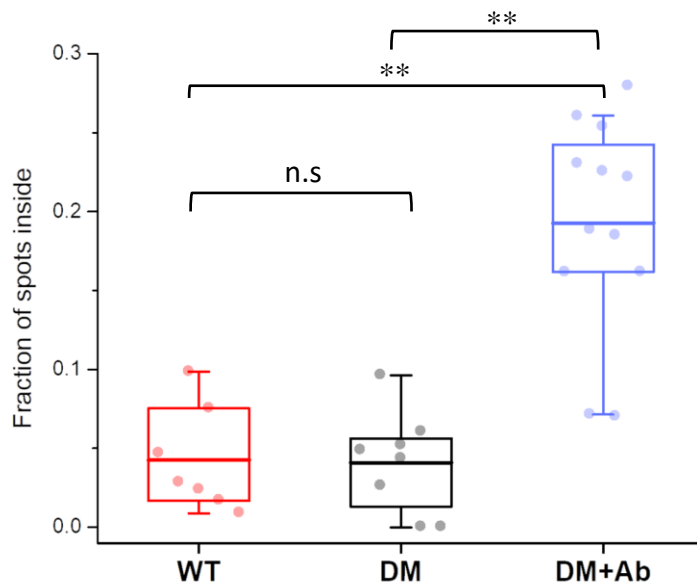


**Fig 29. Nlg1 exhibits oligomerization dependent immobilization in SynGAP condensates**

L cells stably expressing each Nlg-Halo construct ( $\approx 0.6$  spots/ $\mu\text{m}^2$ ) were labelled by incubating with 20 nM TMR-Halo ligand for 30 min, and imaged simultaneously with mCherry-SynGAP and PSD95-EGFP using triple-color TIRF microscopy.

(a) Snapshots from the movies of Nlg-Halo DM, Nlg-Halo WT, and Nlg-Halo DM+Ab imaged with single-molecule sensitivities (green), showing immobilizations (white arrows) in SynGAP LLPS condensates (red). Scale bar = 1  $\mu\text{m}$ .

(b) Cumulative distributions of the immobilization periods of Nlg-Halo DM, Nlg-Halo WT, and Nlg-Halo DM+Ab within SynGAP LLPS condensates.



(c) Mean immobilization durations for each construct.  $n = 41,784$  immobilizations for Nlg-Halo DM, 30,568 for Nlg-Halo WT, and 55,641 for Nlg-Halo DM+Ab.

(d) Fractions of single-molecule spots inside vs. outside the binarized SynGAP LLPS condensate areas at frame zero. Bars, boxes, and whiskers indicate mean values, inter-quartile ranges (25% - 75%), and 10% - 90% range, respectively. Statistical P-values: \* $p < 0.05$ , \*\* $p < 0.01$ , \*\*\* $p < 0.001$ .

### 3.2.3 Valency dependent retention of receptors at the synapse: comparing tetrameric GluA1 to dimeric and monomeric versions

The results from the previous section suggest that Nlg1 relies on its dimerization state to be effectively immobilized in SynGAP LLPS condensates containing PSD95. To extend these results to my initial hypothesis, that trans-membrane receptors rely on multiple binding sites for prolonged immobilizations at the post-synapse, I next used three proteins that can bind to PSD95 and form different sizes of oligomers. The proteins I employed were based on transmembrane AMPA receptor regulatory protein (TARP)  $\gamma 2$  (henceforth referred to as TARP2) due to its ability to bind to PSD95 via its PBM. The three proteins are the following: (1) TARP2, serving as a monomer control molecule, (2) TARP2 linked to the AMPAR subunit GluA1 via a cytoplasmic linker (called Halo-GluA1-TARP2 or GluA1-TARP2), which could form tetramers and was first employed by Shi et al. (2009), and (3) TARP2 linked to the GluA1 mutant with its N-terminal motif deleted (called Halo-GluA1- $\Delta$ NTD-TARP2). GluA1- $\Delta$ NTD was shown to have dramatically reduced fraction of tetramers (Morise et al., 2019). The GluA1 subunit of AMPAR, tagged with the Halo protein at GluA1's N-terminus, was shown to be fully functional in extensive experiments, including electrophysiology, and able to form homo-dimers, trimers, and tetramers by Morise et al. (2019). In TARP2, the Halo tag protein was inserted into the first extracellular loop, at the same position as previous studies (Chamma et al., 2016). See Fig 30. for a summary of all the constructs used in this study.

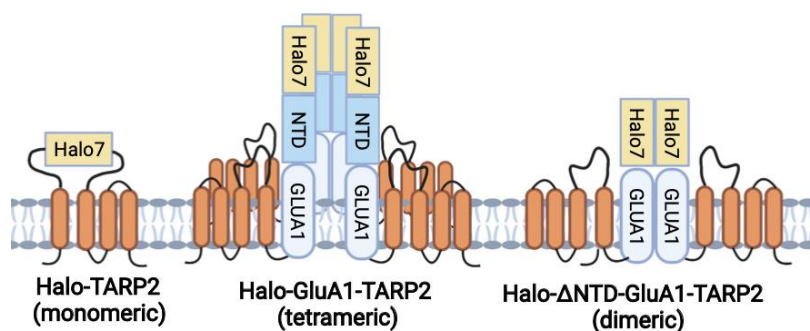


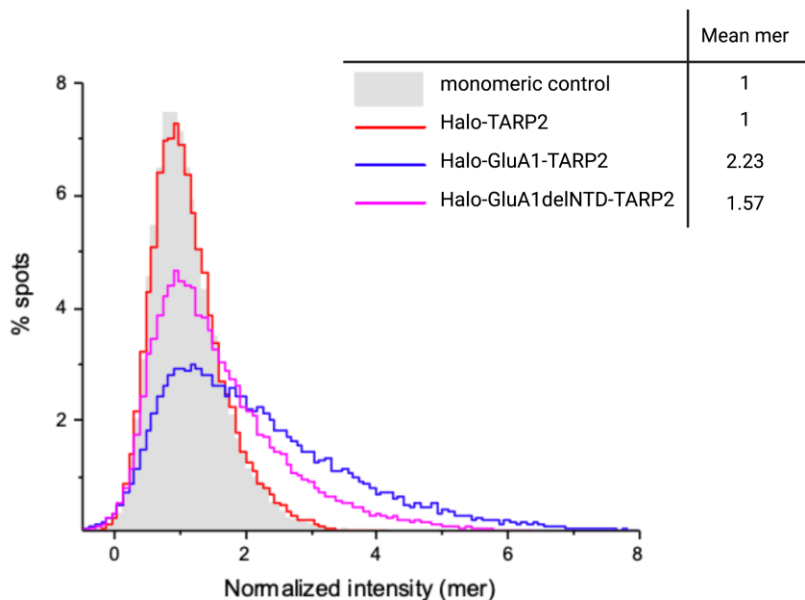
**Fig 30. Schematic of TARP2, GluA1-TARP2, and GluA1-delNTD-TARP2 used for experiments**

Halo-tagged TARP2 (Halo-TARP2), a monomeric receptor (left), Halo-tagged GluA1 linked to TARP2 (Halo-GluA1-TARP2), capable of forming complete tetrameric receptors, with a mean cluster size of 2.23 mer (middle), and Halo-tagged GluA1 with N-terminal deletion (Halo-GluA1- $\Delta$ NTD), which has an impaired ability to form tetramers, with a mean cluster size of 1.57 mer (right).

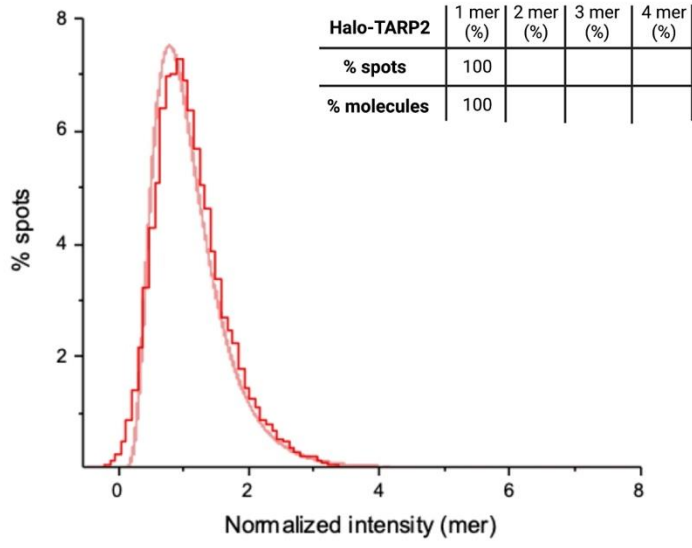
As with all Nlg1 constructs, TARP2 and GluA1 constructs were evaluated to estimate the spot fractions of monomers and various oligomers at similar number densities. All constructs were labelled with TMR-Halo ligand, to achieve labelling efficiency of >90%, and imaged at the same conditions. To estimate the fractions of monomers and various oligomers, the signal intensities of all the individual fluorescent spots detected in the initial twenty frames in the single fluorescent-molecule imaging movies were determined (Fig 31a). The mean single-molecule intensity of the monomer control, Halo-TM was used to normalize the intensities of each AMPAR construct (and the x-axis). This gives the mean stoichiometry for each construct, indicated on the top right of Fig 31a.

Thereafter, the histogram of single-molecule intensities of each AMPAR construct, Halo-TARP2, Halo-GluA1-TARP2, and Halo-GluA1- $\Delta$ NTD-TARP2, were fitted by the sum of multiple lognormal functions, such that each of the constituent lognormal functions estimates the fraction of monomers and various oligomers (Fig 31b, 31c, 31d), as was done for Nlg1 constructs. The intensity distribution for single molecules (monomers) was obtained by using the monomer reference molecule Halo-TM expressed at similar number densities on the plasma membrane, with the fitting using a single lognormal function.

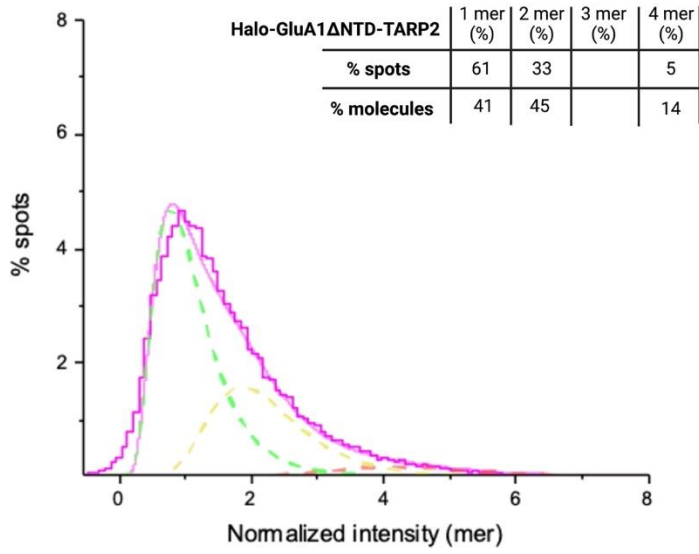
(a)



(b)



(c)



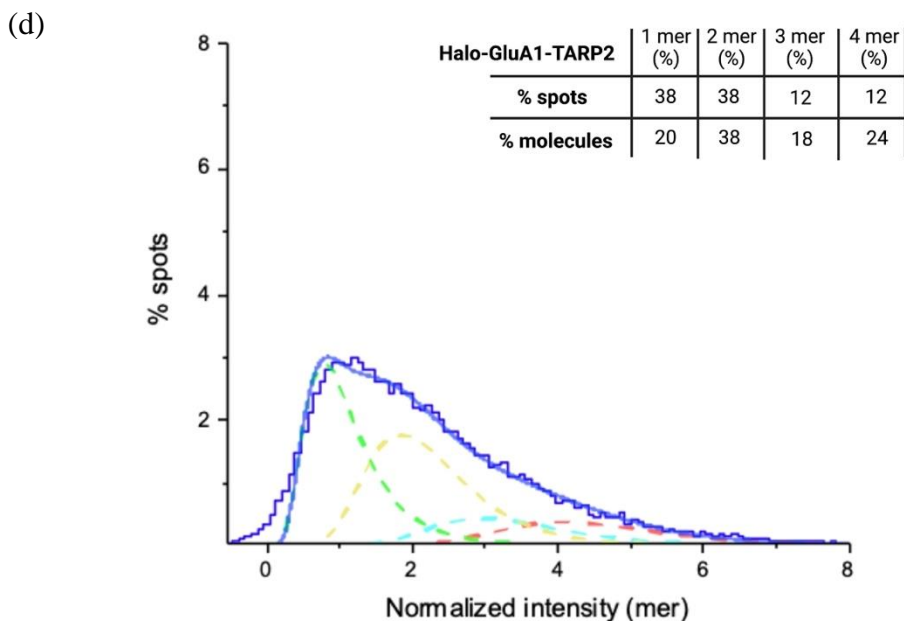


**Fig 31. Assessment of relative stoichiometry of monomers, dimers, trimers, and tetramers, and average stoichiometry for each TARP2/TARP2 linked GluA1 construct used for experiments**

L cells stably expressing each AMPAR construct (or the monomeric control construct) at single-molecule expression levels were labelled by incubating with 20 nM TMR-Halo ligand for 30 min, and single fluorescent-molecule imaging was performed using TIRF microscopy.

(a) Superimposed histograms of the normalized signal intensities of of Halo-TM (monomeric control, grey solid) Halo-TARP2 (orange lines), Halo-GluA1- $\Delta$ NTD-TARP2 (magenta lines), and Halo-GluA1-TARP2 (blue lines).

(b) The distribution for Halo-TARP2 (histogram, orange step lines) could be fitted best by a single lognormal function (solid orange smooth curve), indicating that Halo-TARP2 is monomeric.

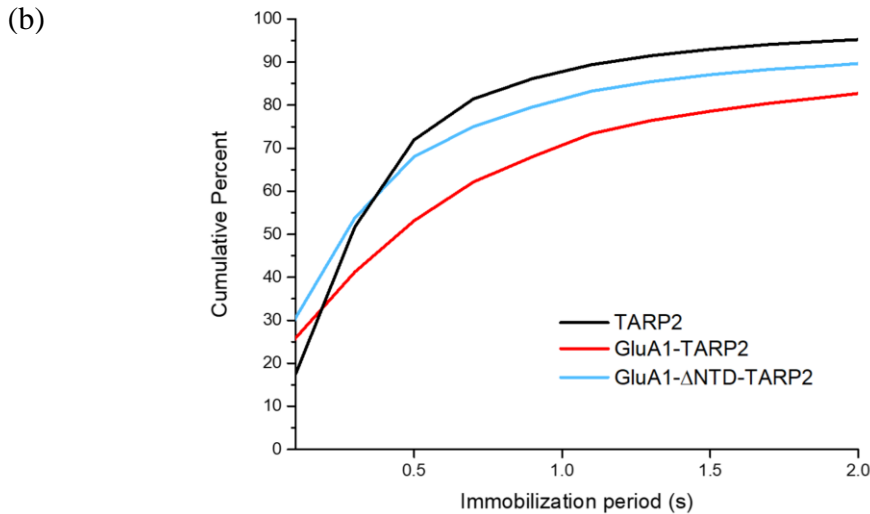
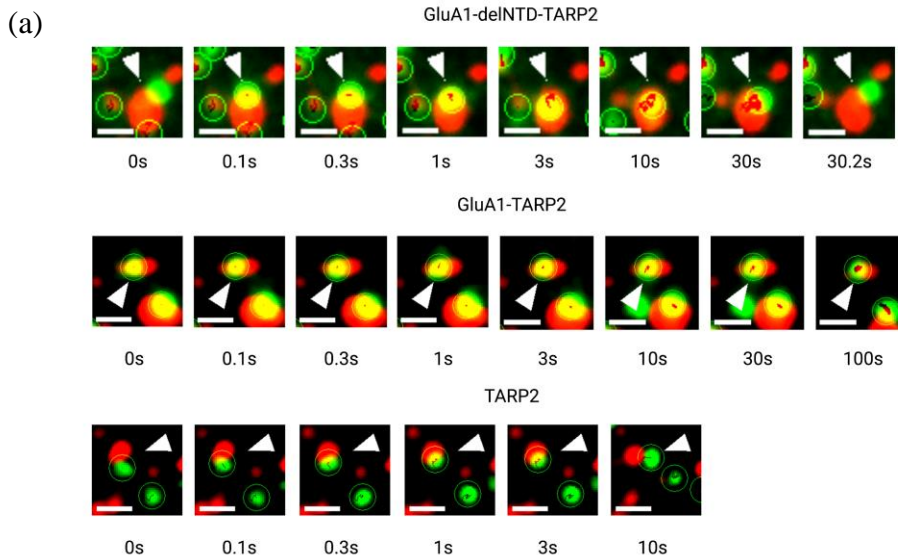
(c) The distribution for Halo-GluA1- $\Delta$ NTD-TARP2 (histogram, step lines) could be fitted best by the sum of three lognormal functions (green, yellow, and red dashed smooth curves indicate each lognormal distribution of monomers, dimers and tetramers respectively; solid smooth curve indicates the sum), indicating that Halo-GluA1- $\Delta$ NTD-TARP2 spots consist of 61% monomers, 33% dimers and 5% tetramers, while 41% of the molecules are monomers, 45% dimers, 14% tetramers.

(d) The distribution for Halo-GluA1-TARP2 (histogram, step lines) could be fitted best by the sum of four lognormal functions (green, yellow, cyan, and red dashed smooth curves indicate each lognormal distribution of monomers, dimers, trimers, and tetramers respectively; solid smooth curve indicates the sum), indicating that Halo-GluA1-TARP2 spots consist of 38% monomers, 38% dimers, 12% trimers, and 12% tetramers, while 20% of the molecules are monomers, 38% dimers, 18% trimers, and 24% tetramers.

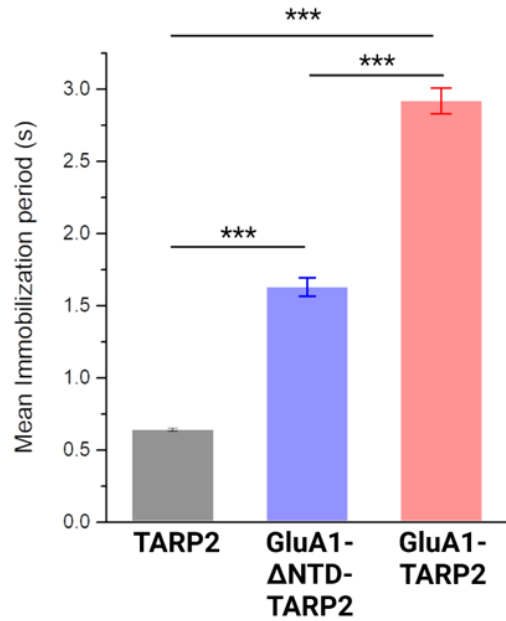
Halo-TARP2 is monomeric (Fig 31b), with the intensity of spots identical to the monomeric control. Halo-GluA1- $\Delta$ NTD spots, at similar number densities, consist of 61% monomers, and 33% dimers, and 5% tetramers (Fig 31c), consistent with the results of Morise et

al., who used Halo-GluA1- $\Delta$ NTD, but without linking it to TARP2. Halo-GluA1-TARP2 spots consist of 38% monomers, 38% dimers, 12% trimers, and 12% tetramers (Fig 31d), again roughly consistent with the results of Morise et al. (2019). These constructs enabled the study of the effect of number of binding sites on the immobilization of receptors in LLPS condensates.

As with the experiments described in section 3.2.2, these constructs were expressed with mCherry-SynGAP and PSD95-EGFP in L cells for triple-color single molecule imaging. Single molecule trajectories of each construct were analyzed as described before. The immobilization period of Halo-TARP2, Halo-GluA1-TARP2, and Halo-GluA1- $\Delta$ NTD-TARP2 molecules is displayed as a cumulative distribution, revealing the difference in immobilizations between monomeric TARP2, dimeric GluA1- $\Delta$ NTD-TARP2, and tetrameric GluA1-TARP2, as shown in Fig 32b.



(c)



(d)

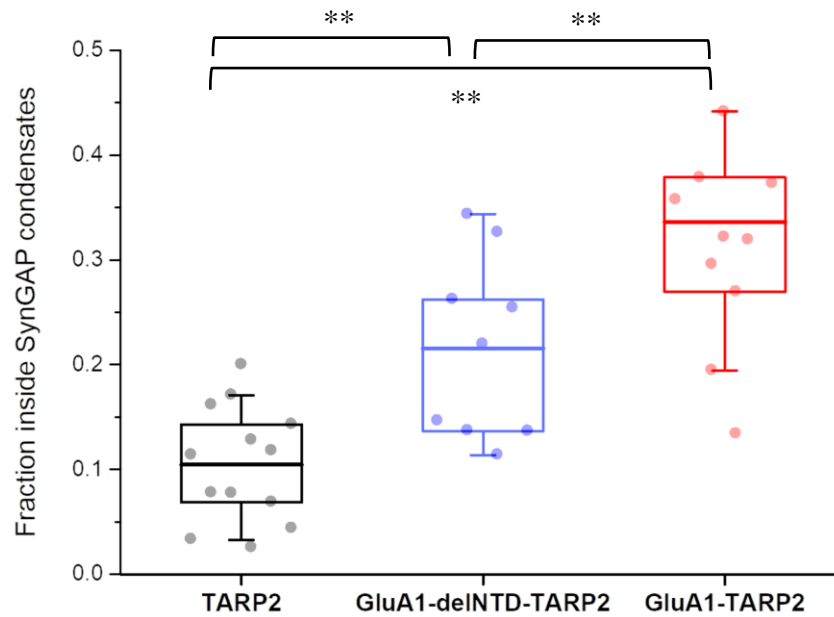


**Fig 32. AMPA receptors exhibit oligomerization dependent immobilization in SynGAP condensates**

L cells stably expressing each AMPAR construct ( $\approx 0.6$  spots/ $\mu\text{m}^2$ ) were labelled by incubating with 20 nM TMR-Halo ligand for 30 min, and imaged simultaneously with mCherry-SynGAP and PSD95-EGFP using triple-color TIRF microscopy.

- (a) Snapshots of single molecule trajectories of Halo-GluA1- $\Delta$ NTD-TARP2, Halo-GluA1-TARP2, and Halo-TARP2 (green) shown immobilizing in SynGAP LLPS condensates (red), indicated by white arrows, with time points under each snapshot. Scale bar = 1  $\mu$ m.
- (b) Cumulative distribution of the immobilization period (in seconds) of trajectories of Halo-TARP2 (black line), Halo-GluA1- $\Delta$ NTD-TARP2 (blue line), and Halo-GluA1-TARP2 (orange line) within SynGAP LLPS condensates
- (c) Mean immobilization durations for each construct. n=29,131 immobilizations for Halo-TARP2; n=42,037 immobilizations for Halo-GluA1- $\Delta$ NTD-TARP2; n=76,652 immobilizations for Halo-GluA1-TARP2.
- (d) Fractions of single-molecule spots inside vs. outside the binarized SynGAP LLPS condensate areas at frame zero. Bars, boxes, and whiskers indicate mean values, inter-quartile ranges (25% - 75%), and 10% - 90% range, respectively. Statistical P-values: \*p<0.05, \*\*p<0.01, \*\*\*p<0.001.

Monomeric TARP2 shows the shortest immobilizations. GluA1-TARP2, which has a mean stoichiometry of 2.23, exhibits the longest immobilizations, while GluA1- $\Delta$ NTD-TARP2, which has a mean stoichiometry of 1.57, is immobilized longer than monomeric TARP2 and shorter than GluA1-TARP2 (Fig 32b). The mean immobilization durations for each construct, estimated from thousands of immobilizations, shown in Fig 32c, indicate there is clear stoichiometry dependent immobilization of AMPAR in SynGAP condensates. While comparisons between TARP2 and Nlg1 can be done qualitatively, it is important to emphasize that the binding affinities of the PDZ domain binding sites on TARP2 and Nlg1 are likely different, and thus the proper comparisons would be between various constructs of Nlg1 or constructs linked to TARP2.

To assess if GluA1- $\Delta$ NTD-TARP2 and GluA1-TARP2 constructs were indeed getting immobilized within SynGAP LLPS condensates, and not just immobilized uniformly due to clustering, the ratio of spots inside SynGAP LLPS condensates to the total number of spots detected, at time zero (the moment when single molecule imaging was started), was estimated, as shown in Fig 32d. TARP2, GluA1- $\Delta$ NTD-TARP2, and GluA1-TARP2 showed clear stoichiometry dependent increase in detections inside SynGAP LLPS condensates (~10% inside for TARP2, ~20% inside for GluA1- $\Delta$ NTD-TARP2, ~33% inside for GluA1-TARP2).

### 3.3 Summary and discussion

The experimental results detailed in this chapter demonstrate that binding avidity could play an important role in receptor recruitment and retention at SynGAP condensates, and thus at the post-synapse.

Nlg1 molecules exhibit oligomerization-dependent immobilizations within SynGAP LLPS condensates. Antibody-induced Nlg1 clusters could be retained in LLPS condensates for durations much longer than Nlg WT and Nlg DM, likely due to the enhanced ‘effective’ affinity of clustered Nlg1, which would increase following the exponent of the number of the binding sites. A significant difference in immobilization durations between Nlg WT and Nlg DM was found. Since only 26% of Nlg-Halo WT spots are dimers at the number densities used in these experiments, further experiments that specifically track dimeric Nlg1 molecules only, are required. The finding that the monomeric mutant of Nlg1 exhibits impaired retention at the synapse supports this hypothesis, which is illustrated in Fig 33.

The principle of oligomerization-enhanced immobilization of receptors holds true for AMPAR as well: fully-functional AMPAR exhibit even longer immobilizations within SynGAP LLPS condensates than N-terminal deletion variant of AMPAR, which in turn exhibit longer immobilizations than monomeric TARP2. The improved retention of tetrameric AMPAR complexes within LLPS condensates at the post-synapse also supports the results of Morise et al. (2019), who postulate that AMPAR receptors mainly turn over by monomer diffusion in and out of the synapse. If tetrameric AMPAR are largely immobilized within the post-synapse, only when AMPAR tetramers break apart into monomers and dimers, would the individual subunits have a significantly reduced ‘effective’ affinity, and be able to diffuse out of the post-synapse. Further single molecule studies that can distinguish between monomeric subunits and full tetramers in live neurons, are needed to clarify the controversial findings of Morise et al. (2019).

My results are also a demonstration of the function of LLPS condensates to recruit and retain full-length fully functional receptors in live cells, and suggest that such LLPS condensates may be involved in recruitment and immobilization of receptors at the post-synapse as well. LLPS condensates could provide an extremely high density of bindings sites, and may be dynamically dispersed and assembled as needed.



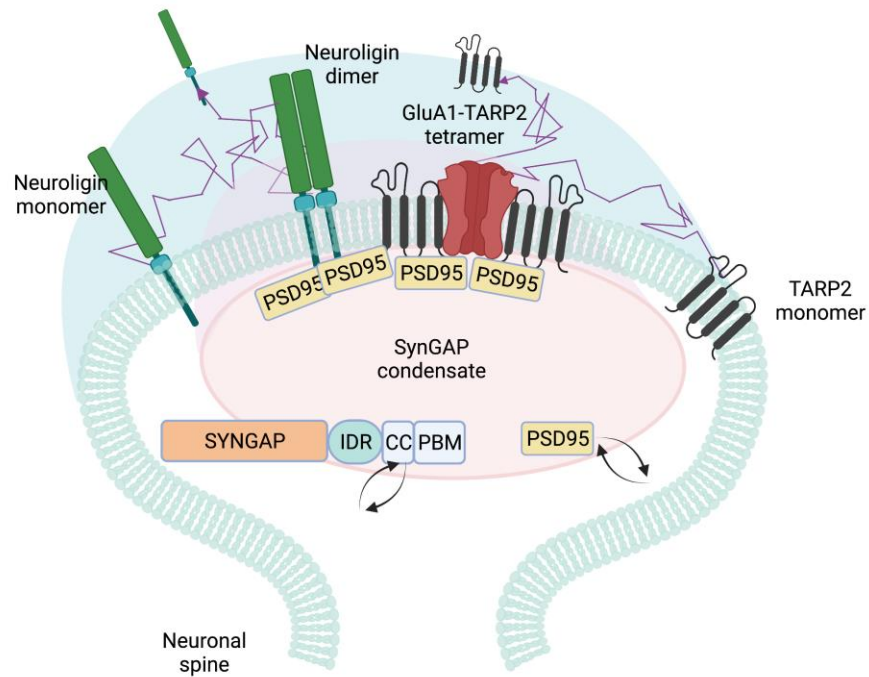


**Fig 33. Proposed model for the oligomerization dependent capture of post-synaptic receptors at SynGAP condensates at the post-synapse**

LLPS condensates of SynGAP, with PSD95 as a client, recruit and immobilize dimeric Nlg1 and tetrameric AMPAR at the post-synapse in a typical neuronal spine.

## Chapter 4. General discussion and future directions

### 4.1 SynGAP's role at the post-synapse: reconciling my results with other studies

SynGAP's function as a structural protein at the post-synapse is still incompletely understood. SynGAP is considered to be inversely related to synaptic potentiation: chemically induced LTP is reported to cause dispersion of SynGAP from neuronal spines, due to CaMKII phosphorylation, and a concomitant increase in AMPAR numbers at the spine (Araki et al., 2015). This inverse relation between SynGAP and AMPA at the synapse is considered due to the GAP activity of SynGAP, whereby SynGAP dispersion following LTP causes activation of Ras activity and this induces a cascade of downstream signals that cause AMPAR insertion in the synapse. However, SynGAP also modulates another small GTPase, Rap, and does this more robustly than for Ras (Krapivinsky et al., 2004). Rap has an opposing effect on synaptic potentiation than Ras (Zhu et al., 2002), and so, SynGAP's dispersion from the synapse, and the effect of this dispersion on Ras activity, is insufficient to explain SynGAP's inverse relation to synaptic potentiation.

A more direct explanation of the inverse relationship of SynGAP with synaptic potentiation is that SynGAP dispersion from the post-synapse following synaptic activity frees up binding domains on PSD95 and thereby makes more "slots" available for other receptors (Opazo et al., 2012). This explanation requires that SynGAP's binding to PSD95 makes some binding domains on PSD95 unavailable. Although this seems to contrast with the results of my experiments, it is possible that SynGAP's binding to PSD95 in LLPS condensates may indeed make some PDZ domain slots unavailable, restricting the number of receptors that can bind to a single PSD95 molecule. While my experiments show that PSD95 molecules in SynGAP LLPS condensates can recruit Nlg1 and AMPAR (via TARP2), they were done at relatively low number densities of receptors, such that at any given time only a few (1-5) receptors were bound to SynGAP condensates. At higher receptor number densities, the number of binding sites available on each PSD95 molecule may indeed be limited by SynGAP's own interactions with PSD95. PSD95's incorporation into LLPS condensates does however dramatically increase the density of available binding sites for receptors at the condensates, even if some of those binding sites are made unavailable due to interactions with SynGAP. However, if PSD95 also forms LLPS condensates with other proteins at the post-synapse, and these interactions do not block any binding sites on PSD95, then SynGAP could indeed function as a negative regulator by occupying PSD95 "slots".

A recent study (Hosokawa et al., 2021) has suggested that another abundant post-synaptic protein, CaMKII, forms LLPS condensates with the cytoplasmic tail of the NMDA receptors subunit GluN2B in the presence of calcium ions. While most of the experiments in this study were done in vitro using fragments of proteins, and very scant live cell data was provided to support the claims made by the authors, some results of this study are of particular interest. A phase-in-phase phenomenon was reported by the authors, whereby CaMKII and GluN2B (more specifically, the cytoplasmic tail of GluN2B), formed a separate liquid phase surrounding an inner liquid phase of PSD95 and the cytoplasmic tail of TARP2 (STGc). Moreover, when the cytoplasmic tail of Nlg1 was added, it also segregated into the PSD95 and STGc (TARP2 cytoplasmic tail) condensates.

The results of Hosokawa et al. show that it is possible that other abundant post-synaptic proteins, such as CaMKII, could also form LLPS condensates. Both STGc (cytoplasmic tail of TARP2) and Nlg1 participate in the inner condensate of the "phase-in-phase", containing PSD95, albeit without the presence of SynGAP. GluN2B and CaMKII remain in the surrounding phase. It is important to note that Nlg1 cytoplasmic tail and PSD95 did not form condensates on their own,

but required a third component, GluN2Bc. These results are consistent with the idea that PSD95 needs a second protein to be incorporated into LLPS condensates. In my experiments, this second protein is SynGAP. Importantly, SynGAP LLPS condensates clearly form at much lower concentrations, of less than 1  $\mu\text{M}$ , in live cells. Hosokawa et al. used concentrations of 10  $\mu\text{M}$  of each protein (fragment) component to see the LLPS condensates in vitro. Thus, SynGAP more readily forms LLPS condensates in live cells, and could therefore be an important aggregator of PSD95 and post-synaptic receptors such as Nlg1 and AMPAR during the early stages of synapse formation, when concentrations of proteins are unlikely to be as high as 10  $\mu\text{M}$  in the dendritic region.

## 4.2 Future experiments

One of the most important remaining issues is to replicate my results in vitro using purified proteins. The in-vitro demonstration showing that SynGAP forms LLPS condensates on its own and that the CC domain and the IDR are essential for LLPS condensate formation would be important. This would support the hypothesis I postulate in this thesis, that SynGAP forms LLPS condensates by itself. These experiments will use the same constructs used in live cell experiments, and tests such as liquid droplet formation and merging, as well as fluorescence recovery after photobleaching (FRAP) will be performed to assess the liquid nature of these condensates in vitro. To perform such experiments, I am collaborating with Dr. Dragomir Milovanovic and his colleagues at DZNE, Berlin to use advanced protein purification methods to accomplish this.

Another important result from Chapter 2, that SynGAP LLPS condensates can be dissolved by CaMKII expression, warrants further study. Synaptic activity induced CaMKII activation could control the dissolution and reformation of SynGAP condensates, and during this process, faster turnover of the receptors and other proteins immobilized within SynGAP LLPS condensates would occur, such as Nlg1 and AMPAR, as well as scaffold proteins like PSD95. While this may seem contrary to the general increase in the spine size and numbers of AMPA receptors associated with LTP, it may in fact be consistent with the hypothesis that the insertion of extra receptors and other proteins into the PSD after LTP requires a dismantling or re-modelling of the PSD (Muller et al., 2000). On the other hand, the dissolution of SynGAP condensates could also reduce SynGAP's ability to recruit PSD95, since PSD95 participates in SynGAP LLPS condensates as a "client". If SynGAP is a negative regulator of synaptic potentiation, my results would fit with the hypothesis of Araki et al., that SynGAP needs to be removed from the post-synapse to allow potentiation to occur, and provides a mechanistic explanation for SynGAP's dispersion from synapses upon CaMKII phosphorylation. Further experiments are required to discriminate between the two possible stated hypotheses:

- A CaMKII expression switch will be developed in L cells, allowing the estimation of SynGAP clustering without CaMKII, after CaMKII expression, and after the inactivation of CaMKII.
- Activation of synapses by glutamate-uncaging will be performed in cultured primary hippocampal neurons, and the mobility of synaptic receptors such as Nlg1 and AMPAR will be assessed by tracking single molecules of these receptors in neuronal spines. The liquid nature of the SynGAP condensates, and their modulation by CaMKII activity, will be assessed by FRAP measurements.

### 4.3 Final summary

In this thesis, I show that:

- SynGAP forms condensates by LLPS, and this requires its IDR and CC domains.
- PSD95 is recruited to SynGAP condensates as a client.
- CaMKII regulates SynGAP LLPS to form/dissolve condensates.
- Nlg1 oligomers can recruit SynGAP condensates to the PM via PSD95.
- GluA1-TARP2 complexes exhibit oligomerization dependent recruitment to SynGAP condensates.
- Binding avidity plays an important role in receptor recruitment and retention at the SynGAP condensates, and may be an important biophysical mechanism at the synapse.

Taken together, these experiments indicate, in living cells, that liquid-liquid phase separation and receptor oligomerization may play an important role in the assembly and function of the post-synapse. They provide much needed clarity on the role of phase-separation, a phenomenon that is increasingly viewed as a vital biophysical mechanism in cells, but for which a majority of data comes from in-vitro experiments that lack sufficient resemblance to live cells.

I hope these findings contribute to our understanding of the biophysical mechanisms by which receptor complexes assemble, turnover, and disassemble at the post-synapse.

## Chapter 5. Materials and methods

### *Cell culture and transfections*

L cells, a kind gift from Rinshi Kasai (Kyoto University) were cultured in Dulbecco's Minimum Essential Medium (DMEM), purchased from Sigma Aldrich (Catalog #: D5796) supplemented with 10% (vol/vol) fetal bovine serum (FBS, Gibco: 10270-106, Lot#: 42G7281K). All of the cells used were mycoplasma free, as determined by using MycoAlert (Lonza: LT07-118) and a Mycoplasma PCR Detection Kit (Beyotime Biotechnology: C0301S). The transfection of cells with the plasmid vectors was performed by lipofection, using the Effectene reagent (Qiagen, catalog #: 301425), according to the manufacturer's recommendations.

For the generation of cell lines stably expressing selected proteins, the cells were transfected with the expression vector (for the pPBpuro expression vector, pCMV-mPBbase was co-transfected). Two days after transfection, the cells were incubated with puromycin (2 µg/ml) containing medium on 10 cm cell-culture grade dishes. After an incubation in the selection medium for a week, cell colonies were partly detached by incubation with 0.25% trypsin, colonies were picked using a pipette tip, and the cells from these colonies replated in glass-bottom dishes (described later in this subsection). The expression levels of isolated cell clones were examined by fluorescence microscopy. The established stable cell lines were routinely cultured in the presence of antibiotics.

For experiments where multiple proteins were expressed in L cells, such as the experiments shown in Figs. 16, 17, 29, and 32, cells were co-transfected with the respective expression vectors using the Effectene transfection reagent according to the manufacturer's recommendation.

For fluorescence microscopy, the cells were plated in a glass-bottom dish with a glass window size of 12 mm in diameter (No.1S, Iwaki: 3971-035), pre-coated with fibronectin (FN, Sigma Aldrich: F1141) by placing 100 µl of 10 µg/ml FN in phosphate buffered saline (PBS: 137 mM NaCl, 8.1 mM NaHPO<sub>4</sub>, 2.7 mM KCl, 1.5 mM KH<sub>2</sub>PO<sub>4</sub>, pH 7.4) on the glass at room temperature for 10 min. The cells were cultured in the complete growth medium for 24–48 h before imaging. For microscope observations, the medium was replaced by a custom ordered Ham's F12 medium (from Nacalai), lacking the following constituents which were then reconstituted at the specified concentrations: 1.8 mM CaCl<sub>2</sub>, 10 nM Cu(II)SO<sub>4</sub>, 30 nM D-Biotin, 300 nM linoleic acid, and 1 mM GlutaMAX. This imaging medium was buffered with 2 mM TES (Dojindo: 348-08371) at pH 7.4. To this medium, a final concentration of 10% (v/v) filtered FBS was added.

### *cDNA constructs*

The cDNAs encoding Halo7, mEGFP, and mCherry were obtained from Promega (G9651) and Clontech (Z2370N, Z2522N), respectively. The cDNAs encoding Nlg1 and Neurexin 1 were PCR amplified from pCAG-NL1AB and pCAG-HA-Nrxn1β AS4(-) vectors, which were a gift from Peter Scheiffele (Addgene plasmid # 15262; <http://n2t.net/addgene:15262>; RRID:Addgene\_15262; Addgene plasmid # 59409; <http://n2t.net/addgene:59409>; RRID:Addgene\_59409). The cDNA encoding PSD95 was a gift from Yuri Nemoto (Kyoto University). The cDNA encoding SynGAP was acquired from the PlasmID repository at Harvard Medical School.

The sequences encoding various proteins were subcloned into the following vectors: pEGFP (Clontech: Z2370N), pCAGplay (a custom vector containing the CMV enhancer and chicken β-actin promoter and rabbit β-globin polyadenylation signal region, developed by Kawaguchi et al., 2006), and pPBpuro (a custom vector with the PiggyBac terminal repeat

sequence and the high expression promoter consisting of chicken  $\beta$  actin promoter, CAG promoter with an artificial intron, and CMV IE, developed by Nakamura et al., 2020). pCMV-mPBase was a kind gift from Michiyuki Matsuda (Kyoto University).

### *Cell aggregation experiments*

For cell aggregation experiments, L cell clones stably expressing the E-cadherin, Nlg1, or Neurexin were grown until 90% confluency in 6 cm cell-culture dishes, and then treated with 1 mL 0.05% trypsin (without EDTA) in Hanks' balanced salt solution (HBSS) buffered with 2 mM TES (Dojindo: 348-08371), and incubated at 37°C for 10 min. Cells were detached with mild tapping, and resuspended in the imaging medium. Cells were then centrifuged at 1,000 RPM for 2 min, and the cell pellet was resuspended in the imaging medium. Cells were counted and diluted to approximately  $10^6$  cells/ml. The cell suspension (300  $\mu$ L) was placed in the 1.5 mL Eppendorf tube and used for cell aggregation experiments. When cells from two different clones were mixed (as in the case of Nlg1 + Nxn cell aggregation assays), 150  $\mu$ L of each cell suspension (at a cell density of  $10^6$  cells/mL) was mixed in a 1.5 mL Eppendorf tube. Cells in each Eppendorf tube were immersed in a water-bath at 37°C with shaking at 100 RPM, and at each indicated time point, the tube was vortexed briefly to resuspend the cells, and an aliquot of 10  $\mu$ L was placed on the cover glass part of the glass-bottom dish and observed by phase-contrast microscopy. Cell 'particles', including both single cells and cell clumps, were counted in the images using a custom ImageJ script. The cell aggregation coefficient was estimated as the number of cell particles detected at the indicated time point divided by the number of cell particles detected at time zero.

### *Confocal imaging and analysis*

To obtain confocal fluorescence images of the cells at 37°C, we employed a custom-built spinning disk confocal microscope based on an Olympus IX83 (placed in a home-built environmental chamber) equipped with an Olympus objective UApoN100XTIR, a Yokogawa confocal unit, CSU-W1, and a Hamamatsu Photonics ORCA-Flash 4.0 V2 plus sCMOS camera. Confocal images of L cells were recorded using the same instrument setting: 30% of the maximum laser power of the Cobolt 488 nm laser and 300 ms integration for each image. The confocal image slices of each L cell were taken every 0.5  $\mu$ m starting from the basal plasma membrane.

To evaluate the clustering coefficient, confocal images of 512x512 pixels taken at 2  $\mu$ m above the basal plasma membrane was analyzed to detect clusters and measure the total cell area (excluding the nucleus) using the open-source machine-learning based imaging software, 'ilastik' (Berg et al., 2019). The clustering coefficient was defined as the total intensity of all pixels identified as 'clusters' in an image, divided by the total area of the cell in pixels. This was plotted against the average intensity of a pixel in the cell area.

### *EGFP reconstitution and imaging*

Purified EGFP (Biovision, catalog #: 4999) was reconstituted in the imaging buffer and imaged by the same confocal microscope with the same instrument setting used to observe L cells for evaluating the cluster coefficient. EGFP was imaged at various concentrations covering the concentration ranges in L cells, and the average pixel intensity of EGFP from at least 3 separate titrations, was plotted as a function of concentration. This data set was fitted with a linear function, which was then used to convert the average pixel intensity of mEGFP-SynGAP constructs to concentrations.

### *Fluorescence labelling of Halo-tagged proteins for single-molecule fluorescence imaging*

To fluorescently label Halo tags bound to target proteins expressed in cells, the cells were incubated at 37°C in complete growth medium containing 20 nM TMR-Halo linker (Promega: G8251), to achieve maximum labelling efficiency for experiments to estimate fractions of monomers, dimers, and oligomers or 60 nM Setau647-Halo linker (custom ordered) for 30 min, in experiments for single-molecule tracking. The labelling efficiency with TMR was estimated as shown in Appendix 1. The percentages of fluorescent proteins were estimated to be  $88 \pm 2.2\%$  for Halo7, and  $75 \pm 2.3\%$  for mEGFP, using the control monomeric proteins mGFP-CD47-Halo7 (Halo7 tag located in the cytoplasm), as shown in Appendix 1. After labelling, cells were washed at least 4 times with imaging medium prior to imaging.

Primary hippocampal neurons were labelled with TMR-Halo linker as described. Labelled neurons were washed with ACSF medium at least 6 times prior to imaging.

### *Neuron culture + viral transfections*

Hippocampi from E17-E19 Wister embryos were dissected and dissociated following the protocol described in Pierce Primary Neuron Isolation Kit (Thermo Fischer, manual number: MAN0016221). Cells were plated at a density of approximately  $4 \times 10^5$  cells/dish on glass-bottom dishes, coated with 0.01% (w/v) poly-L-lysine overnight, and subsequently washed with double distilled water 5 times. A feeder layer of astrocytes that had been originally plated on the circular plastic part of the glass-bottom dishes the day before neuronal culture in DMEM (Sigma-Aldrich) containing 15% FBS (Gibco). The isolated primary neurons were plated in 2 mL MEM containing 2% (v/v) B27 (Invitrogen) and 5% (v/v) FBS. 10  $\mu$ L of AraC was added 24 h after neurons were plated to prevent the proliferation of glial cells. These neurons were imaged between DIV 18 - DIV 21 in artificial cerebrospinal fluid (ACSF) buffered with 10 mM HEPES at pH 7.4.

To express target proteins in primary hippocampal neurons, cDNAs encoding the respective target proteins were incorporated into the pLVSI-CMV Pur vector (Takara, Code #: 6183). Lentivirus particles were produced by transfecting LentiX 293T cells (Takara, Code #: 632180) with the plasmids from the Lentiviral High Titer packaging mix (Takara, Code #: 6194) by following the manufacturer's instructions. Lentivirus particles were added to primary hippocampal neurons at DIV 6-7.

### *Single-molecule fluorescence imaging and analysis*

All single-molecule observations were performed at 37°C, using a microscope housed in a homemade environmental chamber. Fluorescently labelled molecules in cells were excited by total internal reflection (TIR) illumination (for those on the basal PM) using objective-lens-type TIRF microscopes, which were constructed on Olympus and Nikon inverted microscopes (IX-83 and TiE, respectively) equipped with 100x 1.49 NA objective lenses (UApoN100XTIRF and ApoTIRF100XC, respectively). The three-color fluorescence images were separated into the three detection arms of the microscope by a dichroic mirror (Chroma: ZT640rdc-UF3). The detection arms were equipped with bandpass filters of ET525/50m, ET600/50m, or ET700/75m (all from Chroma), and the images were recorded at each arm with a two-stage microchannel plate intensifier (Hamamatsu Photonics: C9016-02MLP24), lens-coupled to a scientific complementary metal oxide semiconductor (sCMOS) camera (ORCA-Flash ver4.0 V2 plus, Hamamatsu Photonics: C11440-22CU). The final magnifications were 133 and 100x, resulting in pixel sizes of ~50 and 65 nm respectively. Only the 642 nm line channel was used for single-molecule observations, while the 488 nm and 561 nm lines were used to image PSD95-EGFP and mCherry-

SynGAP clusters respectively. The incident excitation laser powers at the sample plane were  $0.07 \mu\text{W}/\mu\text{m}^2$  for the 488 nm line (for mEGFP, Coherent: OBIS 488- 100 LS),  $0.06 \mu\text{W}/\mu\text{m}^2$  for the 561 nm line (for TMR, Coherent: OBIS 561-100 LS), and  $0.4 \mu\text{W}/\mu\text{m}^2$  for the 642 nm line (for Setau647, Omicron: LuuXPlus 640-140). For triple-color experiments, the 488 nm and 561 nm line channels, for imaging PSD95-EGFP and mCherry-SynGAP clusters respectively, were imaged at a frame rate of 1 Hz with an exposure of 33 ms, whereas the 642 nm line channel, used for single-molecule imaging of Halo tagged trans-membrane receptors, was imaged at a frame rate of 10 Hz with an exposure of 33ms. All three channels were staggered, with 33 ms intervals between successive images of each channel to minimize background due to cross channel fluorescence. For analysis of single-color movies to estimate the monomer, dimer, and oligomer fractions of Halo-tagged constructs, the incident excitation laser powers at the sample plane was  $0.5 \mu\text{W}/\mu\text{m}^2$ . All other analysis was done in the same way as described above.

Each individual fluorescent spot in the image was identified and tracked by using an in-house computer program, developed by Fujiwara et al. (2016). The superimposition of images in different colors obtained by three separate cameras was conducted using the method developed by Koyama-Honda et al. (2005). Transient immobilization events were detected in single-molecule trajectories by using the same program as for single fluorescent spot tracking, and by setting the upper threshold for diffusing spots at  $0.0083 \mu\text{m}^2/\text{s}$ . Spots that exhibited immobilizations for longer than 0.5 s were selected for further analysis.

To detect whether immobilized spots were located within SynGAP LLPS condensates, images from the 561 nm line channel, used to image SynGAP, were binarized using a custom made ImageJ script. The binarized SynGAP channel masks were then used in an in-house computer program to detect if trajectories of immobilized spots were located inside or outside the binarized areas.

#### *Fluorescence recovery after photobleaching (FRAP) assays and analysis*

For the in-cell fluorescence recovery after photobleaching (FRAP) experiments, the same Nikon inverted microscope was used as described previously. Recordings were done at  $37^\circ\text{C}$ , at 1 Hz, using a 40X oil-immersion lens (Nikon CFI 40X), resulting in a pixel size of 211 nm. The photobleached-observed area was a circular region of  $\sim 1 \mu\text{m}$  in diameter, and photobleaching was performed by illuminating the area with a 488 nm laser beam at 50% of the full laser power for 0.5 s.

#### *Immunofluorescence*

The cultured cells on the FN-coated glass-base dish were fixed with paraformaldehyde (4% w/v) at room temperature (RT) for 20 min. The fixed cells were then washed with HBSS two times, then incubated with 0.1% Triton X-100 and 2% BSA in PBS for 10 min, and then washed two times with the imaging medium containing FBS. The cells were immuno-stained for 1 h with anti-HA primary antibody conjugated to Alexa Fluor 555 (Invitrogen, product number: 26182-A555) at RT. This was followed by four washes with the imaging medium. The cells were then imaged in the imaging medium with home-built TIRF microscope, as described in the section above. Imaging was done with the 561 nm line channel.

#### *Statistical analysis and software*

Conventional TIRF images were processed and analyzed using ImageJ (Schindelin et al., 2012), and ilastik (Berg et al., 2019). Curve fittings were performed using Origin 2016 (OriginLab).



Statistical analyses were performed using OriginPro 2016 and Excel (Microsoft).  $P < 0.05$  was defined as statistically significant. Figures and videos were edited using BioRender (biorender.com) and ImageJ, respectively.

For determining the fractions of monomer, dimers, and oligomers, the signal intensities of all of the individual fluorescent spots detected in the initial twenty frames in single fluorescent-molecule imaging movies were determined, and each histogram was fitted by the sum of four lognormal functions using OriginPro, as previously demonstrated by Morise et al. (2019). Greater oligomer fractions were not detected in the present research. The signal intensity distribution for single molecules (monomers) was obtained by using the monomer reference molecule Halo7-LDLTM expressed at number densities similar to those of the molecules in study. They could always be fitted sufficiently well using a single lognormal function.

#### *Data availability*

All data (including raw data and all analyses) can be made available upon request.

## Bibliography

- Arac, D., Boucard, A.A., Ozkan, E., Strop, P., Newell, E., Sudhof, T.C., and Brunger, A.T. (2007). Structures of neuroligin-1 and the neuroligin-1/neurexin-1 beta complex reveal specific protein-protein and protein-Ca<sup>2+</sup> interactions. *Neuron* *56*, 992-1003. 10.1016/j.neuron.2007.12.002.
- Araki, Y., Hong, I., Gamache, T.R., Ju, S., Collado-Torres, L., Shin, J.H., and Hugarir, R.L. (2020). SynGAP isoforms differentially regulate synaptic plasticity and dendritic development. *Elife* *9*. 10.7554/eLife.56273.
- Araki, Y., Zeng, M., Zhang, M., and Hugarir, R.L. (2015). Rapid dispersion of SynGAP from synaptic spines triggers AMPA receptor insertion and spine enlargement during LTP. *Neuron* *85*, 173-189. 10.1016/j.neuron.2014.12.023.
- Bademosi, A.T., Lauwers, E., Padmanabhan, P., Odierna, L., Chai, Y.J., Papadopoulos, A., Goodhill, G.J., Verstreken, P., van Swinderen, B., and Meunier, F.A. (2016). In vivo single-molecule imaging of syntaxin1A reveals polyphosphoinositide- and activity-dependent trapping in presynaptic nanoclusters. *Nature Communications* *7*, 13660. 10.1038/ncomms13660.
- Berg, S., Kutra, D., Kroeger, T., Straehle, C.N., Kausler, B.X., Haubold, C., Schiegg, M., Ales, J., Beier, T., Rudy, M., et al. (2019). ilastik: interactive machine learning for (bio)image analysis. *Nature Methods* *16*, 1226-1232. 10.1038/s41592-019-0582-9.
- Bliss, T.V.P., and Collingridge, G.L. (2013). Expression of NMDA receptor-dependent LTP in the hippocampus: bridging the divide. *Molecular Brain* *6*, 5. 10.1186/1756-6606-6-5.
- Bosch, M., Castro, J., Saneyoshi, T., Matsuno, H., Sur, M., and Hayashi, Y. (2014). Structural and Molecular Remodeling of Dendritic Spine Substructures during Long-Term Potentiation. *Neuron* *82*, 444-459.
- Brangwynne, Clifford P., Tompa, P., and Pappu, Rohit V. (2015). Polymer physics of intracellular phase transitions. *Nature Physics* *11*, 899-904. 10.1038/nphys3532.
- Budreck, E.C., Kwon, O.-B., Jung, J.H., Baudouin, S., Thommen, A., Kim, H.-S., Fukazawa, Y., Harada, H., Tabuchi, K., Shigemoto, R., et al. (2013). Neuroligin-1 controls synaptic abundance of NMDA-type glutamate receptors through extracellular coupling. *Proceedings of the National Academy of Sciences* *110*, 725-730. 10.1073/pnas.1214718110.
- Cabantous, S., Terwilliger, T.C., and Waldo, G.S. (2005). Protein tagging and detection with engineered self-assembling fragments of green fluorescent protein. *Nature Biotechnology* *23*, 102-107. 10.1038/nbt1044.
- Carlin, R.K., Grab, D.J., Cohen, R.S., and Siekevitz, P. (1980). Isolation and characterization of postsynaptic densities from various brain regions: enrichment of different types of postsynaptic densities. *The Journal of cell biology* *86*, 831-845.

- Catsburg, L.A., Westra, M., van Schaik, A.M., and MacGillavry, H.D. (2022). Dynamics and nanoscale organization of the postsynaptic endocytic zone at excitatory synapses. *Elife* *11*. 10.7554/eLife.74387.
- Chanda, S., Hale, W.D., Zhang, B., Wernig, M., and Sudhof, T.C. (2017). Unique versus Redundant Functions of Neuroligin Genes in Shaping Excitatory and Inhibitory Synapse Properties. *J Neurosci* *37*, 6816-6836. 10.1523/JNEUROSCI.0125-17.2017.
- Chen, B.-S., and Roche, K.W. (2007). Regulation of NMDA receptors by phosphorylation. *Neuropharmacology* *53*, 362-368.
- Chen, H.-J., Rojas-Soto, M., Oguni, A., and Kennedy, M.B. (1998). A Synaptic Ras-GTPase Activating Protein (p135 SynGAP) Inhibited by CaM Kinase II. *Neuron* *20*, 895-904. 10.1016/S0896-6273(00)80471-7.
- Chen, X., Nelson, C.D., Li, X., Winters, C.A., Azzam, R., Sousa, A.A., Leapman, R.D., Gainer, H., Sheng, M., and Reese, T.S. (2011). PSD-95 Is Required to Sustain the Molecular Organization of the Postsynaptic Density. *The Journal of Neuroscience* *31*, 6329. 10.1523/JNEUROSCI.5968-10.2011.
- Chen, X., Vinade, L., Leapman, R.D., Petersen, J.D., Nakagawa, T., Phillips, T.M., Sheng, M., and Reese, T.S. (2005). Mass of the postsynaptic density and enumeration of three key molecules. *Proc Natl Acad Sci U S A* *102*, 11551-11556. 10.1073/pnas.0505359102.
- Cheng, D., Hoogenraad, C.C., Rush, J., Ramm, E., Schlager, M.A., Duong, D.M., Xu, P., Wijayawardana, S.R., Hanfelt, J., Nakagawa, T., et al. (2006). Relative and absolute quantification of postsynaptic density proteome isolated from rat forebrain and cerebellum. *Mol Cell Proteomics* *5*, 1158-1170. 10.1074/mcp.D500009-MCP200.
- Chetkovich, D.M., Chen, L., Stocker, T.J., Nicoll, R.A., and Brecht, D.S. (2002). Phosphorylation of the Postsynaptic Density-95 (PSD-95)/Discs Large/Zona Occludens-1 Binding Site of Stargazin Regulates Binding to PSD-95 and Synaptic Targeting of AMPA Receptors. *The Journal of Neuroscience* *22*, 5791. 10.1523/JNEUROSCI.22-14-05791.2002.
- Choquet, D., and Triller, A. (2003). The role of receptor diffusion in the organization of the postsynaptic membrane. *Nat Rev Neurosci* *4*, 251-265. 10.1038/nrn1077.
- Craven, S.E., El-Husseini, A.E., and Brecht, D.S. (1999). Synaptic Targeting of the Postsynaptic Density Protein PSD-95 Mediated by Lipid and Protein Motifs. *Neuron* *22*, 497-509. 10.1016/S0896-6273(00)80705-9.
- Dahan, M., Levi, S., Luccardini, C., Rostaing, P., Riveau, B., and Triller, A. (2003). Diffusion dynamics of glycine receptors revealed by single-quantum dot tracking. *Science* *302*, 442-445.
- Dean, C., Scholl, F.G., Choih, J., DeMaria, S., Berger, J., Isacoff, E., and Scheiffele, P. (2003). Neurexin mediates the assembly of presynaptic terminals. *Nature neuroscience* *6*, 708-716.

Dosemeci, A., and Jaffe, H. (2010). Regulation of phosphorylation at the postsynaptic density during different activity states of Ca<sup>2+</sup>/calmodulin-dependent protein kinase II. *Biochemical and Biophysical Research Communications* 391, 78-84.

Eggermann, E., Bucurenciu, I., Goswami, S.P., and Jonas, P. (2012). Nanodomain coupling between Ca<sup>2+</sup> channels and sensors of exocytosis at fast mammalian synapses. *Nature Reviews Neuroscience* 13, 7-21. 10.1038/nrn3125.

Feinberg, E.H., Vanhoven, M.K., Bendesky, A., Wang, G., Fetter, R.D., Shen, K., and Bargmann, C.I. (2008). GFP Reconstitution Across Synaptic Partners (GRASP) defines cell contacts and synapses in living nervous systems. *Neuron* 57, 353-363. 10.1016/j.neuron.2007.11.030.

Frey, S., Richter, R.P., and Görlich, D. (2006). FG-Rich Repeats of Nuclear Pore Proteins Form a Three-Dimensional Meshwork with Hydrogel-Like Properties. *Science* 314, 815-817. 10.1126/science.1132516.

Fujiwara, T.K., Iwasawa, K., Kalay, Z., Tsunoyama, T.A., Watanabe, Y., Umemura, Y.M., Murakoshi, H., Suzuki, K.G., Nemoto, Y.L., Morone, N., and Kusumi, A. (2016). Confined diffusion of transmembrane proteins and lipids induced by the same actin meshwork lining the plasma membrane. *Mol Biol Cell* 27, 1101-1119. 10.1091/mbc.E15-04-0186.

Gamache, T.R., Araki, Y., and Huganir, R.L. (2020). Twenty Years of SynGAP Research: From Synapses to Cognition. *J Neurosci* 40, 1596-1605. 10.1523.

Giannone, G., Mondin, M., Grillo-Bosch, D., Tessier, B., Saint-Michel, E., Czondor, K., Sainlos, M., Choquet, D., and Thoumine, O. (2013). Neurexin-1beta binding to neuroligin-1 triggers the preferential recruitment of PSD-95 versus gephyrin through tyrosine phosphorylation of neuroligin-1. *Cell Rep* 3, 1996-2007. 10.1016/j.celrep.2013.05.013.

Giese, K.P., Fedorov, N.B., Filipkowski, R.K., and Silva, A.J. (1998). Autophosphorylation at Thr286 of the  $\alpha$  Calcium-Calmodulin Kinase II in LTP and Learning. *Science* 279, 870-873. 10.1126/science.279.5352.870.

Gray, N.W., Weimer, R.M., Bureau, I., and Svoboda, K. (2006). Rapid redistribution of synaptic PSD-95 in the neocortex in vivo. *PLoS Biol* 4, e370. 10.1371/journal.pbio.0040370.

Groc, L., Heine, M., Cousins Sarah, L., Stephenson, F.A., Lounis, B., Cognet, L., and Choquet, D. (2006). NMDA receptor surface mobility depends on NR2A-2B subunits. *Proceedings of the National Academy of Sciences* 103, 18769-18774. 10.1073/pnas.0605238103.

Holler, S., Kostinger, G., Martin, K.A.C., Schuhknecht, G.F.P., and Stratford, K.J. (2021). Structure and function of a neocortical synapse. *Nature* 591, 111-116. 10.1038/s41586-020-03134-2.

Hsueh, Y.-P., and Sheng, M. (1999). Requirement of N-terminal Cysteines of PSD-95 for PSD-95 Multimerization and Ternary Complex Formation, but Not for Binding to Potassium Channel Kv1.4 \*. *Journal of Biological Chemistry* 274, 532-536. 10.1074/jbc.274.1.532.

Irie, M., Hata, Y., Takeuchi, M., Ichtchenko, K., Toyoda, A., Hirao, K., Takai, Y., Rosahl, T., and Südhof, T. (1997). Binding of neuroligins to PSD-95. *Science* *277*, 1511-1515.

Isaac, J.T.R., Nicoll, R.A., and Malenka, R.C. (1995). Evidence for silent synapses: Implications for the expression of LTP. *Neuron* *15*, 427-434.

Jacob, T.C., Bogdanov, Y.D., Magnus, C., Saliba, R.S., Kittler, J.T., Haydon, P.G., and Moss, S.J. (2005). Gephyrin regulates the cell surface dynamics of synaptic GABAA receptors. *Journal of Neuroscience* *25*, 10469-10478.

Jeong, J., Pandey, S., Li, Y., Badger, J.D., 2nd, Lu, W., and Roche, K.W. (2019). PSD-95 binding dynamically regulates NLGN1 trafficking and function. *Proc Natl Acad Sci U S A* *116*, 12035-12044. 10.1073/pnas.1821775116.

Jurado, S., Goswami, D., Zhang, Y., Molina, Alfredo J.M., Südhof, Thomas C., and Malenka, Robert C. (2013). LTP Requires a Unique Postsynaptic SNARE Fusion Machinery. *Neuron* *77*, 542-558.

Kawaguchi, S.-y., and Hirano, T. (2006). Integrin  $\alpha3\beta1$  suppresses long-term potentiation at inhibitory synapses on the cerebellar Purkinje neuron. *Molecular and Cellular Neuroscience* *31*, 416-426.

Kellermayer, B., Ferreira, J.S., Dupuis, J., Levet, F., Grillo-Bosch, D., Bard, L., Linarès-Loyez, J., Bouchet, D., Choquet, D., Rusakov, D.A., et al. (2018). Differential Nanoscale Topography and Functional Role of GluN2-NMDA Receptor Subtypes at Glutamatergic Synapses. *Neuron* *100*, 106-119.e107.

Kerchner, G.A., and Nicoll, R.A. (2008). Silent synapses and the emergence of a postsynaptic mechanism for LTP. *Nature reviews. Neuroscience* *9*, 813-825. 10.1038/nrn2501.

Kim, E., Naisbitt, S., Hsueh, Y.-P., Rao, A., Rothschild, A., Craig, A.M., and Sheng, M. (1997). GKAP, a Novel Synaptic Protein That Interacts with the Guanylate Kinase-like Domain of the PSD-95/SAP90 Family of Channel Clustering Molecules. *Journal of Cell Biology* *136*, 669-678. 10.1083/jcb.136.3.669.

Kim, E., and Sheng, M. (2004). PDZ domain proteins of synapses. *Nat Rev Neurosci* *5*, 771-781. 10.1038/nrn1517.

Kim, J.H., Liao, D., Lau, L.-F., and Huganir, R.L. (1998). SynGAP: a Synaptic RasGAP that Associates with the PSD-95/SAP90 Protein Family. *Neuron* *20*, 683-691. 10.1016/S0896-6273(00)81008-9.

Koyama-Honda, I., Ritchie, K., Fujiwara, T., Iino, R., Murakoshi, H., Kasai, R.S., and Kusumi, A. (2005). Fluorescence imaging for monitoring the colocalization of two single molecules in living cells. *Biophys J* *88*, 2126-2136. 10.1529/biophysj.104.048967.

Lomo, T. (1966). Frequency potentiation of excitatory synaptic activity in dentate area of hippocampal formation. (Blackwell Science Ltd PO BOX 88, OSNEY MEAD, OXFORD OX2 ONE, OXON, ENGLAND), pp. 128-&.

Lowenthal, M.S., Markey, S.P., and Dosemeci, A. (2015). Quantitative mass spectrometry measurements reveal stoichiometry of principal postsynaptic density proteins. *J Proteome Res* *14*, 2528-2538. 10.1021/acs.jproteome.5b00109.

MacGillavry, H.D., Song, Y., Raghavachari, S., and Blanpied, T.A. (2013). Nanoscale scaffolding domains within the postsynaptic density concentrate synaptic AMPA receptors. *Neuron* *78*, 615-622. 10.1016/j.neuron.2013.03.009.

Matsuzaki, M., Honkura, N., Ellis-Davies, G.C.R., and Kasai, H. (2004). Structural basis of long-term potentiation in single dendritic spines. *Nature* *429*, 761-766. 10.1038/nature02617.

Mehta, N.B., Molisch, A.F., Wu, J., and Zhang, J. (2006). Approximating the Sum of Correlated Lognormal or, Lognormal-Rice Random Variables. 11-15 June 2006. pp. 1605-1610.

Milovanovic, D., Wu, Y., Bian, X., and De Camilli, P. (2018). A liquid phase of synapsin and lipid vesicles. *Science* *361*, 604-607. 10.1126/science.aat5671.

Mondin, M., Labrousse, V., Hosy, E., Heine, M., Tessier, B., Levet, F., Poujol, C., Blanchet, C., Choquet, D., and Thoumine, O. (2011). Neurexin-neuroigin adhesions capture surface-diffusing AMPA receptors through PSD-95 scaffolds. *J Neurosci* *31*, 13500-13515. 10.1523/JNEUROSCI.6439-10.2011.

Moser, E.I., Krobot, K.A., Moser, M.-B., and Morris, R.G.M. (1998). Impaired Spatial Learning after Saturation of Long-Term Potentiation. *Science* *281*, 2038-2042. 10.1126/science.281.5385.2038.

Muller, D., Toni, N., and Buchs, P.-A. (2000). Spine changes associated with long-term potentiation. *Hippocampus* *10*, 596-604.

Mutch, S.A., Fujimoto, B.S., Kuyper, C.L., Kuo, J.S., Bajjalieh, S.M., and Chiu, D.T. (2007). Deconvolving Single-Molecule Intensity Distributions for Quantitative Microscopy Measurements. *Biophysical Journal* *92*, 2926-2943.

Nair, D., Hosy, E., Petersen, J.D., Constals, A., Giannone, G., Choquet, D., and Sibarita, J.B. (2013). Super-resolution imaging reveals that AMPA receptors inside synapses are dynamically organized in nanodomains regulated by PSD95. *J Neurosci* *33*, 13204-13224. 10.1523/JNEUROSCI.2381-12.2013.

Nakamura, A., Oki, C., Kato, K., Fujinuma, S., Maryu, G., Kuwata, K., Yoshii, T., Matsuda, M., Aoki, K., and Tsukiji, S. (2020). Engineering Orthogonal, Plasma Membrane-Specific SLIPT Systems for Multiplexed Chemical Control of Signaling Pathways in Living Single Cells. *ACS Chemical Biology* *15*, 1004-1015. 10.1021/acscchembio.0c00024.

- Nose, A., Nagafuchi, A., and Takeichi, M. (1988). Expressed recombinant cadherins mediate cell sorting in model systems. *Cell* 54, 993-1001. 10.1016/0092-8674(88)90114-6.
- Okabe, S., Kim, H.-D., Miwa, A., Kuriu, T., and Okado, H. (1999). Continual remodeling of postsynaptic density and its regulation by synaptic activity. *Nature Neuroscience* 2, 804-811. 10.1038/12175.
- Opazo, P., Sainlos, M., and Choquet, D. (2012). Regulation of AMPA receptor surface diffusion by PSD-95 slots. *Curr Opin Neurobiol* 22, 453-460. 10.1016/j.conb.2011.10.010.
- Penn, A.C., Zhang, C.L., Georges, F., Royer, L., Breillat, C., Hosy, E., Petersen, J.D., Humeau, Y., and Choquet, D. (2017). Hippocampal LTP and contextual learning require surface diffusion of AMPA receptors. *Nature* 549, 384-388. 10.1038/nature23658.
- Poulopoulos, A., Soykan, T., Tuffy, L.P., Hammer, M., Varoqueaux, F., and Brose, N. (2012). Homodimerization and isoform-specific heterodimerization of neuroligins. *Biochem J* 446, 321-330. 10.1042/BJ20120808.
- Ribic, A., and Biederer, T. (2019). Emerging Roles of Synapse Organizers in the Regulation of Critical Periods. *Neural Plast* 2019, 1538137-1538137. 10.1155/2019/1538137.
- Schindelin, J., Arganda-Carreras, I., Frise, E., Kaynig, V., Longair, M., Pietzsch, T., Preibisch, S., Rueden, C., Saalfeld, S., Schmid, B., et al. (2012). Fiji: an open-source platform for biological-image analysis. *Nature Methods* 9, 676-682. 10.1038/nmeth.2019.
- Sheng, M., and Hoogenraad, C.C. (2007). The postsynaptic architecture of excitatory synapses: a more quantitative view. *Annu Rev Biochem* 76, 823-847. 10.1146/annurev.biochem.76.060805.160029.
- Shi, Y., Lu, W., Milstein, A.D., and Nicoll, R.A. (2009). The stoichiometry of AMPA receptors and TARPs varies by neuronal cell type. *Neuron* 62, 633-640. 10.1016/j.neuron.2009.05.016.
- Shibata, A.C., Fujiwara, T.K., Chen, L., Suzuki, K.G., Ishikawa, Y., Nemoto, Y.L., Miwa, Y., Kalay, Z., Chadda, R., Naruse, K., and Kusumi, A. (2012). Archipelago architecture of the focal adhesion: membrane molecules freely enter and exit from the focal adhesion zone. *Cytoskeleton (Hoboken)* 69, 380-392. 10.1002/cm.21032.
- Shipman, S.L., and Nicoll, R.A. (2012). Dimerization of postsynaptic neuroligin drives synaptic assembly via transsynaptic clustering of neuroligin. *Proc Natl Acad Sci U S A* 109, 19432-19437. 10.1073/pnas.1217633109.
- Specht, C.G., and Triller, A. (2008). The dynamics of synaptic scaffolds. *Bioessays* 30, 1062-1074. 10.1002/bies.20831.

Sturgill, J.F., Steiner, P., Czervionke, B.L., and Sabatini, B.L. (2009). Distinct domains within PSD-95 mediate synaptic incorporation, stabilization, and activity-dependent trafficking. *J Neurosci* 29, 12845-12854. 10.1523/JNEUROSCI.1841-09.2009.

Sudhof, T.C. (2008). Neuroligins and neuroligins link synaptic function to cognitive disease. *Nature* 455, 903-911. 10.1038/nature07456.

Sugiyama, Y., Kawabata, I., Sobue, K., and Okabe, S. (2005). Determination of absolute protein numbers in single synapses by a GFP-based calibration technique. *Nat Methods* 2, 677-684. 10.1038/nmeth783.

Trotter, J.H., Hao, J., Maxeiner, S., Tsetsenis, T., Liu, Z., Zhuang, X., and Sudhof, T.C. (2019). Synaptic neuroligin-1 assembles into dynamically regulated active zone nanoclusters. *J Cell Biol* 218, 2677-2698. 10.1083/jcb.201812076.

Tsetsenis, T., Boucard, A.A., Arac, D., Brunger, A.T., and Sudhof, T.C. (2014). Direct visualization of trans-synaptic neuroligin-neuroligin interactions during synapse formation. *J Neurosci* 34, 15083-15096. 10.1523/JNEUROSCI.0348-14.2014.

Uchida, N., Honjo, Y., Johnson, K.R., Wheelock, M.J., and Takeichi, M. (1996). The catenin/cadherin adhesion system is localized in synaptic junctions bordering transmitter release zones. *Journal of Cell Biology* 135, 767-779. 10.1083/jcb.135.3.767.

Wright, P.E., and Dyson, H.J. (2014). Intrinsically disordered proteins in cellular signalling and regulation. *Nature Reviews Molecular Cell Biology* 16, 18-29. 10.1038/nrm3920.

Xu, W., Schlüter, O.M., Steiner, P., Czervionke, B.L., Sabatini, B., and Malenka, R.C. (2008). Molecular Dissociation of the Role of PSD-95 in Regulating Synaptic Strength and LTD. *Neuron* 57, 248-262. 10.1016/j.neuron.2007.11.027.

Zeng, M., Chen, X., Guan, D., Xu, J., Wu, H., Tong, P., and Zhang, M. (2018). Reconstituted Postsynaptic Density as a Molecular Platform for Understanding Synapse Formation and Plasticity. *Cell* 174, 1172-1187 e1116. 10.1016/j.cell.2018.06.047.

Zeng, M., Shang, Y., Araki, Y., Guo, T., Huganir, R.L., and Zhang, M. (2016). Phase Transition in Postsynaptic Densities Underlies Formation of Synaptic Complexes and Synaptic Plasticity. *Cell* 166, 1163-1175 e1112. 10.1016/j.cell.2016.07.008.

Zhang, H., Zhang, C., Vincent, J., Zala, D., Benstaali, C., Sainlos, M., Grillo-Bosch, D., Daburon, S., Coussen, F., Cho, Y., et al. (2018). Modulation of AMPA receptor surface diffusion restores hippocampal plasticity and memory in Huntington's disease models. *Nature Communications* 9, 4272. 10.1038/s41467-018-06675-3.

Zhao, Y., Chen, S., Swensen, A.C., Qian, W.-J., and Gouaux, E. (2019). Architecture and subunit arrangement of native AMPA receptors elucidated by cryo-EM. *Science* 364, 355-362. 10.1126/science.aaw8250.



## Appendices

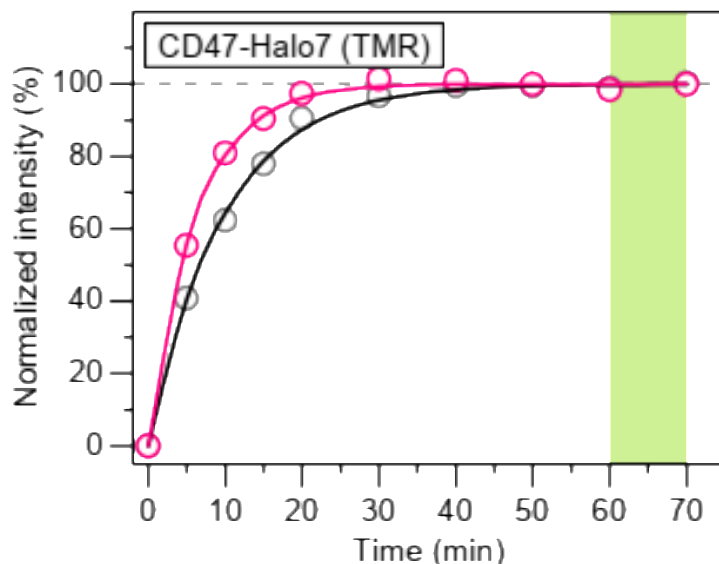
### Appendix 1- Labelling efficacy of TMR-Halo ligand for Halo tagged trans-membrane proteins

To estimate the labelling efficacy of Halo-tagged trans-membrane proteins in live cells, using TMR dye conjugated with Halo ligand, plasma membrane signal of Halo-tagged CD47 protein, in live cells, was measured with increasing incubation periods with TMR dye. Two different concentrations of TMR dye, 5 nM and 2.5 nM, were used. In the observation period after 60 min, the concentration of TMR dye was doubled, to ensure that no unlabeled protein remained. As shown in Fig 35a and 35b below, incubation with TMR dye at a concentration of 5 nM or higher, for a period of 30 min, was sufficient to label almost all CD47 molecules.

To estimate the percentage of Halo and mEGFP tagged molecules that were actually fluorescent, taking into account misfolding, slow folding, and cleavage of the tagged proteins, a monomeric molecule, with both Halo and mEGFP tags, GFP-CD47-Halo (intracellular Halo tag) was labelled with SaraFluor650-Halo. The percentage of Halo spots colocalized with mEGFP spots, and the percentage of mEGFP spots colocalized with Halo spots was estimated using single-molecule imaging and colocalization analysis, as shown in Fig 35c.

The experiments to estimate labelling efficacy were performed by Dr. Taka-aki Tsunoyama from the Membrane Cooperativity Unit, OIST.

(a)



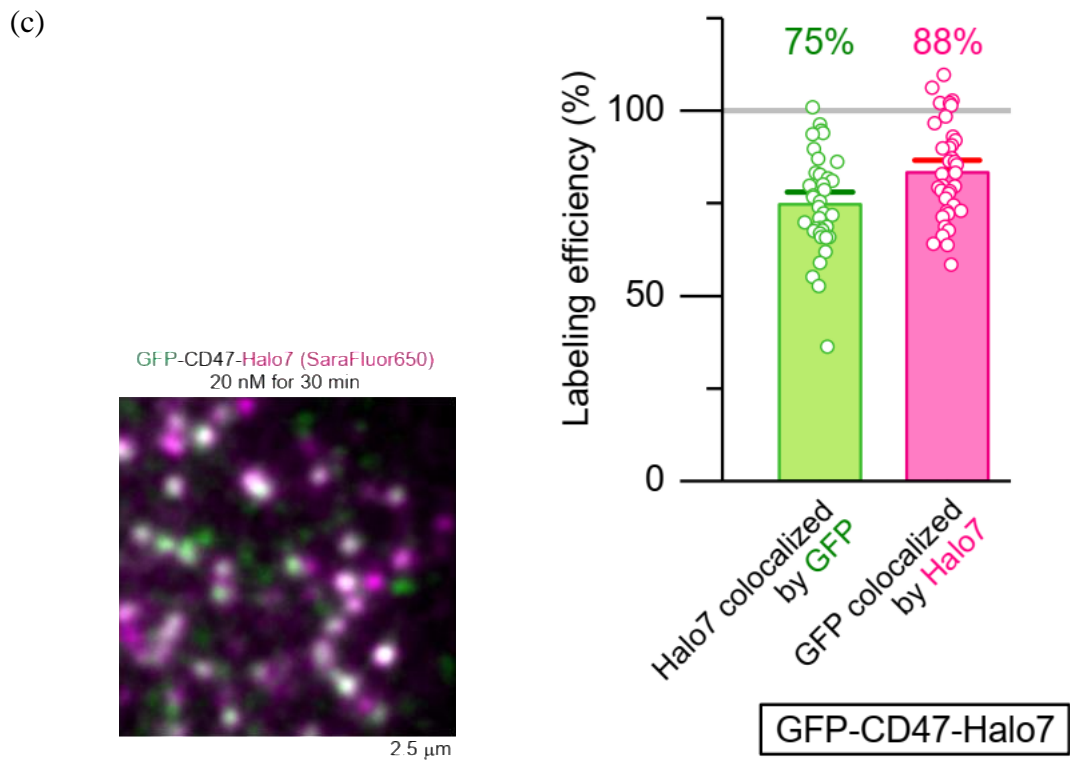
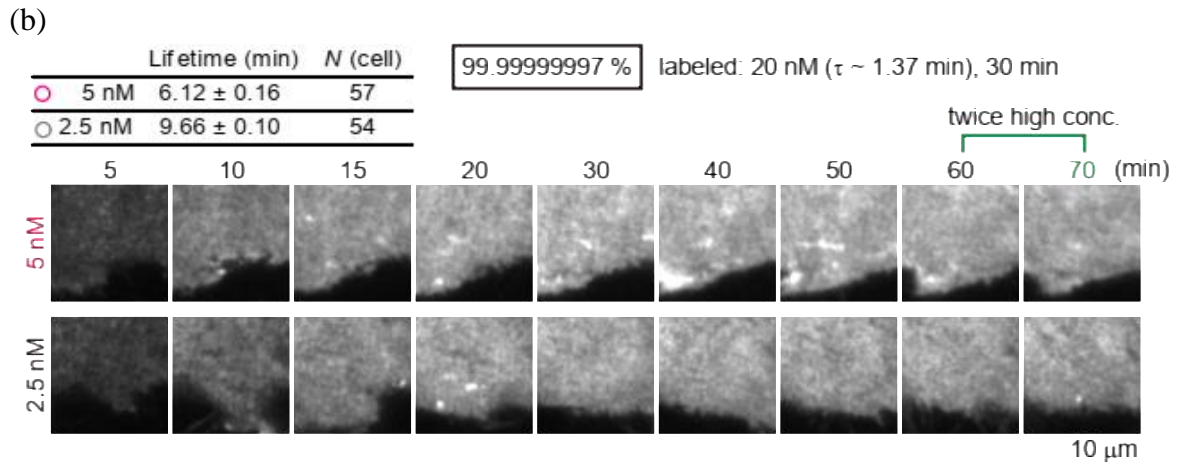


Fig 35. (a) Intensity of plasma membrane signal of CD47-Halo molecules expressed in T24 cells plotted against incubation time, tagged with 5 nM (magenta curve) or 2.5 nM (black curve) TMR-Halo dye.

(b) Fitting of the curves in (a) with logarithmic functions yielded labelling lifetimes of 6 min and 9.6 min respectively for 5 nM and 2.5 nM TMR-Halo. Thus, by incubating cells with 20 nM TMR-Halo for 30 min, more than 99% of all molecules could be labelled

(c) Colocalization of mEGFP and Halo (labelled with TMR-Halo) spots of a monomeric molecule containing both mEGFP and Halo tags, mEGFP-CD47-Halo, used to assess the percentage of

mEGFP tags that are fluorescent (75%) and the percentage of Halo tags that can be fluorescently labelled (88%).